INSTITUTO POTOSINO DE INVESTIGACIÓN CIENTÍFICA Y TECNOLÓGICA, A.C.

POSGRADO EN CIENCIAS APLICADAS

Carbon nanostructured adsorbents for the removal of toxic metals from aqueous solution

Tesis que presenta

Nancy Verónica Pérez Aguilar
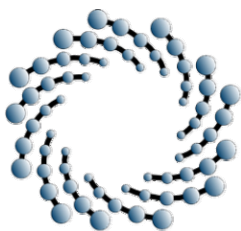
Para obtener el grado de

Doctor en Ciencias Aplicadas

En la opción de

Ciencias Ambientales

Director de la Tesis:

José René Rangel Méndez

San Luis Potosí, S.L.P., Abril de 2010

IPICYT

La tesis **"Carbon nanostructured adsorbents for the removal of toxic metals from aqueous solution"** presentada para obtener el Grado de Doctor en Ciencias Aplicadas en la opción de Ciencias Ambientales fue elaborada por **Nancy Verónica Pérez Aguilar** y aprobada el día **15 de Abril de 2010** por los suscritos, designados por el Colegio de Profesores de la División de Ciencias Ambientales del Instituto Potosino de Investigación Científica y Tecnológica, AC.

Dr. José René Rangel Méndez
(Director de la Tesis)

Dr. Emilio Muñoz Sandoval
(Sinodal)

Dr. Roberto Leyva Ramos
(Sinodal)

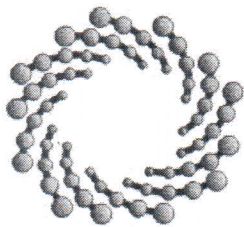Dr. Vladimir Alonso Escobar Barrios
(Sinodal)

CRÉDITOS INSTITUCIONALES

Instituto Potosino de Investigación Científica y Tecnológica, A.C.

Acta de Examen de Grado

El Secretario Académico del Instituto Potosino de Investigación Científica y Tecnológica, A.C., certifica que en el Acta 010 del Libro Primero de Actas de Exámenes de Grado del Programa de Doctorado en Ciencias Aplicadas en la opción de Ciencias Ambientales está asentado lo siguiente:

En la ciudad de San Luis Potosí a los 15 dias del mes de abril del año 2010, se reunió a las 16:00 horas en las instalaciones del Instituto Potosino de Investigación Científica y Tecnológica, A.C., el Jurado integrado por:

Dr. Vladimir Alonso Escobar Barrios	**Presidente**	**IPICYT**
Dr. Roberto Leyva Ramos	**Secretario**	**UASLP**
Dr. Emilio Muñoz Sandoval	**Sinodal**	**IPICYT**
Dr. José René Rangel Méndez	**Sinodal**	**IPICYT**

a fin de efectuar el examen, que para obtener el Grado de:

DOCTORA EN CIENCIAS APLICADAS EN LA OPCIÓN DE CIENCIAS AMBIENTALES

sustenta la C.

Nancy Verónica Pérez Aguilar

sobre la Tesis intitulada:

Carbon nanostructured adsorbents for the removal of toxic metals from aqueous solution

que se desarrolló bajo la dirección de

Dr. José René Rangel Méndez

El Jurado, después de deliberar, determinó

APROBARLA

Dandose por terminado el acto a las 18:40 horas, procediendo a la firma del Acta los integrantes del Jurado. Dando fe el Secretario Academico del Instituto.

A petición de la interesada y para los fines que a la misma convengan, se extiende el presente documento en la ciudad de San Luis Potosí, S.L.P., México, a los 15 días del mes de abril de 2010.

Dr. Marcial Bonilla
Secretario Académico

INSTITUTO POTOSINO
DE INVESTIGACIÓN
CIENTÍFICA Y TECNOLÓGICA, A.C.

IPICYT
SECRETARIA ACADEMICA

Mtra. Ivonne Lizette Cuevas Vélez
Jefa del Departamento de Asuntos Escolares

DEDICATORIA

A la memoria de papá, Domitilo Pérez García (q.e.p.d.)

Papá por treinta o cuarenta años,
amigo de mi vida todo el tiempo
protector de mi miedo, brazo mío,
palabra clara, corazón resuelto.

Algo le falta al mundo, y tú te has puesto
a empobrecerlo mas, y a hacer a solas
tus gentes tristes y tu Dios contento.

Y es en vano llorar. Y si golpeas
las paredes de Dios, y si te arrancas
el pelo o la camisa,
nadie te oye jamás, nadie te mira.
No vuelve nadie, nada. No retorna
el polvo de oro a la vida.

Jaime Sabines

Con amor a mi familia:
a mamá Ma. de Jesús Aguilar
a Gaby, Pepe, Lilí, Tito
a Dany y Angelito

AGRADECIMIENTOS

TABLE OF CONTENTS

LIST OF TABLES

LIST OF FIGURES

xvi

SUPPORTING INFORMATION

Appendix A

Appendix B

onto ox-CNx. Runs 6, 7 and 8 were performed at initial cadmium concentration of approximately C_{A0} 4, 9 and 19 mg/L respectively, at pH 6 and 200 rpm.

Appendix C

ABSTRACT

Nowadays most bodies of water are polluted by toxic heavy metals, which persist for long periods even at low concentrations. Permissible limits for toxic heavy metals in drinking water are continuously reviewed to protect human health. Accomplishment of established regulations requires the improvement of current technologies and the development of new ones. Nanotechnology has the potential to preserve water quality enabling its reuse, through development of nanoparticles to detect, prevent, and remove toxic heavy metals by adsorption. However, nanoparticles should be immobilized prior to be applied to water treatment to prevent their liberation and negative impact on the environment.

Early adsorption studies of toxic metals (cadmium, lead, copper, nickel, zinc and chromium) were performed with oxidized carbon nanotubes of single wall (SWNT) and multiwall (MWNT). Reported results showed that compared to activated carbon, carbon nanotubes had higher adsorption capacity, shorter equilibrium time and the possibility of being regenerated and used through several cycles.

In this study, oxidized nitrogen-doped multiwall carbon nanotubes (ox-CNx) showed 1.8 and 1.4 times higher adsorption capacity for cadmium and lead than ox-MWNT and oxidized granular activated carbon (ox-ACF), but 0.65 times lower than for ox-SWNT, at ph 5 and 25 °C. The small size, geometry and surface chemical composition of ox-CNx are the key factors for their higher adsorption capacity than ox-MWNT and activated carbon. Metal-exhausted ox-CNx could be regenerated and reused since more than 90% of the mass of both metals adsorbed was desorbed.

Morphology determines adsorption kinetic, as pointed out equilibrium times for cadmium adsorption onto different carbon nanotubes: around 15, 25 and 180 min for oxidized CNx, MWNT and SWNT, respectively, at initial cadmium concentration of 4 mg/L and pH 6. Cadmium adsorption could have a stronger diffusion effect onto the longest and most strongly entangled ox-SWNT, compared to the shorter ox-MWNT and ox-CNx. The intraparticle diffusion model fitted best the

experimental kinetic data with lower deviations than 5% and calculated diffusivity coefficients of about 2.4E-11, 4.2E-9 and 1.1E-9 cm^2/s, for ox-SWNT, ox-CNx and ox-MWNT, respectively, considered as single nanotubes, at initial cadmium concentration of 4 mg/L, pH 6 and 200 rpm.

Nanoestructured adsorbents were obtained supporting oxidized carbon nanotubes (ox-CNx) in polyurethane: nanotube loading of 2.5% (composite C1) and 1% plus 5% SBR (composite C3). Dynamic adsorption tests were performed in bed-packed columns with composites C1 and C3; about 5 and 7 bed volumes of cadmium solution were processed by C1 and C3, respectively, before bed saturation. Physical and chemical interactions between oxygen surface groups of carbon nanotubes and polymer chains could disable adsorption sites of carbon nanotubes. Consecutive cycles of adsorption-desorption suggested that nanotubes were firmly supported by the polymeric matrix. Obtained composites can be used in water treatment systems while preventing carbon nanotubes dispersion. Further research is required to effectively support carbon nanotubes or other nanoparticles preserving their adsorptive features.

Keywords: Water treatment, adsorption, carbon nanotubes, composites, adsorption kinetic, bed-packed column

RESUMEN

En la actualidad gran parte de los cuerpos de agua superficiales y subterráneos están contaminados por metales tóxicos, lo que implica un riesgo para la salud humana y la biodiversidad de los ecosistemas. Para obtener la calidad del agua establecida en las normas, se requieren tecnologías de purificación y tratamiento cada vez más eficientes. La nanotecnología ha surgido como una alternativa para preservar la calidad de este recurso.

En la presente investigación se probaron nanotubos de carbono dopados con nitrógeno oxidados (ox-CNx), para adsorber cadmio y plomo en solución acuosa. La capacidad máxima de adsorción de cadmio (q_m) sobre ox-CNx fue 1.8 y 1.4 veces mayor que la de ox-MWNT y carbón activado oxidado (ox-ACF), respectivamente, pero 0.65 veces menor que la de ox-SWNT. Factores como la geometría, la composición química y menor tamaño de partícula de los nanotubos ox-CNx pudieron determinar su mayor capacidad de adsorción de cadmio en relación con ox-MWNT y carbón activado. Además, es posible desorber más del 90% de los metales adsorbidos utilizando soluciones ácidas (pH 2) y reutilizar estos nanotubos (ox-CNx) durante varios ciclos, manteniendo su capacidad de adsorción.

La morfología juega un papel determinante en la cinética de adsorción con nanotubos de carbono. Se estudio la cinética de adsorción de cadmio sobre ox-CNx, ox-SWNT y ox-MWNT, por medio de experimentos en lote. El equilibrio se alcanzó en aproximadamente 15, 25 y 180 min para ox-CNx, ox-MWNT y ox-SWNT, respectivamente, con soluciones de cadmio de concentración inicial de 4 mg/L a pH 6. El mecanismo de difusión en el interior de los nanotubos fue más evidente en ox-SWNT. Estos nanotubos son más largos, con diámetro interno más pequeño y se entrelazan formando aglomerados, a diferencia de los ox-MWNT y ox-CNx. El modelo de difusión intraparticular se ajustó mejor a los datos experimentales, que los modelos de pseudo-segundo orden y de difusión externa, con desviaciones menores a 5%. Los coeficientes de difusión calculados con este

modelo fueron 4.2E-9, 1.1E-9 y 2.4E-11 cm^2/s para nanotubos individuales de ox-CNx, ox-MWNT y ox-SWNT, respectivamente, a una concentración inicial de cadmio de 4 mg/L, a pH 6 y 200 rpm.

Los nanotubos ox-CNx se inmovilizaron en poliuretano para obtener un adsorbente nanoestructurado. Estos nanotubos se seleccionaron considerando su mayor capacidad de adsorción de cadmio que los ox-MWNT, además de su cinética de adsorción más rápida que la de los ox-MWNT y ox-SWNT. Los compositos preparados con ox-CNx tuvieron concentraciones de 2.5% y 5% en peso (compositos C1 y C2), además de 1% en peso de nanotubos más 5% de SBR (composito C3). En el composito ocurrieron interacciones físicas y químicas entre los grupos superficiales de los nanotubos y el polímero. Como resultado, la concentración de sitios de adsorción disponibles en la superficie de los nanotubos disminuyó de manera significativa. Los compositos C1 y C3 se empacaron en columnas de lecho fijo para realizar pruebas de adsorción dinámicas; C1 y C3 procesaron aproximadamente 5 y 7 volúmenes de lecho de solución de cadmio, respectivamente, antes de la saturación del lecho. Ciclos consecutivos de adsorción-desorción mostraron que los nanotubos permanecieron en la matriz polimérica. Los compositos obtenidos son un medio de soporte seguro que permitirían la aplicación de nanotubos de carbono en sistemas de tratamiento de agua, evitando su dispersión. Es necesario continuar investigando cómo incrementar el porcentaje de nanotubos de carbono en los compositos a la vez mantener sus propiedades de adsorción.

Palabras clave: Tratamiento de agua, adsorción, nanotubos de carbono, compositos, cinética de adsorción, columna empacada

NOMENCLATURE

AAS	Atomic absorption spectroscopy
AC	Activated carbon
GAC	Granular activated carbon Filtrasorb® 400 from Calgon Carbon Corporation
ATRFTIR	Fourier transformed infrared spectroscopy by attenuated total reflectance
BV	Bed-packed volume (cm^3)
C	Solution concentration (mg/L)
C_A	Concentration of cadmium in solution at time t (mg/cm^3)
C_{Ao}	Initial concentration of cadmium in solution (mg/cm^3)
$C_{A\infty}$	Concentration of cadmium at equilibrium (mg/cm^3)
$C_{A,r}$	Concentration of cadmium in the pore volume at a distance r (mg/cm^3)
$C_{A,R}$	Concentration of cadmium in solution at the external surface (mg/cm^3)
C_0	Initial cadmium concentration (mg/L)
C_e	Concentration of cadmium solution at equilibrium (mg/L)
C_i	Concentration of cadmium solution at time interval i (mg/L)
C_S	Equilibrium concentration of cadmium on the surface of solid nanoparticle (mg/cm^3)
CNx	Nitrogen-doped carbon nanotubes
D_{corr}	Dimensionless effective diffusion coefficient (cm^2/h)
$D_{e,p}$	Effective pore volume diffusivity (cm^2/h)

D_i	Ionic diffusivity of cadmium (cm^2/h)
D_i^0	Ionic diffusivity of cadmium at diluted concentrations (cm^2/h)
D_s	Intraparticle diffusion coefficient (cm^2/h)
d_p	Nanoparticle diameter (cm)
DTA	Differential thermal analysis
DRIFTS	Fourier transformed infrared spectroscopy by diffuse reflectance
EBCT	Empty bed contact time (min)
ENP	Engineered nanoparticles
FeOOH	Iron oxide nanoparticles
HRTEM	High resolution transmission electron microscopy
K	Langmuir isotherm constant (L/mg-min)
K_1	Adsorption kinetic constant (L/mg-min)
K_2	Desorption kinetic constant (L/min)
k_L	Liquid film mass transfer coefficient (cm/h)
k_2	Constant rate of pseudo-second order sorption (g/mg-min)
m	Mass of adsorbent (mg)
MWNT	Multiwall carbon nanotubes
nZVI	Zero valent-iron nanoparticles
ox-GAC	Nitric acid-oxidized activated carbon by 1 h
ox-CNx	Nitric acid-oxidized nitrogen-doped carbon nanotubes
ox-CNx-1h	Nitric acid-oxidized nitrogen-doped carbon nanotubes by 1h
ox-CNx-3h	Nitric acid-oxidized itrogen-doped carbon nanotubes by 3h
ox-CNx-5h	Nitric acid-oxidized nitrogen-doped carbon nanotubes by 5h
ox-MWNT	Nitric acid-oxidized multiwall carbon nanotubes
ox-SWNT	Nitric acid-oxidized single wall carbon nanotubes

PAC-F400	Powder activated carbon Filtrasorb 400
pH_{PZC}	pH of point of zero charge
pH_{SP}	Slurry pH
PZC	Point of zero charge
Q	Influent flow rate (cm^3/min)
q	Adsorption capacity (mg/g)
q_e	Adsorption capacity at equilibrium (mg/g)
q_m	Maximal surface concentration, Langmuir isotherm constant (mg/g)
q_{max}	Maximum adsorption capacity (mg/g)
q	Mass of metal adsorbed per unit mass of adsorbent (mg/g)
q_m	Langmuir isotherm constant (mg/g)
q_t	Adsorption capacity at time t (mg/g)
r	Distance in radial direction of nanoparticle (cm)
R	Radius of the nanoparticle (cm)
S	Outer surface area of the adsorbent particle per unit mass of adsorbent (cm^2/g)
S_{BET}	Specific surface per unit mass of adsorbent determined by BET method (m^2/g)
S_V	Surface area of the adsorbent particle per unit volume of the adsorbent particle (cm^{-1})
SEM	Scanning electron microscopy
STEM	Scanning transmission electron microscopy
SWNT	Single wall carbon nanotubes Elicarb® from Thomas Swan
t	Time (min)
T	Absolute temperature (K)
TAS	Total acidic sites (mmol/g)
TGA	Thermo-gravimetric analysis
Tg	Glass transition temperature (°C)

Tm	Melting temperature (°C)
V	Volume of cadmium solution (L)
V_A	Molar volume of cadmium at its boiling temperature (cm^3/mol)
V_P	Pore volume per unit mass of nanoparticles (cm^3/g)
XRD	X-ray diffraction
ρ_s	Solid density of nanoparticles (g/cm^3)
ρ_p	Apparent density of nanoparticles (g/cm^3)
ϵ_p	Void fraction of nanoparticle adsorbent (g/cm^3)
τ	Tortuosity factor
φ	Dimensionless concentration of cadmium in solution
φ_{exp}	Experimental dimensionless concentration of cadmium at equilibrium
φ_{pred}	Dimensionless concentration of cadmium in solution predicted with the diffusion model
φ_∞	Dimensionless concentration of cadmium at equilibrium

CHAPTER 1

Carbon Nanostructured Adsorbents for the Removal of Toxic Metals from Aqueous Solution. State of the Art

1.1 INTRODUCTION

Water plays a key role in human societies. Proper management of water resources is an essential component of growth, social and economic development, poverty reduction and sustainable environmental development. The availability of water resources and their management is determinant in a country's growth strategy (WWAP, 2009). As world population grows, there is a challenge of having sufficient water of the right quality, at the right place and at the right time. However, this resource becomes increasingly scarce relative to demand. Great efforts are necessary to protect the water supply for humans, biodiversity and ecosystems (WWF4, 2006a).

That is why all countries are encouraged to optimize water consumption at the same time as preventing its pollution. Several actions are suggested, such as water recycling and reuse, adoption of international standards for water quality, and more investment in wastewater treatment and sanitation infrastructure, with preference for small-scale and local solutions. These actions require technological innovation for efficient operation of current water infrastructure, even more to design new cost-effective technologies (WWF4, 2006 b).

Advancement of knowledge and understanding of water treatment at different levels of sophistication has resulted in better technological options. Emerging nanotechnology can offer significant opportunities for the water sector. This new knowledge would result in using nanoparticles, nanofiltration or other products improving water quality. It is possible that application of nanotechnology to water treatment and purification systems would have lower overall costs; as well as

reduce the complexity of large centralized systems (Savage and Diallo, 2005; WWAP, 2006; 2009).

1.1.1 Water Pollution by Toxic Metals and Technologies for Treatment

Population growth has increased water demand for almost all productive activities such as agriculture, industry, energy and transportation. The wastewater from these activities containing high loads of toxic substances such as toxic metals is frequently discharged into water bodies. These contaminants have the potential for long-range transport, dispersal and deposition. Nowadays most bodies of water, either surface or groundwater sources, are polluted with toxic metals, which persist for long periods even at low concentrations (WWAP, 2003).

Toxic metals cannot be destroyed or broken down through treatment or environmental degradation, leading to different human health problems such as lead poisoning and cancer (USEPA, 1999). International standards for water quality list as priority toxic metals: lead, cadmium, mercury, chromium, nickel, silver, thallium and zinc. These standards are guideline values that are reasonably achievable through practical treatment technologies. However, these values are revised continuously. It is necessary to improve current technologies and to develop new ones (WHO, 2006).

In this research, lead and cadmium were selected as model toxic metal pollutants of water. A brief description of these metals, water pollution sources, and toxicology are presented in the following sections.

1.1.1.1 Water Pollution by Lead

The World Health Organization recommends a guideline value for the maximum allowable limit of 0.01 mg/L for lead in drinking water (WHO, 2006). This value can vary in each country depending on available technologies. In Mexico the corresponding value is also 0.01 mg/L (NOM-127-SSA1-1994, 2000).

Lead is principally used in the production of lead-acid batteries, solder and alloys. Lead is rarely present in tap water as a result of its dissolution from natural sources; rather, its presence is primarily due to plumbing systems containing lead in pipes, solder, fittings or the service connections. The amount of lead dissolved from the plumbing system depends on several factors including pH, temperature and hardness of the water. Lead concentrations in drinking-water are generally below 5 mg/L, although much higher concentrations (above 100 mg/L) have been measured where lead fittings are present. Infants, children up to 6 years of age and pregnant women are most susceptible to its adverse health effects. Lead accumulates in the skeleton impeding calcium metabolism, both directly and by interfering with vitamin D metabolism. Lead is toxic to the central and peripheral nervous systems, inducing subencephalopathic neurological and behavioral effects. Lead and its compounds are classified as possible human carcinogen. However, there is evidence from studies in humans that adverse neurotoxic effects other than cancer may occur at very low concentrations of lead and that a guideline value derived on this basis would also be protective for carcinogenic effects. Most lead in drinking-water arises from plumbing, and the remedy consists principally of removing plumbing and fittings containing lead (WHO, 2006).

Lead in aqueous solutions participates in a series of consecutive proton transfers that determine their chemical compounds in solution. The lead speciation diagram (Fig. 1.1) shows the distribution of species present in aqueous solution as a function of pH. Lead ion (Pb^{2+}) is stable below pH 5.5, then species $PbOH^+$, $Pb(OH)_2$, $Pb(OH)^{3-}$ are consecutively formed as a result of hydrolysis reactions (Stumm and Morgan, 1996).
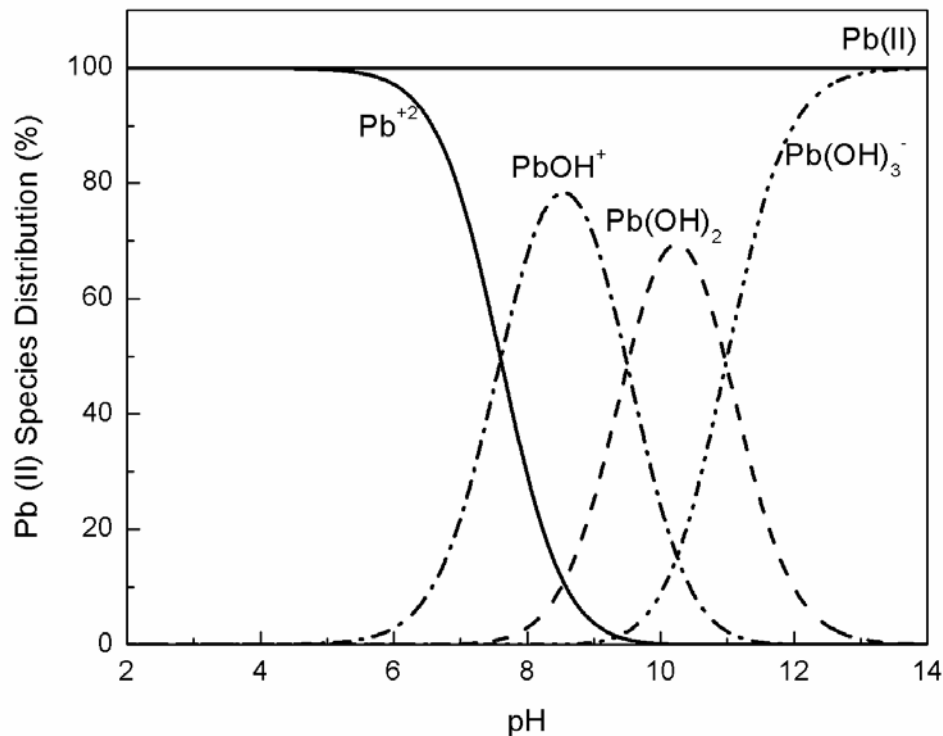
Fig. 1.1 Species distribution of 4×10^{-4} M Pb (II) in aqueous solution at 25 °C.

1.1.1.2 Water Pollution by Cadmium

The World Health Organization recommends a threshold limit guideline value of 0.003 mg/L for cadmium in drinking water (WHO, 2006). This value can vary in each country in function of available technologies. In Mexico, the corresponding value is 0.005 mg/L (NOM-127-SSA1-1994, 2000).

Cadmium metal and its compounds are used in the steel industry, plastics and in batteries. Cadmium is released to the environment in wastewater, and diffuse pollution is caused by contamination from fertilizers and local air pollution. Contamination of drinking-water may also be caused by impurities in the zinc of galvanized pipes and solders, and some metal fittings.

Food is the main source of daily exposure to cadmium. The daily oral intake is from 10 to 35 µg. Smoking is a significant additional source of cadmium exposure.

Cadmium accumulates primarily in the kidneys and has a long biological half-life in humans of 10 to 35 years. There is evidence that cadmium is carcinogenic when it is inhaled. However, there is no evidence of carcinogenicity by ingestion and no clear evidence for the genotoxicity of cadmium. The kidney is the main target organ for cadmium toxicity. The critical cadmium concentration in the renal cortex is about 200 mg/kg and would be reached after a daily dietary intake of about 175 µg per person for 50 years.

Speciation of cadmium in aqueous solution (Fig. 1.2) shows that at a concentration of $7x10^{-4}$ M (78 mg/L), cadmium ion (Cd^{2+}) is stable below pH 7.8; then species $CdOH^+$, $Cd(OH)_2$, $Pb(OH)^{3-}$ are consecutively formed as result of hydrolysis reactions (Stumm and Morgan, 1996).
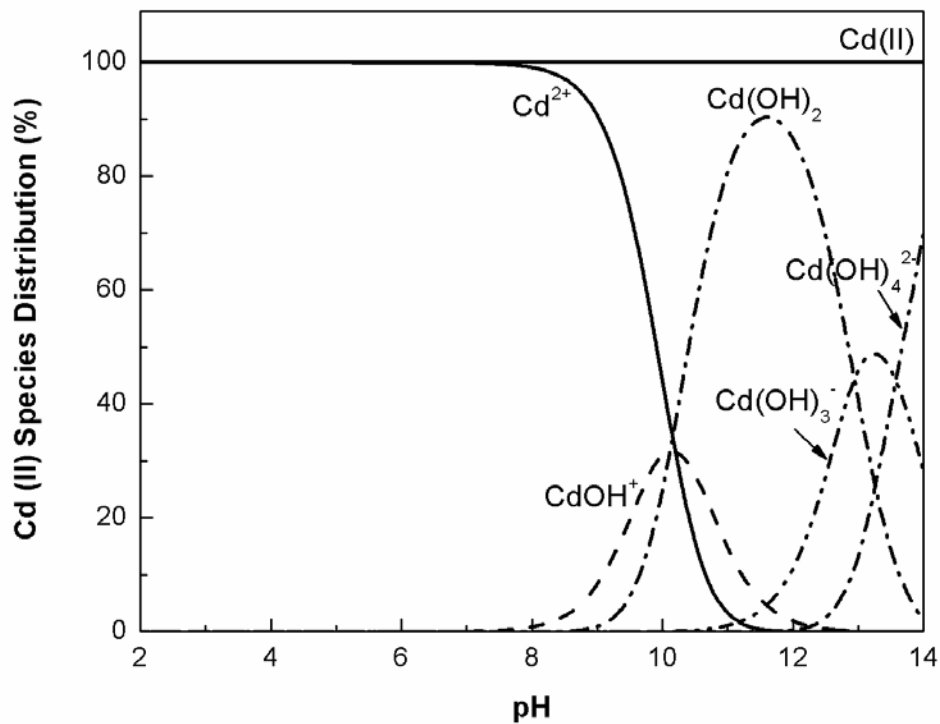
Fig. 1.2 Species distribution of $7x10^{-4}$ M Cd (II) in aqueous solution at 25 °C.

1.1.1.3 Water Treatment Technologies Available to Remove Toxic Metals

Drinking water purification and wastewater treatment will invariably be required to reduce both health risks and negative environmental impacts. Different technologies can be employed to remove pollutants as toxic metals: chemical precipitation, coagulation-flocculation, membrane filtration, ion exchange and adsorption. A brief review of advantages and limitations of these technologies are described as follows (Kurniawan et al., 2006):

a) Chemical precipitation. After pH adjustment to the basic conditions (pH 11), the dissolved metal ions are converted to the insoluble solid phase via a chemical reaction with a precipitant agent such as lime, lime plus sodium carbonate, or sodium hydroxide. Typically the precipitated metal from the solution is in the form of hydroxides, sulfides, or carbonates. The precipitate can then be removed from the treated water by clarification (settling) and/or filtration. Lime precipitation can be employed to effectively treat inorganic effluent with a metal concentration higher than 1000 mg/L. Other advantages are the simplicity of the method, inexpensive equipment requirement and wide availability of chemicals used. The main disadvantages are the necessity for large amounts of chemicals to reduce metals to an acceptable level for discharge. Since precipitated metals cannot be economically recovered from sludge, this requires further treatment increasing cost due to sludge disposal. Other disadvantages are slow metal precipitation, poor settling and aggregation of metal precipitates, and the long-term environmental impacts of sludge disposal.

b) Coagulation-flocculation. In coagulation colloidal particles are destabilized by adding a chemical coagulant, usually salts of aluminum or iron, to overcome the repelling forces between particles. To increase the particle size, coagulation is followed by flocculation of the unstable particles into bulky flocs. Typical coagulant doses are 2–5 mg/L as aluminum or 4–10 mg/L as iron. The precipitated floc removes suspended and dissolved contaminants by the mechanisms of charge

neutralization, adsorption and entrapment. The floc is removed from the treated water by subsequent processes such as sedimentation, flotation or filtration. This method can treat effluents with a metal concentration between 100 to 1000 mg/L, at pH ranging from 11 to 11.5 for optimum efficiency. The main advantages of the method are improved sludge settling, bacterial inactivation capability and sludge stability. The disadvantages are a high operational cost due to chemical consumption and further requirement for final disposal of sludge.

c) Membrane processes. Membranes have become an increasingly available filtration technology which can separate a wide range of substances organic and inorganic present in water. They can also be used in industrial and drinking water treatment, wastewater treatment and brackish and seawater desalination, at costs that are being reduced substantially. In function of the size of the particle to be retained, various types of membrane filtration can be employed: ultrafiltration (UF), nanofiltration (NF) and reverse osmosis (RO).

UF utilizes membranes of pore size in the range from 5 to 20 nm; UF can achieve more than 90% of removal efficiency with a metal concentration ranging from 10 to 112 mg/L at pH ranging from 5 to 9.5 and at 2 to 5 bar of pressure. NF has unique properties between UF and RO membranes, because its separation mechanism involves steric (sieving) and electrical (Donnan) effects. The significance of this membrane process lies in its small pore size and membrane surface charge, which allows charged solutes smaller than the membrane pores to be rejected along with the bigger neutral solutes and salts. NF can treat effluents with a metal concentration of 2000 mg/L with more than 90% of removal efficiency. NF can effectively remove metals at a wide pH interval of 3 to 8 and at a pressure of 3 to 4 bar. RO operates by applying a greater hydrostatic pressure than the osmotic pressure of the feeding solution. In general, RO is more effective for heavy metal removal from inorganic solutions, since efficiencies for metal removal are over 97% with a metal concentration ranging from 21 to 200 mg/L. Depending on the characteristics of the membrane such as porosity, material, hidrophylicity, thickness, roughness and charge of the membrane, RO works effectively at a wide

pH range from 3 to 11 and 5 to 15 bars of pressure. Pressure is the major parameter controlling effectiveness of metal removal: a higher pressure ensures higher metal removal, and thus higher energy consumption. Other advantages of RO include a high water reflux rate, high salt rejection, resistance to biological attack, mechanical strength, chemical stability and the ability to withstand high temperatures.

The main disadvantages of membrane processes are the decrease in performance due to membrane fouling, with adverse effects on the membrane system causing flux decline, an increase in transmembrane pressure and the biodegradation of the membrane materials, resulting in a high operational of cost for the system.

d) Ion exchange. In this process a reversible exchange of ions between the solid and liquid phases occurs, where an insoluble substance (resin) removes ions from a solution, and releases other ions of like charge in a chemically equivalent amount without any structural change of the resin. The process takes place without the formation of chemical bonds, hence it is possible to recover the metal loaded by using adequate reagents (Zagorodni, 2007). Ion exchange resins are cross-linked polymers carrying fixed functional groups or sites, usually sulfonic acid ($-RSO_3^-$). Ion exchange is effective to treat inorganic effluent with a metal concentration in the range from 10 to 100 mg/L, in acidic conditions at pH ranging from 2 to 6. This process does not present sludge disposal problems. Appropriate pretreatment of the effluent is required prior to using an ion exchange process, as the removal of suspended solids.

Ion exchange resembles adsorption because in both cases a solid takes up a dissolved species. The characteristic difference between these two phenomena is in the stoichiometric nature of ion exchange. Every ion exchanged from the solution is replaced by an equivalent amount of another ion of the same charge. In adsorption, on the other hand, a solute is usually taken up non-stoichiometrically without being replaced.

e) Adsorption. This is a mass transfer operation by which a substance is transferred from the liquid phase to the surface of a solid and becomes bound by physical and/ or chemical interactions. Adsorption is used in drinking water treatment as tertiary process, for the removal of color and odor for achieving regulatory requirements. The primary adsorbent materials used in the adsorption process for drinking water treatment are activated carbons (Suzuki, 1990; Bansal et al., 1998; Bansal and Goyal, 2005). Recently research has pointed out low-cost adsorbents derived from agricultural waste, industrial by-products or natural materials for the removal of heavy metals. Use of granular activated carbon (GAC) is considered to be the best available technology for removing low-solubility contaminants such as toxic metals in trace concentrations (Radovic, 2001). A broader description of this technology is included in the following section.

1.1.1.4 Adsorbents for Toxic Metals

Some adsorbent materials are capable to remove toxic metal from aqueous solutions such as activated carbons, zeolites, clays and polymeric resins.

a) Zeolites are porous crystalline aluminosilicates which comprise assemblies of SiO_4 and AlO_4 tetrahedra joined together through the sharing of oxygen atoms. Commercially the most important are chabazite, faujasite and mordenite. Cavities contained within the zeolite framework are connected by regular channels of molecular dimensions, into which adsorbate molecules can penetrate. The internal porosity is high and thus the majority of adsorption takes place internally. For this reason zeolites are capable of effectively remove adsorbates on the basis of size, shape and other properties such as polarity.

b) Clays can be synthesized or found in natural deposits. These comprise layered silicates which take in guest molecules between their siliceous layers causing their crystals to swell.

9

Fuller's earth is an activated natural montmorillonite. Its pore size is altered and its surface area increased (150-250 m^2/g) by acid treatment. It is relatively inexpensive and which it is in cationic form is capable of adsorbing a range of polar molecules as toxic metal ions (Thomas and Crittenden, 1998).

c) Polymeric resins are cross-linked polymers carrying fixed ions which can be stoichiometrically exchanged for other ions of the same sign. Some groups are able to form chelate structures with metal ions. The most typical example of ion exchange resin is sulphonated polystyrene cross-linked with divinylbenzene. The group –SO$_3$H can exchange the hydrogen ion for any other cation, aditionally it can bear a wide diversity of functional groups (Zagorodni, 2007).

1.1.1.5 Adsorption of Toxic Metals on Activated Carbon

Activated carbon (AC) has been proven to be an effective adsorbent for the removal of a wide variety of organic compounds and heavy metals dissolved in aqueous media (Yin et al., 2007). Activated carbon is produced by the combustion of carbonaceous material, normally wood, coal, coconut shells or peat. This activation produces a porous material with a large surface area (500–1500 m^2/g) (Bansal et al., 1998; Bansal and Goyal, 2005).

The usefulness of activated carbons derives mainly from its large micropore and mesopore volumes, with a high surface area between 300 and 4000 m^2/g. They also have analogous surface chemical groups of organic compounds (Fig. 1.3) (Yang, 2003). The surface of activated carbons can display acidic, basic and/or neutral characteristics depending on the presence of these functional groups, which can be modified through chemical treatment with different reagents (nitric acid, sulfuric acid, hydrogen peroxide, or sodium hypochlorite). Some surface acidic functional groups include carboxyl, carbonyl, lactone, hydroxyl and carboxylic anhydride. These specific functional groups are essential for the

adsorption of heavy metals due to reactions to form complexes as indicated by the equation 1.1 (Yin et al, 2007):

$$M^{n+} + n(-COOH) \leftrightarrow (-COO)_n M + nH^+ \qquad\qquad (1.1)$$
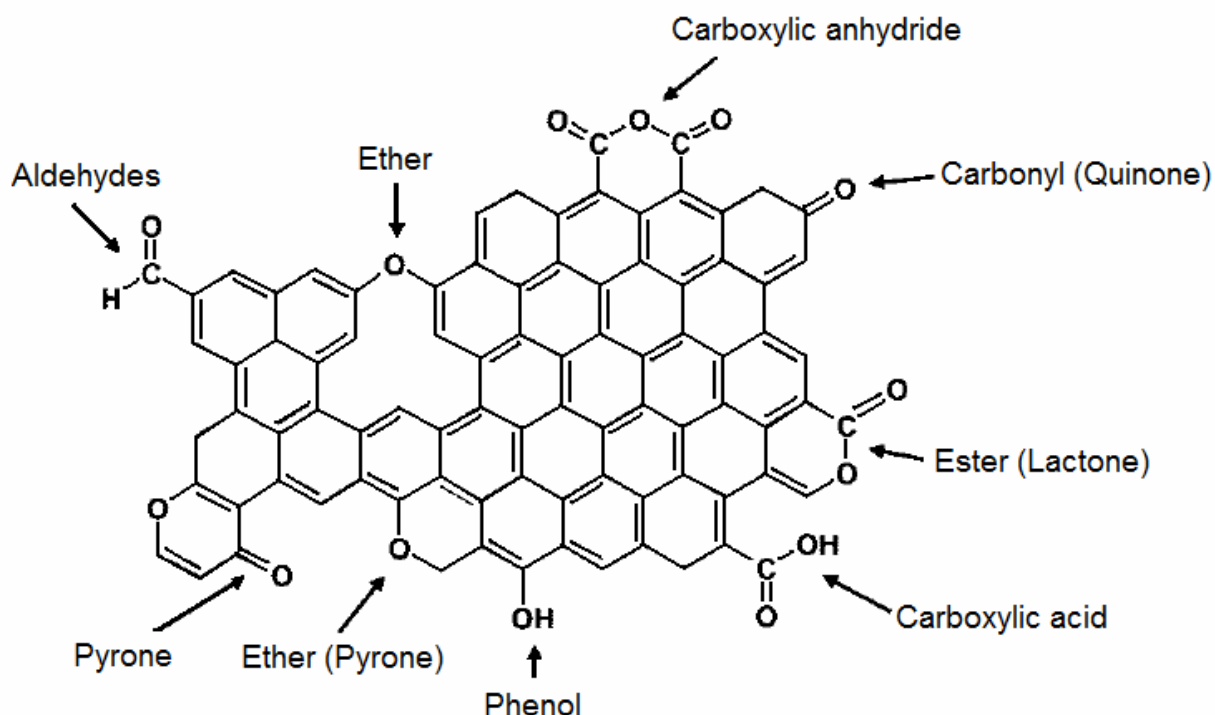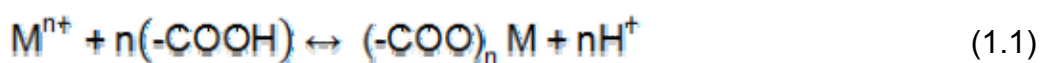
Fig. 1.3 Representation of oxygen functional groups present on the carbon activated surface.

Acidic and basic functional surface groups impart a polar character to the surface of activated carbons by interaction with water. Ionization of these surface groups depends strongly on the pH of the solution and leads to a charged interface between the surface and the bulk solution. In addition, these surface groups are subjected to a wide variety of inter- and intra-molecular interactions including inductive, mesomeric, tatuomeric, steric and hydrogen-bonding. The heterogeneity in the surface chemistry of activated carbons makes it difficult to delineate a specific mechanism of adsorption of heavy metals on the surface of carbons, but it is clear that the extent of adsorption of metal ions on activated carbons is related to

11

the amount of surface oxygen-containing groups (Contescu et al., 1997; Radovic, 2001; Bansal and Goyal, 2005).

Adsorption of heavy metals in solution depends very much on pH and it has been found that it occurs at 1 to 2 pH units below the value that is required for precipitation of the metal hydroxide. In general, activated carbons are capable of adsorbing many of the toxic metals such as copper, lead, zinc, nickel, cadmium, mercury, chromium, cobalt and silver. Many works have been reviewed and discussed by several authors (Radovic, 2001; Bansal and Goyal, 2005).

Adsorption at the solution-carbon interface is already widely used on large scale water treatment to remove toxic metals. Carbon capacity is strongly dependent on the water source and is greatly reduced by the presence of background organic compounds (Cooney, 1999). Activated carbons are normally used either in powdered (PAC) or in granular (GAC) form. The choice between PAC and GAC will depend upon the frequency and dosage required. PAC would be preferred where low dosage rates are required. PAC is dosed as slurry into the water and is removed by subsequent treatment processes. Its use is therefore restricted to surface water treatment with existing filters. GAC in fixed-bed adsorbers is used much more efficiently than PAC dosed into the water. The service life of a GAC bed is dependent on the capacity of the carbon, and the contact time between the water and the carbon (empty bed contact time, EBCT). EBCT is controlled by the flow rate of the water, often values for EBCTs are in the range from 5 to 30 min. Metal ions exhausted activated carbons are normally used only once before their disposal (WHO, 2006).

So far activated carbon has been used as an all-purpose adsorbent, but future applications of adsorption are limited by the availability of new, better and cheaper adsorbents (Yang, 2003).

1.2 NANOTECHNOLOGY DEVELOPMENT AND POTENTIAL APPLICATIONS TO WATER TREATMENT

The expansion of scientific knowledge and technological applications is changing the way in which water is used, cleaned and reused, to meet human, economic and environmental needs. Nanotechnology has been emerging rapidly; it has been predicted that it will exert strong influence on the technologies related to supply, use and management of water resources (WWAP, 2009).

Nanotechnology is the manipulation of matter for particular applications at the atomic, molecular, or macromolecular levels, using a length scale of approximately one to one hundred nanometers in any dimension (USEPA, 2007). Nanotechnology can develop new materials with enhanced properties and attributes, resulting of larger surface area per unit of volume and quantum effects that occur at the nanometer scale (Renn and Roco, 2006).

Applications of nanotechnology will penetrate nearly all sectors and spheres of life (communication, health, labour, mobility, housing, relaxation, energy, food) and will be accompanied by changes in the social, economic, ethical and ecological spheres. Already nanomaterial-containing products are available in U.S. markets including coatings, computers, clothing, cosmetics, sports equipment and medical devices (Renn and Roco, 2006; Hristozov and Malsch, 2009).

Nanomaterials are all materials with sizes on the nanoscale in at least one of their dimensions, while nanoparticles (NP) are nanosized in at least two dimensions. The nomenclature nanoparticle includes particles as well as fibrous materials and tubes, but it excludes materials, such as coatings, films and multilayers. Two types of nanoparticles can be distinguished: naturally occurring ones such as those produced in volcanoes, forest fires or as combustion by-products, and engineered nanoparticles (ENP), deliberately developed to be used in application (Hristozov and Malsch, 2009).

The United States Environmental Protection Agency has classified the current nanomaterials as follows (USEPA, 2007):

a) Carbon-based materials: Composed mostly of carbon; spherical and ellipsoidal carbon nanomaterials are referred to as fullerenes, while cylindrical ones are called nanotubes.

b) Metal-based materials: Include quantum dots, nanogold, nanosilver and metal oxides.

c) Dendrimers: Are nanosized polymers built from branched units. The surface of a dendrimer has numerous chain ends, which can be tailored to perform specific chemical functions.

d) Composites: Combine nanoparticles with other nanoparticles or with larger, bulk-type materials.

Characteristics of nanomaterials such as enhanced reactivity, surface area, subsurface transport, and/or sequestration, could benefit environmental remediation by faster and more economical processes than current conventional approaches. It is necessary to understand how to best apply nanotechnology for pollution prevention as well as in environmental detection, monitoring and remediation. Environmental remediation is the degradation or sequestration of chemical and radiological contaminant, reducing the risks to human and environmental receptors (USEPA, 2007).

Nanotechnology shows particular promise for water resources, to improve water quality through water treatment or remediation. Key areas are desalinization, water purification, wastewater treatment and monitoring. The first three areas involve the use of nanofiltration technology, nanomaterials and nanoparticles to remove or reduce water contaminants. Monitoring involves the use of new sensor technology coupled with micro and nanofabrication technology. Nanosensors would be highly accurate and portable for detection of biological and chemical water contaminants, present in very low concentrations (Tour, 2007; WWAP, 2009).

Nanotechnology-based water treatments could replace current chemicals for which existing technologies are inefficient or costly, and could eventually permit human

use of heavily polluted and saline water for drinking, sanitation and irrigation (Weber, 2002; Savage and Diallo, 2005). ENP applied to water treatment might control the destination, transport, and bioavailability of toxic metals and other contaminants through adsorption, redox reaction, and other biogeochemical processes. However, the stability and aggregation behavior of ENP in water could impact their reactivity and efficacy in contaminant treatment (He et al., 2008).

There are several reviews about using ENP and nanomaterials to remove metal ions from aqueous solutions or wastewater. So far the most promising results have been obtained using carbonaceous nanomaterials (fullerenes, SWNT and/ or MWNT), biopolymers, zero-valent iron and nanocrystalline titanium oxide (TiO_2) (Savage and Diallo, 2005; Li et al., 2007; Mauter and Elimelech, 2008; Shannon et al., 2008; Theron et al., 2008).

Applications involving dispersive uses of nanomaterials in water have the potential for wide exposures to aquatic life and humans (USEPA, 2007). It is possible that ENP can cause novel environmental problems and/or impose risks to human health. It is very important to study the environmental destination of ENP in order to understand their pathways of environmental and human exposure. At this point of time and stage of knowledge, it is impossible to make any collective judgment about the potential risks of exposure to nanomaterials (Renn and Roco, 2006).

The destination of ENP in water is determined by factors such as aqueous solubility, reactivity of the ENP with the chemical environment and their interaction with certain biological processes. Some ENP might be removed from water by processes such as sorption to soil and sediment particles, biotic and/ or abiotic degradation (hydrolysis and photocatalysis). Nonetheless, some insoluble ENP can be stabilized in aquatic environments by interaction with natural organic matter (NOM) or humic acids (Hristozov and Malsch, 2009).

To facilitate accurate risk assessment of ENP, all research strategies involving ENP must have a strong focus on their characterization. Hence, the identification of clear causality between ENP properties and the adverse effects they cause would

be more accurate. For all types of ENPs, the most suitable dose-descriptors need to be determined in terms of their surface area, mass, morphology and chemical composition (Renn and Roco, 2006; Hristozov and Malsch, 2009). Considering this situation, adequate immobilization of nanoparticles before their use in water-related applications could prevent their dispersion, and their probable adverse environmental effects.

Nanotechnology-based applications to the water sector are still under fundamental research, and it is unclear when they will be ready for wide-scale use. These new technologies must compete against currently used technologies, looking for cheaper solutions that meet government standards. In addition, it is necessary to overcome factors such as availability of nanomaterials in large scale and lack of knowledge and regulations about their environmental and health impacts (WWAP, 2009).

1.2.1   Adsorbent Nanoparticles for Toxic Metals

Research and development of novel materials with increased capacity, affinity and selectivity for heavy metals and other water pollutants is being performed. Benefits from using nanomaterials may derive from their enhanced reactivity, surface area and sequestration characteristics. Some materials possessing unique functionalities potentially applicable to heavy metal remediation and purification from water are carbon nanotubes, biopolymers and zero-valent iron nanoparticles.

Advances in genetic and protein engineering techniques have enabled the construction of protein-based nanobiomaterials with metal-binding properties with enhanced specifity and affinity compared to chemical adsorbents. The use of tunable metal-binding biopolymers, based on elastin-like polypetides is emerging as a promising technology for heavy metal remediation from aqueous wastes. Bioploymers have structurally similar characteristics to the mammalian protein elastin; the most interesting feature of this protein is their ability to undergo reversible phase transition under a range of temperature, pH and ionic strength, which are properties for recovery of the metal-polymer complexes. After extraction

of metals, the aggregated polymers can be reused for subsequent cycles (Kostal et al., 2005).

Iron nanoparticle technology represents one of the first generation nanoscale environmental technologies, receiving considerable attention for its potential applications in groundwater treatment and site remediation. The greatest interest is in the use of zero-valent iron nanoparticles (Fe^0; nZVI), for which reactivity is driven by oxidation of the Fe^0 core. Their higher reactivity compared to their microscale counterparts has been attributed to the greater density and higher intrinsic reactivity of their surface sites. Extensive laboratory studies have demonstrated that nZVI nanoparticles are effective for the transformation heavy metal ions such as lead, copper, nickel, and chromium. Both, reduction and surface complex formation are reported as the mechanisms for ion transformation (Li and Zhang, 2006).

1.2.2 Carbon Nanotubes: Synthesis, Properties and Modification

Carbon nanotubes (CNT) are key elements in nanotechnology. The structure of carbon nanotubes is depicted as a rolled segment of a single graphite layer, called a graphene sheet (Fig. 1.4). It is formed by linking each carbon atom to three equivalent neighbors in a trigonal planar fashion (C-C distance, 1.42 Å) (Dresselhaus, 1997; Dresselhaus et al., 2001). Carbon nanotubes structured by only one graphene sheet are known as single-wall carbon nanotubes (SWNT). If carbon nanotubes contain several coaxial SWNT, these are called multiwall carbon nanotubes (MWNT), in which graphene sheets are separated from one another by approximately 0.34 nm, the interlayer distance of graphite (Dresselhaus et al., 2001).
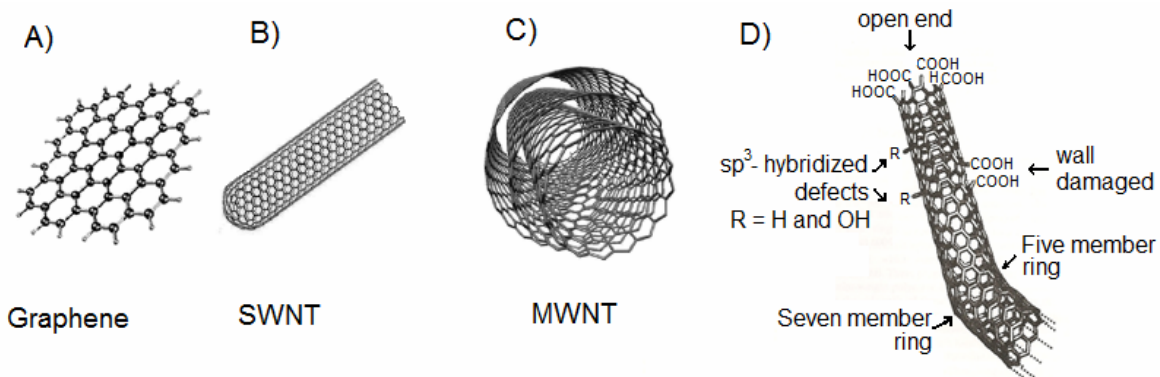
Fig. 1.4 Fundamental structure for (A) graphene sheet, (B) single-wall carbon nanotube, SWNT, (C) multiwall carbon nanotube, MWNT (modified figure from Mauter and Elimelech, 2008) and (D) typical defects and functional groups in an oxidized carbon nanotube (modified figure from Hirsch, 2002).

Synthesis of carbon nanotubes can be carried out by several techniques, at high temperatures (above 3200 °C) or at medium temperatures (lower than 1000 °C). High-temperature routes involve sublimating graphite in a reduced atmosphere of rare (inert) gases, and condensing resulting vapor under a high temperature gradient. Used methods for sublimating graphite could be: an electric arc formed between two electrodes made in graphite, an ablation induced by a pulsed laser, or a vaporization induced by a solar or a continuous laser beam. Medium-temperature routes are based on catalytic chemical vapor deposition (CVD) processes. CVD make possible the growth of carbon nanotubes of various sizes and shapes, from carbon-containing gaseous compounds which decompose catalytically on transition-metal particles (Loiseau et al., 2006).

High-temperature methods produce high quality nanotubes, particularly SWNT in relatively large quantities. Meanwhile, CVD processes are more flexible and easier to be scaled up. CVD processes are becoming the major way for synthesizing carbon nanotubes in a controlled way. Depending on the experimental conditions, it is possible to selectively grow SWNT or MWNT. However, SWNT can only be

produced with metallic catalyst whichever the synthesis process used (Dresselhaus et al., 2001).

Carbon nanotubes have a very stable structure due to sp^2 covalent bonds between carbon atoms. Moreover, cylindrical curvature gives some sp^3 character to the C–C bonding, resulting in the richness and diversity of the physical and chemical properties of carbon nanotubes. Only perfect graphene sheets are chemically inert, but surface defects existing on carbon nanotubes constitute reactive sites (Niyogi et al., 2002; Tománek et al., 2008). It is possible to modify and control the physicochemical properties of carbon nanotubes by doping processes, which consist of introducing either non-carbon atoms or molecules at small concentrations, in the plane of the graphene network. This process can tailor the electronic, vibrational, chemical and/ or mechanical properties of nanotubes, useful for a wide range of applications (Terrones et al., 2002; 2008).

Doping carbon nanotubes with nitrogen atoms induce crystalline disorder in the graphene sheets, when using lower concentrations than 6.5 wt%. From an electronic point of view, one would expect an excess of electron donors on the nitrogen-rich areas, thus being more reactive when compared to crystalline graphite. For nitrogen-doped carbon nanotubes, two types of C–N bonds could occur: the first is a three-coordinated N atom within the sp^2- hybridized network, with the presence of additional electrons. These doped tubes are more likely to react strongly with acceptor molecules. The second type is the pyridine type (two-coordinated N), which can be incorporated in the nanotube lattice; an additional carbon atom is removed from the framework (Terrones et al., 2008). Nitrogen-doped carbon nanotubes can be obtained by using processes such as the arc-discharge method, laser-ablation method and chemical vapor deposition method. In general these tubular structures, produced by using the CVD process, reveal a stacked-cone or compartmentalized morphologies (bamboo-type) and the degree of tubular perfection decreases as a result of the N incorporation into the hexagonal carbon lattice (Nevidomskyy et al., 2003; Terrones, 2003; Terrones et al., 2008).

Besides doping, chemical modification of carbon nanotubes with different functional groups for specific applications is a major growth area nowadays (Tománek et al., 2008; Wang et al., 2009). Functionalization can be used to modify the interface between the environment and the outer wall of CNTs (Fig. 1.4D). This would, for example, modify solubility and facilitate dispersion in a given medium. The tips are the most reactive part of the CNTs because it is where the highest strains are located and where the carbon atoms have some sp^3 character (Hirsch, 2002). All oxidizing treatments involve the use of acidic solutions or thermal treatment (HNO_3, $KMnO_4$ + H_2SO_4, $K_2Cr_2O_7$, H_2O_2, CO_2, O_2), which will attack the tips in order of priority, but structural defects located on the walls (heptagon-pentagon pairs for example) will be attacked as well to a smaller extent (Niyogi et al., 2002; Ovejero et al., 2006). All these treatments will degrade the carbon nanotubes depending on the strength of the oxidizing agent and the duration of the treatment. Oxidation of CNTs leads to the formation of chemical groups such as carboxyl functions, lactones, ketones, or hydroxyl groups. These organic functions can be used to graft other functional groups or molecules (Hirsch, 2002; Tasis et al., 2006).

1.2.3 Adsorption of Toxic Metals on Carbon Nanotubes

Carbon nanotubes have been tested as adsorbent of toxic metals in aqueous solution obtaining promising results; most of the studies have been conducted with MWNT. Early studies were done by Li et al., (2002), who used MWNT oxidized with nitric acid to adsorb lead in aqueous solution. The maximum adsorption capacity at room temperature and pH 5 was 17.5 mg/g. Since then, the same researchers have reported the adsorption of lead, copper, and cadmium onto MWCNT: the maximum adsorption capacities were 97.08 mg/g for lead, 24.49 mg/g for copper and 10.86 mg/g for cadmium at room temperature, pH 5.0 and metal ion equilibrium concentration of 10 mg/L. It was also found that the adsorption capacities of the MWCNT were 3 to 4 times larger than those of powder activated carbon and granular activated carbon (Li et al., 2003a). After that, more studies have been performed: copper ions were removed by oxidized MWNT and

their maximum adsorption capacity was 27.6 mg/g at pH 5.2 (Li et al., 2003b). Also different reagents have been used to modify the nanotubes: hydrogen peroxide (H_2O_2), potassium permanganate ($KMnO_4$) and nitric acid (HNO_3). The oxidized nanotubes removed cadmium with maximum adsorption capacities of 2.6, 5.1 and 11 mg/g, respectively, at the cadmium equilibrium concentration of 4 mg/L (Li et al., 2003 c). Nitric acid solutions are the most used oxidizing agent to attach oxygen-containing groups onto carbon nanotubes to modify their surface properties for metal ions adsorption. Furthermore, adsorption equilibrium tests at different temperatures were conducted to evaluate the effect on adsorption capacity; it was found that adsorption with carbon nanotubes is an endothermic process (Li et al., 2005). Also, carbon nanotubes synthesized by using different conditions of precursor, catalyst and temperature (xylene-Fe-800°C, benzene-Fe-1150°C, propylene-Ni-750°C or methane-Ni-650°C) were tested to adsorb lead. It was found that those synthesized with methane-Ni-650°C had a higher lead adsorption capacity (82.6 mg/g at pH 5), because their less crystalline structure and higher concentration of carboxylic groups (Li et al., 2006).

The adsorption capacity of MWNT for several metal ions has been evaluated at different conditions of ionic strength, pH, temperature, foreign ions, etc. Some of these studies include kinetics analysis of the experimental data by the pseudo-second order reaction model. Published results for maximum nickel adsorption capacity are 9.8 mg/g at 30 °C and pH 6.5 (Chen and Wang, 2006), 49.6 mg/g at room temperature and pH 6 (Kandah and Meunier, 2007), 38.46 mg/g at room temperature and pH 7, for MWNT oxidized by sodium hypochlorite (Lu et al., 2008), and 7.4 mg/g due to the effect of polyacrylic acid (PAA), with a structure like that of natural organic matter (NOM) (Yang et al., 2009).

Few studies have been carried out to test the more expensive SWNT which have higher adsorption capacity than MWNT. Lu and Chiu (2006) observed a maximum zinc adsorption capacity of 44 mg/g at room temperature and pH 7 for oxidized SWNT, versus 32.7 mg/g for oxidized MWNT. Increasing temperature enhanced the maximum zinc adsorption capacity for oxidized SWNT to 46.9 mg/g at 45°C

and pH 7 (Lu et al., 2006). The maximum nickel adsorption capacity onto oxidized SWNT is 47.85 mg/g at room temperature and pH 7 versus 38.46 mg/g for oxidized MWNT (Lu et al., 2008).

Recently, two adsorption studies were conducted with nitrogen-doped carbon nanotubes (CNx) to remove metal ions from aqueous solutions. Maximum adsorption capacity of 31 mg/g (Andrade-Espinosa et al., 2008) and 21.6 mg/g, at pH 7 (Perez -Aguilar et al., 2010) were obtained for cadmium and 28.9 mg/g at pH 5 for lead (Perez -Aguilar et al., 2010).

In general, carbon nanotubes have shown better adsorption capacities for toxic metal ions in aqueous solution than activated carbons. Their adsorptive features besides a more efficient regeneration, and shorter time to reach equilibrium than activated carbon, have led to a search for an adequate use of CNT in devices as membranes and filters for water purification systems (Rao et al., 2007; Stafiej and Pyrzynska, 2007; Wang et al., 2007a,b; Yang et al., 2009).

Adsorption processes are designed on the basis of equilibrium and rate information; thus many of carbon nanotubes adsorption properties remain largely unexplored (Yang, 2003; Li et al., 2007). The overall rate of adsorption of a metal ion on a porous material can be described by two main steps: the external mass transfer from the bulk liquid to the solid surface, followed by mass transport of adsorbate molecules into the particle; this is the most typical of the rate steps in solid adsorbents and is referred to as intraparticle diffusion (Cooney, 1999). Most research studies about adsorption with carbon nanotubes in liquid phase have minimized the role of intraparticle diffusion in kinetics adsorption, assuming that the adsorption reaction is the controlling step. The evaluation of adsorption kinetics is necessary considering the different types of existing carbon nanotubes. The physical structure and the chemical properties should be involved in adsorption kinetics of toxic metals.

Furthermore, considering the risk of liberating carbon nanotubes to water sources, it is necessary to effectively immobilize these nanostructures, in a way that their application is possible in adsorber or filter devices for water treatment.

1.3   MOTIVATION FOR THIS RESEARCH

Nanotechnology is evolving rapidly, offering the possibility to design and obtain customized materials for specific applications from a molecular level, more accurately and economic than current bulk methods.

The development of highly efficient nanotechnology-based water treatment and purification systems will occur in the near future. These will offer higher reliability of treatment, enabling reduction of equipment size, more energy saving, simplification and cost reduction compared to conventional technologies.

Carbon nanotubes are key nanomaterials in nanotechnology. The graphene sheet is the fundamental structure of carbon nanotubes, likewise in activated carbon, the most used adsorbent. Hence, the development of carbon nanotube adsorbents for water applications is of special interest. Current knowledge on carbon chemistry has allowed the modification of graphene sheets, and consequently the chemical properties of carbon nanotubes. Hence, there is a broad range of possibilities to design carbon nanotubes for specific uses and/or to remove certain pollutants. A better performance of the carbon nanotube as adsorbents is expected compared to currently used activated carbons.

Development of devices based on carbon nanotubes for water treatment systems are in the early stages. Parameters of adsorption at equilibrium, adsorption kinetics, and adsorption column tests are necessary. So far, most of the reported studies on adsorption on carbon nanotubes have been performed at equilibrium. To our knowledge there are not published studies on adsorption kinetic and/or column tests with carbon nanotubes, which is an area of opportunity to contribute to the knowledge of the use of carbon nanotubes in water treatment systems.

Finally, there are challenges and difficulties associated with the dissemination of nanotechnology, which is especially important for developing countries such as Mexico. Most of the time new technologies are very expensive because they are imported from industrialized countries. In addition, scarcity of human resources with appropriate technical knowledge and abilities might prevent the optimum operative efficiency of these novel tools. These are the main reasons that motivated exploring and contributing to the current knowledge of using nanotechnology in water treatment.

1.4   GENERAL AND SPECIFIC OBJECTIVES

This research is focused on nitrogen doped and nitric acid oxidized carbon nanotubes. The general aim is to evaluate the adsorption performance of carbon nanotubes to remove toxic metals present in aqueous solutions. This objective was covered from two different approaches: through batch adsorption experiments by using suspended nanotubes, and dynamic adsorption experiments by using bed packed columns with supported nanotubes in a polymeric composite.

To achieve the main goal, the following specific objectives were established: selecting cadmium and lead in aqueous solution as model metal ions.

I. To conduct the physical and chemical characterization of carbon nanotubes by several techniques to understand interactions between the nanotubes surface and heavy metal ions in aqueous solution, in order to suggest an adsorption mechanism.

II. To evaluate the adsorption capacity at equilibrium of modified novel nitrogen-doped carbon nanotubes (CNx), and to compare their performance with single carbon nanotubes (SWNT), multiwall carbon nanotubes (MWNT), as well as with commercially available activated carbon.

III. To evaluate adsorption kinetic of carbon nanotubes, specifically of oxidized single wall carbon nanotubes (SWNT), multiwall carbon nanotubes (MWNT) and

nitrogen-doped carbon nanotubes (CNx), in order to compare the effect of different morphologies over intraparticle diffusion of cadmium ions.

IV. To support carbon nanotubes in a polymeric matrix in order to obtain a nanostructured adsorbent (composite) that can be used in packed columns, to conduct dynamic adsorption tests of the model metal ions through consecutive adsorption-desorption cycles.

1.5   HYPOTHESIS

A high concentration of oxygen-containing functional groups can be attached to carbon nanotubes, in consequence, these will considerably increase their adsorption capacity. These oxygenated surface groups will also enhance the dispersion of nanotubes in a polymeric matrix, which will permit the effective support of CNT into a composite. Moreover, the nanometric size of carbon nanotubes could allow fast adsorption kinetic.

1.6   STRUCTURE OF THE THESIS

This thesis is organized as follows:

Chapter 1 presents a general background about pollution of water by toxic metals, and a description of the currently used technologies in water treatment with emphasis on adsorption with activated carbon. It also contains a review of the state-of-the-art techniques of adsorption of toxic metal with carbon nanotubes.

Chapter 2 includes the evaluation of oxidized nitrogen-doped carbon nanotubes (CNx) to adsorb cadmium and lead in aqueous solution. Equilibrium adsorption as well as the comparison of the affinity of CNx toward these two metals is presented. The cadmium adsorption capacity of oxidized CNx (ox-CNx) is compared to that for commercially available activated carbon (AC) and single-wall carbon nanotubes (SWNT).

Chapter 3 presents results of cadmium adsorption kinetic on different types of carbon nanotubes: ox-CNx, ox-SWNT and ox-MWNT. Data analysis includes modeling with diffusion models and a kinetic model of pseudo-second order. The adsorption kinetic performance of carbon nanotubes is compared to that for non-porous iron oxide hydrous nanoparticles.

Chapter 4 includes the development of nanostructure composites based on carbon nanotubes and polyurethane. Breakthrough curves of three composites are discussed based on interactions between carbon nanotubes and the polymer.

Chapter 5 presents a general discussion of the results obtained in previous chapters. It also includes general conclusions of the research and perspectives for the development of nanostructured adsorbents based on carbon nanotubes for water treatment.

CHAPTER 2

Adsorption of Cadmium and Lead onto Oxidized Nitrogen-doped Multiwall Carbon Nanotubes in Aqueous Solution: Equilibrium and Kinetic

Abstract

Nitrogen-doped multiwall carbon nanotubes (CNx) were chemically oxidized and tested to adsorb cadmium and lead from aqueous solution. Physicochemical characterization of carbon nanotubes included morphological analysis, textural properties, and chemical composition. In addition the cadmium adsorption capacity of oxidized-CNx was compared to commercially available activated carbon and single wall carbon nanotubes. Carboxylic and nitro groups on the surface of oxidized CNx shifted the point of zero charge from 6.6 to 3.1, enhancing their adsorption capacity for cadmium and lead to 0.083 and 0.139 mmol/g, respectively, at pH 5 and 25 °C. Moreover, oxidized-CNx had higher selectivity for lead when both metal ions were in solution. Kinetic experiments for adsorption of cadmium showed that the equilibrium was reached at about 4 minutes. Finally, the small size, geometry and surface chemical composition of oxidized-CNx are the key factors for their higher adsorption capacity than activated carbon.

2.1   INTRODUCTION

The number and range of contaminants entering water supplies resulting from human activities have grown in the past few years, with access to clean water causing serious problems (Shannon et al., 2008). Pollution of water with toxic metals even at trace concentrations represents a severe risk for human health and other biological systems, due to the metals' resistance to biodegradation and accumulation in living tissues (World Health Organization [WHO] 2006). Adsorption is a physicochemical process often used to remove these pollutants present at trace levels in water, with activated carbon (AC) being the most commonly used adsorbent (Bansal et al., 1988; Radovic, 2001; Bansal and Goyal, 2005; Corapcioglu and Huang, 1987; Budinova et al., 1994). Modifications of AC through chemical functionalization are often made to develop their capacity for certain contaminants (Yin et al., 2007; El-Sheik, 2008).

However, it is imperative to develop new methods to treat and purify water to fit emerging regulations concerning toxic metals present in water. In order to minimize the use of chemicals and their impact on the environment, the global trend is to encourage research in developing more efficient, affordable and compact water treatment systems. It has been mentioned that many difficulties involving water quality could be resolved or greatly mitigated using nanotechnology (Weber, 2002; Savage and Diallo, 2005). Nanotechnology research is growing rapidly, and the creation and use of small size structures with novel properties could enormously contribute to improve the performance of a material (Tour, 2007).

Carbonaceous nanostructures of different forms, specifically as single- and multiple-walled carbon nanotubes are currently considered to be the key elements in nanotechnology. These are being extensively studied to take advantage of their properties in numerous fields of application (Terrones et al., 2001; Ajayan and Zhou, 2001). Specifically, SWNT and MWNT have been evaluated as adsorbents of toxic metals in water with promising results to implement in water purification systems (Srivastava et al., 2004; Yang, 2003). In early studies, several research

projects have used functionalized carbon nanotubes, mainly oxidized with strong acids such as nitric or sulfuric acid; their results showed that oxidized carbon nanotubes had better adsorption capacities than activated carbons and other sorbent materials (Li et al., 2002; 2003a; b; c; 2005; 2006; 2007; Rao et al., 2007; Stafiej and Pyrzynska, 2007; Wang et al., 2007a; b; c; Di et al., 2006; Lu et al., 2006; Kandah and Meunier, 2007; Lu and Chiu, 2006).

Recently has emerged a new generation of carbon nanostructures as nitrogen-doped carbon nanotubes (CNx) that have nitrogen atoms incorporated into the graphitic lattice (Czerw et al., 2001; Terrones et al., 2002; 2004; Nevidomskyy et al., 2003). These new structures have shown very different physical and chemical properties compared to their undoped counterparts. Nitrogen atoms lead to localized electronic states that disrupt the nanotube π-cloud, making the nanotube chemically active; these regions with a high electronic state could be utilized to introduce new types of functional groups. Consequently, a wide range of applications are expected for these CNx (Glerup et al., 2003; Xiong et al., 2005; Ewels and Glerup, 2005; Maldonado et al., 2006; Sumpter et al., 2007).

Research into the use of CNx as an adsorbent of toxic metals present in aqueous solution is still scanty (Andrade-Espinosa et al., 2008); hence, the main goal of this study lies in the oxidation of CNx to improve their performance as adsorbents of toxic metals in water, specifically for cadmium (Cd^{2+}) and lead (Pb^{2+}). This research also included the CNx affinity for these two metals and their kinetics of adsorption for cadmium. In addition, this research allowed us to compare the CNx cadmium adsorption capacity with other commercially available carbonaceous materials, such as activated carbon (AC) and single-wall carbon nanotubes (SWNT), previously treated in the same way as oxidized-CNx.

2.2 EXPERIMENTAL

2.2.1 Synthesis and Chemical Oxidation of CNx

The CNx were synthesized by chemical vapor deposition by using bencylamine as precursor and ferrocene as catalyst, in argon atmosphere in a tubular quartz reactor at 800 °C for 30 minutes (Terrones, 2004). The oxidation of CNx was carried out in a three-mouthed reactor connected to a distilling column, containing nanotubes and concentrated nitric acid (69%), at a ratio of 1 mg of CNx per mL of solution. The suspension was heated up to 80 ± 3 °C for 1 h, 3 h or 5 h. Then, the reactor was removed from the water bath and cooled down to room temperature; the nanotubes were separated from the acid solution, repeatedly washed with deionized water until achieving a neutral pH, and dried in an oven at 105 ºC for 24 hours (Andrade-Espinosa et al., 2008). Oxidized nanotubes were identified as ox-CNx-1h, ox-CNx-3h and ox-CNx-5h.

2.2.2 Characterization of Pristine and Oxidized CNx

2.2.2.1   Morphological Characterization

The structure and morphological characteristics of pristine and oxidized CNx were observed by a UHRSEM FEI XL30 field emission microscope, equipped with a STEM detector. For scanning electron microscopy (SEM), the samples were placed on a carbon film stuck to an aluminum pin holder. The microscope was operated at 12 kV. For scanning transmission electron microscopy (STEM) the microscope was operated at 15 kV and in the bright field mode; a low concentration of carbon nanotubes (0.01% wt) was dispersed in methanol by using an ultrasonic processor, and then placed onto a TEM grid.

The X-ray diffraction patterns of carbon nanotubes were recorded on a X-Ray diffractometer Bruker D8 Advance equipped with standard Cu Ka radiation (λ=0.15418 nm). The analysis were conducted at room temperature in the range from 10 to 90 2θ degrees with step size of 0.02 degrees/min. Raman spectra were

performed on an inVia Raman Renishaw system. The analysis conditions used were: 632.8 nm wavelength laser, 1% laser power, 45-60 s time exposure, and the collected range was 100-3500 cm^{-1}. The average of three measurements on each sample was reported.

2.2.2.2 Physical and Chemical Characterization

Textural properties of the pristine and oxidized carbon nanotubes were determined by nitrogen adsorption of previously dried samples at 105 °C by 24 h. The surface area and pore size distribution were calculated from nitrogen adsorption isotherms at 77 K performed in a Micromeritics ASAP 2010 surface-area analyzer. The surface area and pore volume were estimated by the BET method and the BJH method, respectively.

The chemical composition of pristine and oxidized CNx (1.5-2.0 mg) was determined by elemental analysis using an ECS CHNSO analyzer model 4010. Every sample was analyzed twice and the average was reported as content of carbon, nitrogen, hydrogen and oxygen (by difference). In addition the ash content was determined through calcinations of samples at 900 °C for 2 h.

Functional groups attached onto carbon nanotubes were identified by Fourier-transformed infrared spectroscopy by diffuse reflectance (DRIFTS) with a Perkin-Elmer FT-IR spectrophotometer. Spectra were acquired in extra-dry air atmosphere at 32 scans, from 4000 cm^{-1} to 650 cm^{-1} with a resolution of 4 cm^{-1}. Prior, samples of 0.2 to 0.5 mg of pristine and oxidized CNx were diluted in 0.1 g of KBr IR grade, Moreover, thermo-gravimetric analysis (TGA) and differential thermal analysis (DTA) were performed by a TA Instruments Q500 High resolution V6.7. Each sample (0.008-0.012 g) was placed in a platinum container and heated up from 50 °C to 1000 °C at a heating rate of 50 °C/min by using the high-resolution dynamic option with a heating rate of 4 °C/min; a 60 mL/min of nitrogen gas was used as a carrier throughout the experiment.

The surface functional groups were quantitatively measured by the Boehm's titration method (Boehm 1994) with 0.01 g of sample dispersed in 10 mL of 0.01 M solution of sodium hydroxide, and stirred in a sealed glass vessel for 48 h at 25 °C. After this period, the suspension was filtrated using a polycarbonate membrane of 0.2 μm, and obtained samples were titrated with 0.01 M hydrochloric acid. The volume required to neutralize the unreacted base was registered, and the concentration of acidic sites was calculated by the difference between the initial and final concentration of base solution.

The surface charge distribution and pH point of zero charge (pH_{PZC}) of pristine and oxidized carbon nanotubes were determined by titration. A 0.05 M sodium chloride solution (electrolyte) was prepared and degassified with nitrogen gas. Then, a series of glass vials containing 0.01 g of sample were put into contact with 10-10.25 mL of electrolyte, and the total volume was adjusted to 10.5 mL with different volumes of 0.01 M hydrochloric acid or sodium hydroxide to reach a final pH in the range of 2-10. Blank assays were prepared in the same way. The containers were stirred in an orbital shaker for 48 h at 25 °C and 80 rpm; after this period, the pH of every sample was measured.

2.2.3 Adsorption/Desorption and Selectivity of Cadmium and Lead

Analytical grades of cadmium nitrate and lead nitrate were used to prepare solutions of known initial concentration. In order to prevent the metals precipitation as determined by speciation diagrams calculated with the software visual-Minteq v.2.0, the adsorption capacity of ox-CNx-5h was determined by batch adsorption isotherms at 25 °C and with pH 5, 6 and 7 for cadmium, and pH 4 and 5 for lead in aqueous solution. As mentioned, stock solutions for each metal were prepared, and further diluted to the required concentrations. In several glass vials, 10 mL of solution were contacted with 0.01 g of ox-CNx. The vials were placed in a water bath at 25 °C for approximately 5 days, and the pH was adjusted daily by adding 0.01 M NaOH or HNO_3 until it remained constant (± 0.15). Then each solution was filtered with a polycarbonate membrane of 0.2 μm of pore diameter, and the

concentration at equilibrium was determined. Initial and equilibrium concentrations of each metal were measured by atomic absorption spectroscopy (AAS) in a Perkin Elmer AAnalyst 400, and the mass of metal adsorbed by the nanotubes was computed by a mass balance.

The adsorption capacity of the oxidized-CNx was compared to granular activated carbon Filtrasorb® 400, (GAC), from Calgon Carbon Corporation, and single wall carbon nanotubes (SWNT), Elicarb® SW from Thomas Swan. ACF-400 was milled with an agatha bead mill to reduce its particle size to about 370 μm, and then it was oxidized with concentrated nitric acid at 80 ± 3 °C for 1 h and labeled as ox-ACF. In the meantime SWNT were oxidized for 5 h and labeled as ox-SWNT.

After the adsorption equilibrium was reached, the desorption procedure was carried out. Half of the initial volume of solution in contact with the metal-loaded ox-CNx-5h, was substituted with an equal volume of acidic solution at pH 2 ± 0.1 (prepared by dilution of nitric acid in deionized water) to attain a new equilibrium for 24 h. Then, the solutions were filtered through polycarbonate membranes of 0.2 μm, and the concentration of metal was measured by AAS. The mass of metal desorbed by ox-CNx-5h was computed by a mass balance. Moreover, the selectivity of ox-CNx-5h for cadmium and lead at equimolar concentrations was determined by adsorption isotherm at pH 5; the initial concentration of both contaminants ranged from 0.1 to 0.7 mM.

2.2.4 Kinetic Experiments

The adsorption kinetic study was performed for cadmium in solution at pH 6 and room temperature (22 ±1 °C). A suspension of 0.088 g of ox-CNx in 11 mL of deionized water was prepared and shaken it until was homogeneous. Several disposable syringes of 10 mL were used to hold 9 mL of cadmium solution of a known initial concentration at pH 6. Then, 1 mL of ox-CNx suspension was added to the syringes which were sealed, and shaken at 20 rev/min from 30 s to 20 min. At a specific period in time, each syringe was removed from the shaker, and the solution was filtered through a polycarbonate membrane of 0.2 μm pore diameter,

to measure the cadmium concentration. This procedure was also carried out for ACF-400, previously powdered to a particulate size of about 370 μm.

2.3   RESULTS AND DISCUSSION

2.3.1 Synthesis of Nitrogen-doped Carbon Nanotubes (CNx) and their Oxidation by Nitric Acid

Nitrogen-doped carbon nanotubes, with bamboo-like structure, are usually strongly aggregated as depicted by Terrones et al., (2002). Nitrogen atoms could be incorporated into the graphitic lattice in two ways as pyridine-like or graphite-like sites (Czerw et al., 2001; Terrones et al., 2002; Nevidomskyy et al., 2003; Ewels and Glerup 2005; Choi et al., 2005a; van Dommele et al., 2008). The oxidation of CNx was carried out to attach acidic oxygenated groups to their surface (Ago et al., 1999; Zhang et al., 2003; Tasis et al., 2006), while the purification took place through mineralization of amorphous carbon particles. Eventually, long periods of oxidation cut off the structure of nanotubes as detailed by Zhang et al., (2003); to prevent excessive consumption of nanotubes, some physicochemical features of these were traced along oxidation time.

2.3.2 Physical and Chemical Properties of Pristine and Oxidized Carbon Nanotubes

Morphological analysis of carbon nanotubes showed the separation of bundles of nanotubes and damage to their structure after the oxidation process. Van der Waals forces that kept CNx aggregated were overcome by repulsion forces, as result of reducing the π-conjugation of nanotubes and enhancing the surface dipoles by oxygen-containing functional groups (Ago et al., 1999). Figure 2.1 presents SEM and TEM micrographs of pristine nanotubes (Fig. 2.1a-c) and of those oxidized by 5 h (Fig. 2.1d-f). The oxidation defects also occurred at the tips of nanotubes where particles of catalyst were removed (Fig. 2.1b, e); the edges of these carbon nanotubes were available for successive reactions by electrophilic attack (Zhang et al., 2003). Moreover, as the oxidation advanced, the tips of the

tubes became thinner as shown in Fig. 2.1d and e, and the nanotubes become shortened. Dimensions of about 40-80 nm in external diameter and 80 μm in length were observed for pristine CNx. After oxidation, ox-CNx-5h were 30-60 nm in external diameter and 70 μm in length.
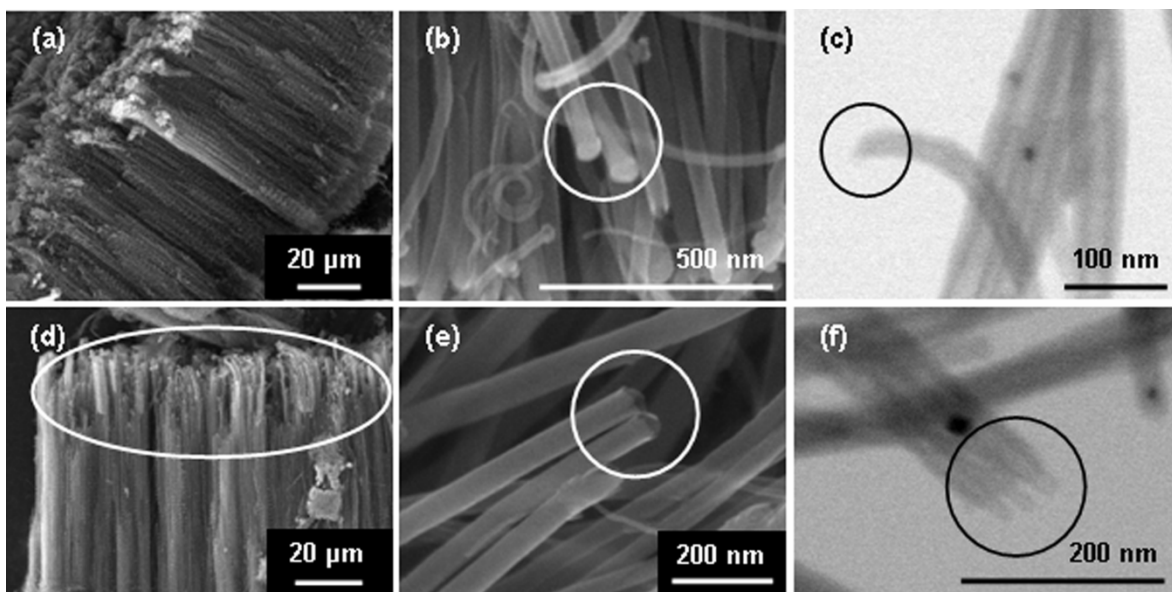
Fig. 2.1 **a,b** SEM images of pristine CNx. **c** STEM image of a tip of CNx before oxidation with nitric acid. **d, e** SEM images of nitric acid oxidized CNx by 5 h at 80 °C. **f** STEM image of the tips of nitric acid oxidized CNx by 5 h at 80 °C. The *circles* at the tips of the nanotubes show some changes due to the oxidative process.

X-Ray diffraction patterns of pristine nanotubes and ox-CNx-5h (Fig. 2.2) supported the morphological results related to the diminishing of the nanotubes outer diameter, mainly through the reflection of the (002) plane, located at 26.52° for pristine nanotubes and 26.4° for ox-CNx-5h. This peak corresponds to interlayer spacing between the graphene layers; it often has low intensity due to the corrugated hexagonal networks within the doped tubes (Zamudio et al., 2006; Peng and Liu 2006; Xiong et al., 2005). The interlayer spacing was slightly larger for ox-CNx-5h than for pristine nanotubes (d_{002} = 3.371 Å and 3.358 Å, respectively), as a result of the higher repulsive intertube force between the inner

and smaller tubes, which became exposed after the tips of the external tubes were dissolved by oxidation (Kiang et al., 1998; Ovejero et al., 2006).
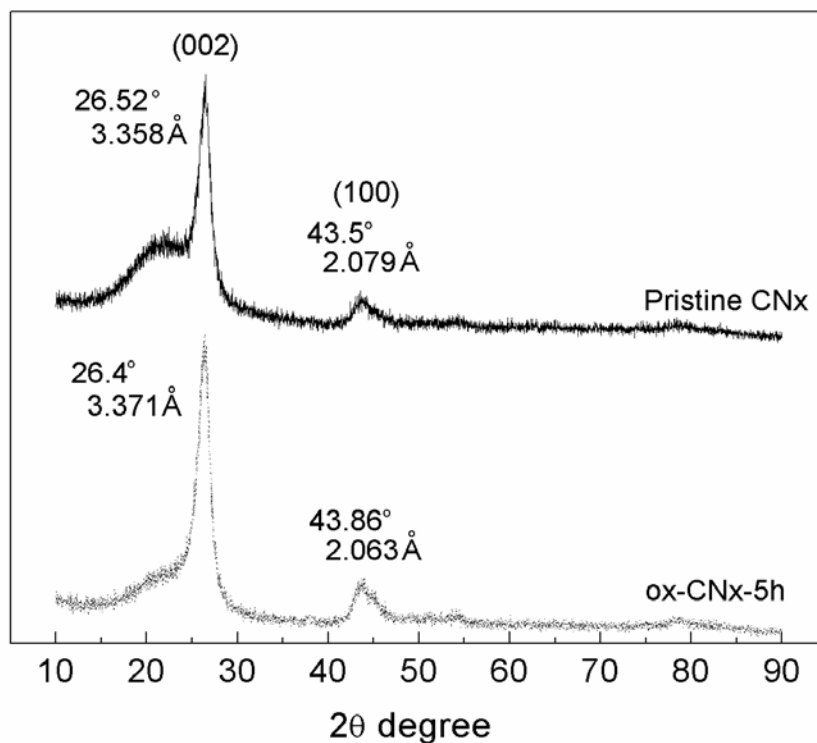
Fig. 2.2   XRD spectra for pristine CNx and nitric acid oxidized CNx by 5 h (ox-CNx-5h), at 80 ± 3°C.

Changes in morphology of oxidized carbon nanotubes were associated with their surface area and porosity, Table 2.1 presents the main results. These were similar to those reported by Andrade-Espinosa et al., (2008) for oxidized CNx, and Li et al., (2006) for pure multiwall carbon nanotubes (CNT), with values between 47-145 m^2/g for surface area and 0.18-0.54 cm^3/g for pore volume. The oxidation process led to the gradual dissolution of the catalyst located at the tips of nanotubes; thus their internal surface was unblocked and the BET surface area of the oxidized CNx by 1 h, 3 h and 5 h increased by 11, 17 and 23 m^2/g, respectively, when compared to pristine CNx. Ash analysis of carbon nanotubes revealed an iron content of 5.6±0.05 % w/w in CNx and 1.08±0.06 % w/w in ox-CNx-5h, which means that a greater part of the internal surface was accessible during and after the oxidation

process. Eventually, defects along the walls became pores that let the surface of the inner tubes available, resulting in an increase in the pore volume (Zhang et al., 2003). However, the interspace between nanotubes made the main contribution to enhance the cumulative pore volume by up to 1.65 times in ox-CNx-5h. Nitrogen adsorption isotherms (not included) depicted this effect, first observed from SEM micrographs; they had a type IV shape with hysteresis type H3 according to IUPAC classification, proper of aggregates of particles such as carbon nanotubes (Rouquerol et al., 1999). Moreover, the loops were close to the saturation pressure ($p/p0$ = 0.9) as result of a capillary condensation process in the interparticle space between the tubes (Inoue, 1998).

Table 2.1   Surface area and pore volume of micropores (d_p < 2nm)   and mesopores (2 nm < dp < 50 nm) of pristine CNx and oxidized CNx by periods of 1 h, 3 h, and 5 h, determined by nitrogen adsorption at 77 K

Sample	BET surface area (m^2/g)	BJH cumulative pores volume (cm^3/g)	BJH pore volume of micropores (cm^3/g)	BJH pore volume of mesopores (cm^3/g)
Pristine CNx	58± 2.31	0.224	0.016	0.066
ox-CNx-1h	69 ± 0.80	0.334	0.019	0.088
ox-CNx-3h	75 ± 0.78	0.351	0.017	0.088
ox-CNx-5h	81 ± 1.08	0.370	0.016	0.103

As the oxidation of carbon nanotubes was carried out in liquid phase, oxygen-containing functional groups were attached along their entire length (Ago et al., 1999; Zhang et al., 2003). Raman spectroscopy evidenced the enhancement in defects density along the walls of the carbon nanotubes when longer periods of oxidation were applied. Spectra of Fig. 2.3 show the main bands of carbon materials: the graphite band (G-band), the disorder-induced phonon mode (D-band), the second order D-band (D*-band) and some peaks related to stretch vibrations of the –CH_2 bonding (Liu et al., 2004; Choi et al., 2005b). The relative

intensity between the D-band and G-band (I_D/I_G ratio) was 1.098 for pristine nanotubes and 1.1003, 1.1287 and 1.2287 for oxidized CNx by 1 h, 3h, and 5 h, respectively. These values indicate a continuously covalent bonding of oxygenated groups along the walls of nanotubes, disrupting the aromatic system of π-electrons (Antunes et al., 2007; Zhang et al., 2004; Dyke and Tour, 2004). Furthermore, the huge overlap between bands D and G and the shoulder which was nearly 1100-1200 cm^{-1} is associated with the presence of nitrogen atoms into the graphene lattice (Maldonado et al., 2006). The overlap between bands D and G was gradually reduced while the oxidation time increased, probably as a result of the transformation of pyridine-type nitrogen and quaternary nitrogen onto the lattice of outer nanotubes and into the form of aliphatic functions (e.g. amide) (Pamula and Rouxhet, 2003).
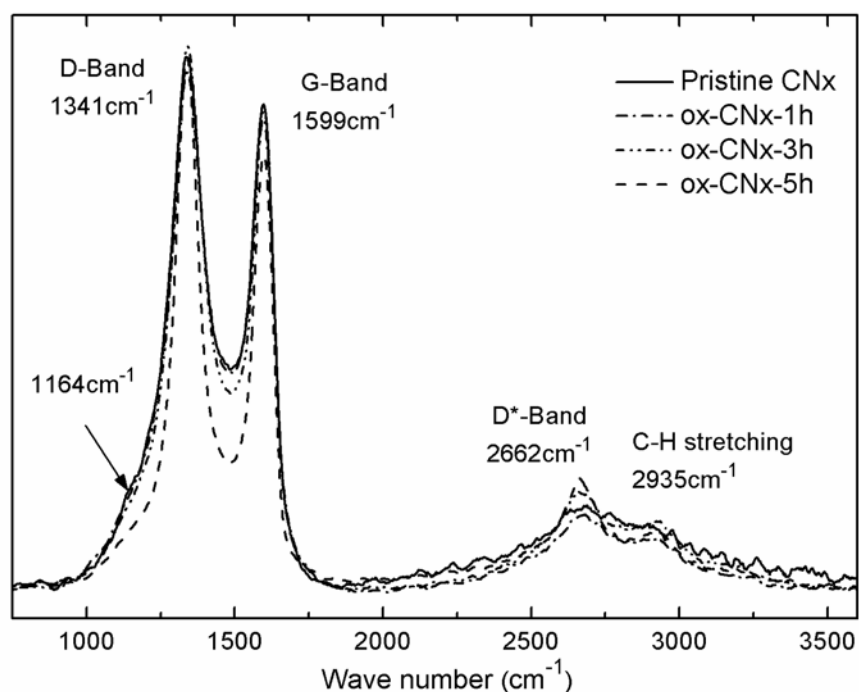
Fig. 2.3 RAMAN spectra of pristine nanotubes and nitric acid oxidized CNx for 1 h, 3 h, and 5 h at 80 ± 3 °C.

Reactions between carbon materials and nitric acid involve strong electrophilic species in solution, which form nitrogen oxides that eventually are reduced to N_2

through oxidation of carbon (Zawadski, 1980). As a result, the oxygen content increases; introduction of a small content of nitrogen has been reported, mainly due to the introduction of nitro (-NO$_2$) groups (Zawadski, 1980; Bradsher and Barker, 1964; Gomez-Serrano et al., 1997; Chen and Wu, 2004). This effect was monitored by determining the elemental composition of pristine nanotubes and partially oxidized CNx (Table 2.2). An important increment in oxygen content was registered as the carbon content was reduced, caused by the destruction of graphene lattice by electrophilic reaction (Ago et al., 1999; Zhang et al., 2003; Tasis et al., 2006; Ovejero et al., 2006; Zawadski, 1980). The hydrogen content also increased in oxidized nanotubes, maybe as a result of the introduction of carboxylic groups (Zawadski, 1980; Bradsher and Barker, 1964; Gomez-Serrano et al., 1997; Chen and Wu, 2004). However, the nitrogen content remained almost constant; because of this content, these atoms could probably change from pyridinic-type or quaternary-type to an aliphatic form (Pamula and Rouxhet, 2003). An equilibrium could be established between the consumption of nitrogen atoms of the lattice and the attachment of nitrogen atoms in some sites of the lattice as nitro groups, as occurs when oxidizing some organic molecules or activated carbons with nitric acid (Pamula and Rouxhet, 2003; Zawadski, 1980; Bradsher and Barker, 1964; Gomez-Serrano et al., 1997; Chen and Wu, 2004).

Table 2.2 Chemical composition of pristine CNx and nitric acid oxidized CNx at 80 ± 3 °C

Sample	% C	% N	% H	% O (by difference)
Pristine CNx	82.2 ± 3.36	1.3 ± 0.002	0.8 ± 0.01	15.6 ± 3.35
ox-CNx-1h	79.5 ± 1.07	1.4 ± 0.042	1.3 ± 0.27	17.8 ± 1.76
ox-CNx-3h	77.2 ± 4.26	1.4 ± 0.18	1.2 ±0.02	20.2 ± 4.30
ox-CNx-5h	73.5 ± 1.25	1.3 ± 0.35	1.4 ± 0.24	23.8 ± 1.28

The acid character of the attached groups onto the surface of nanotubes was measured by the concentration of total acidic sites (TAS) and expressed as mmol/m^2 (Table 2.3). In relation to pristine CNx, the TAS of modified CNx increased 1.8, 3.8 and 4.9 times as the oxidation time increased 1 h, 3 h, and 5 h, respectively. These values showed the same trend as those reported by Andrade-Espinosa et al., (2008), and for oxidized CNx-3h the TAS concentration was almost 20% higher for the nanotubes used in this study due to their higher length and outer diameter.

Table 2.3   Concentration of total acid sites (TAS) of pristine nanotubes and oxidized CNx for 1 h, 3 h and 5 h, determined by Boehm's titration method at 25 °C

Sample	TAS (mmol/g)	TAS (mmol/m^2)
Pristine CNx	0.208 ± 0.059	0.0036 ± 0.0010
ox-CNx–1h	0.441 ± 0.096	0.0064 ± 0.0014
ox-CNx–3h	1.022 ± 0.035	0.0136 ± 0.0005
ox-CNx–5h	1.423 ± 0.161	0.0176 ± 0.0020

The main functional group attached to oxidized carbon nanotubes was carboxylic, as identified by FTIR spectroscopy. Comparison between spectra of pristine nanotubes and oxidized CNx by 5 h (Fig. 2.4) showed that the bands at 1444 cm^{-1} (Misra et al., 2007), 1373 cm^{-1} and 1251 cm^{-1} (Choi et al., 2004), attributed to vibration of multiwall nanotubes and C-N bonding in CNx, were overcome by several vibrations in carbonyl and carboxylic functionalities in the range of 1720 to 1250 cm^{-1} (Pamula and Rouxhet, 2003; Zawadski, 1980; Gomez-Serrano et al., 1997). A strong band appeared from 3600 cm^{-1} to 3300 cm^{-1} by the stretching of the bonding -OH of carboxylic group in oxidized nanotubes (Pamula and Rouxhet, 2003; Zawadski, 1980; Gomez-Serrano et al., 1997; Chen and Wu, 2004; Coates, 2000). The nitro group (–NO$_2$) is isoelectronic with the carboxylate ion group and their spectra are very similar, but a weak feature related to nitro group was

observed at 1535 cm^{-1} for oxidized nanotubes (Zawadski, 1980; Gomez-Serrano et al., 1997; Coates, 2000).
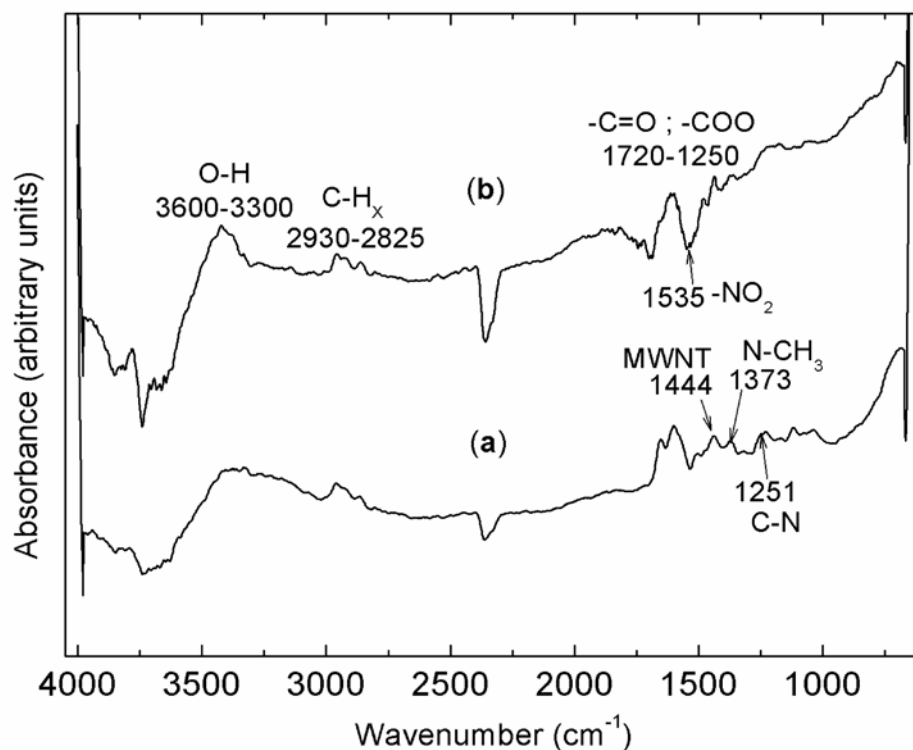
Fig. 2.4 FTIR spectra of *(a)* pristine CNx and *(b)* nitric acid oxidized CNx by 5 h at 80 ± 3°C.

Further characterization of CNx by thermal analysis (Fig. 2.5) showed that ox-CNx-5h had a higher mass loss by almost four times compared to pristine nanotubes, due to the oxygen functional groups and defects attached to the lattice (McKee and Vecchio, 2006). For pristine CNx, the most important transition occurred near 920 °C as result of decomposition of neutral or basic groups, probably as quinone groups (Bansal and Goyal, 2005). On the other hand, 5-h oxidized CNx showed more transitions: approximately 1% weight loss around 250 °C, probably due to decomposition of nitro groups (Pappas et al., 1970); a mass loss of about 22% from 300 °C to 650 °C due to carboxylic groups decomposition as CO_2 (Otake and Jenkins, 1993); a mass loss of nearly 8% in the range 750-850 °C due to phenolic and carbonyl groups decomposition as CO complexes, and above 900°C a mass

loss of nearly 3% occurred, probably due to the disintegration of neutral groups (Bansal and Goyal, 2005). Trends in the physical structure and surface chemistry of CNx along the oxidation time suggested that 5 h of treatment was the most suitable period to functionalize CNx without severe damage to their structures. Hence, the adsorption tests were carried out with 5-h oxidized CNx, labeled as ox-CNx hereafter.
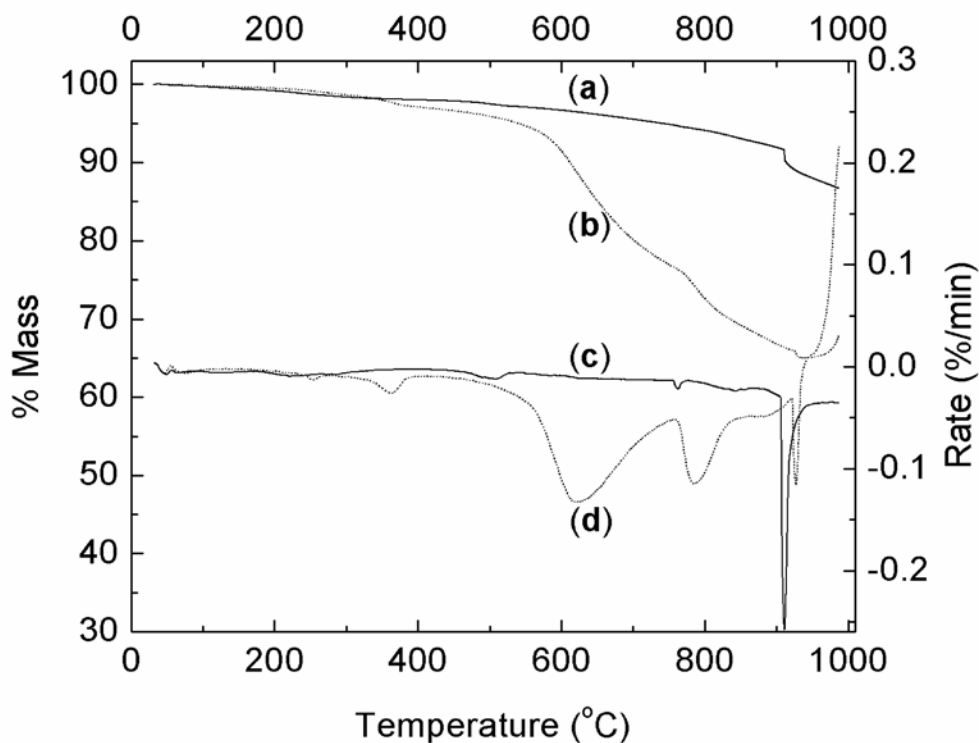
Fig. 2.5 Mass-loss profiles for *(a)* pristine nanotubes and *(b)* oxidized CNx by 5 h, heated up from 40 °C to 1000 °C under nitrogen atmosphere. Decomposition rates derived from mass-loss profiles of the same samples were included and labeled as *(c)* and *(d)*, respectively.

2.3.3 Surface Chemistry of CNx Nanotubes and their Cadmium and Lead Adsorption Capacity

The oxygen-containing surface groups attached to ox-CNx shifted the point of zero charge (pH_{PZC}) from pH 6.6 to pH 3.1 for ox-CNx, as is observed from the proton-binding curves reported in Fig. 2.6. Maldonado et al., (2006) reported a pH_{PZC} of 9 for CNx doped with 4% of nitrogen, while the value reported herein for pristine CNx is almost 2.5 units of pH lower, probably due to the lower nitrogen content (1-2%). The pH_{PZC} for ox-CNx was more than one unit of pH lower than the value reported by Andrade-Espinosa et al., (2008), which was due to a more severe oxidation of the CNx in this study.
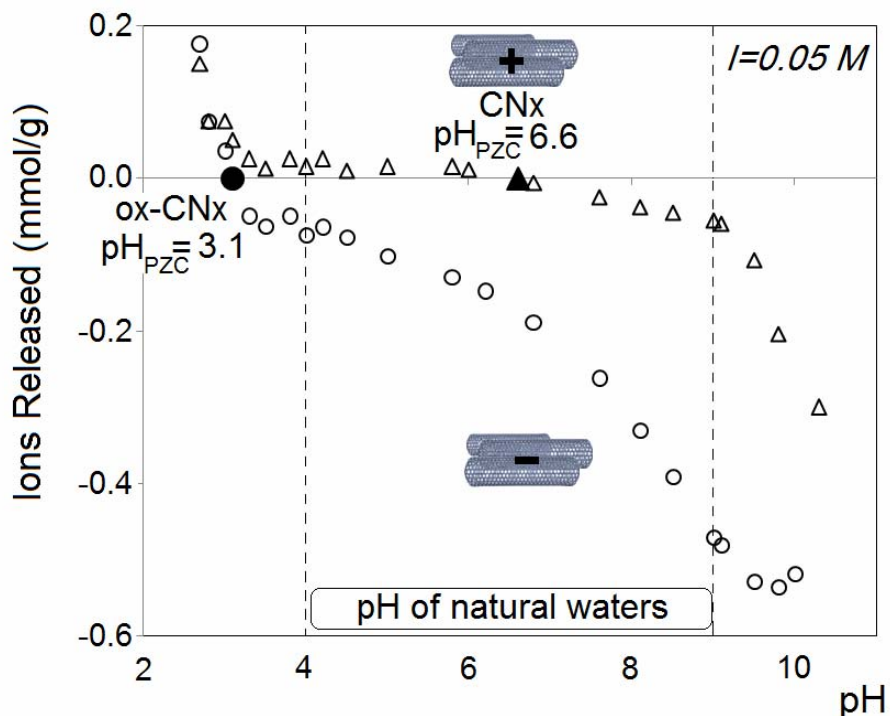
Fig. 2.6 Proton-binding curves for pristine nitrogen-doped carbon nanotubes (CNx) and oxidized nanotubes (ox-CNx) determined at 25 °C and 0.05 M ionic strength.

The low pH_{PZC} of ox-CNx means that at pH of natural waters, their surface is negatively charged and can adsorb positively charged species, such as toxic

metals. Adsorption isotherms were determined at different pH values to evaluate the capacity of ox-CNx to adsorb cadmium and lead (Fig. 2.7). The increasing adsorption capacity observed for each metal when the pH went up was related to the higher concentration of available carboxylic groups, as can be deduced from the proton-binding curve (Fig. 2.6).

Data of the adsorption isotherms of lead were correlated with Langmuir model (Fig. 2.7a); the maxima adsorption capacities (q_{max}) were 0.083 mmol/g and 0.139 mmol/g at pH values 4 and 5, respectively. Li et al., (2006) reported a q_{max} of 0.071 mmol/g for lead at pH 5 for nitric acid oxidized (140 °C by 1 h) multiwall carbon nanotubes, almost half of the ox-CNx at pH 5. The experimental data for adsorption of cadmium were better depicted by the Freundlich model (Fig. 2.7b); the values for parameter K were 0.083 mmol-L/g, 0.165 mmol-L/g and 0.192 mmol/L-g at pH 5, 6 and 7, respectively. Comparing these data with those reported by Li et al., (2003c) for nitric acid-oxidized (140 °C by 1 h) pure-carbon nanotubes, ox-CNx had 1.8 times higher cadmium adsorption capacity at pH 5. The mechanism of adsorption of cationic species in aqueous solution can occur by electrostatic interactions and formation of complexes with carboxylic groups, as was explained by Wang et al., (2007c).

In order to determine the regeneration grade of exhausted ox-CNx at each evaluated pH (4-7), desorption isotherms (not shown here) were carried out at 25 °C. The pH attained at the desorption equilibrium was between 2.4 and 2.6, and more than 90% of the mass of both adsorbed metals was desorbed, indicating that metal saturated ox-CNx can be regenerated and reutilized.

The selectivity of adsorption for lead and cadmium was evaluated with both metals in solution at pH 5 and 25 °C (Fig. 2.8). At low concentration of both metals, there is enough concentration of acidic sites for adsorption of lead and cadmium, but as the concentration of both metals in solution increased, lead was preferentially adsorbed instead of cadmium.
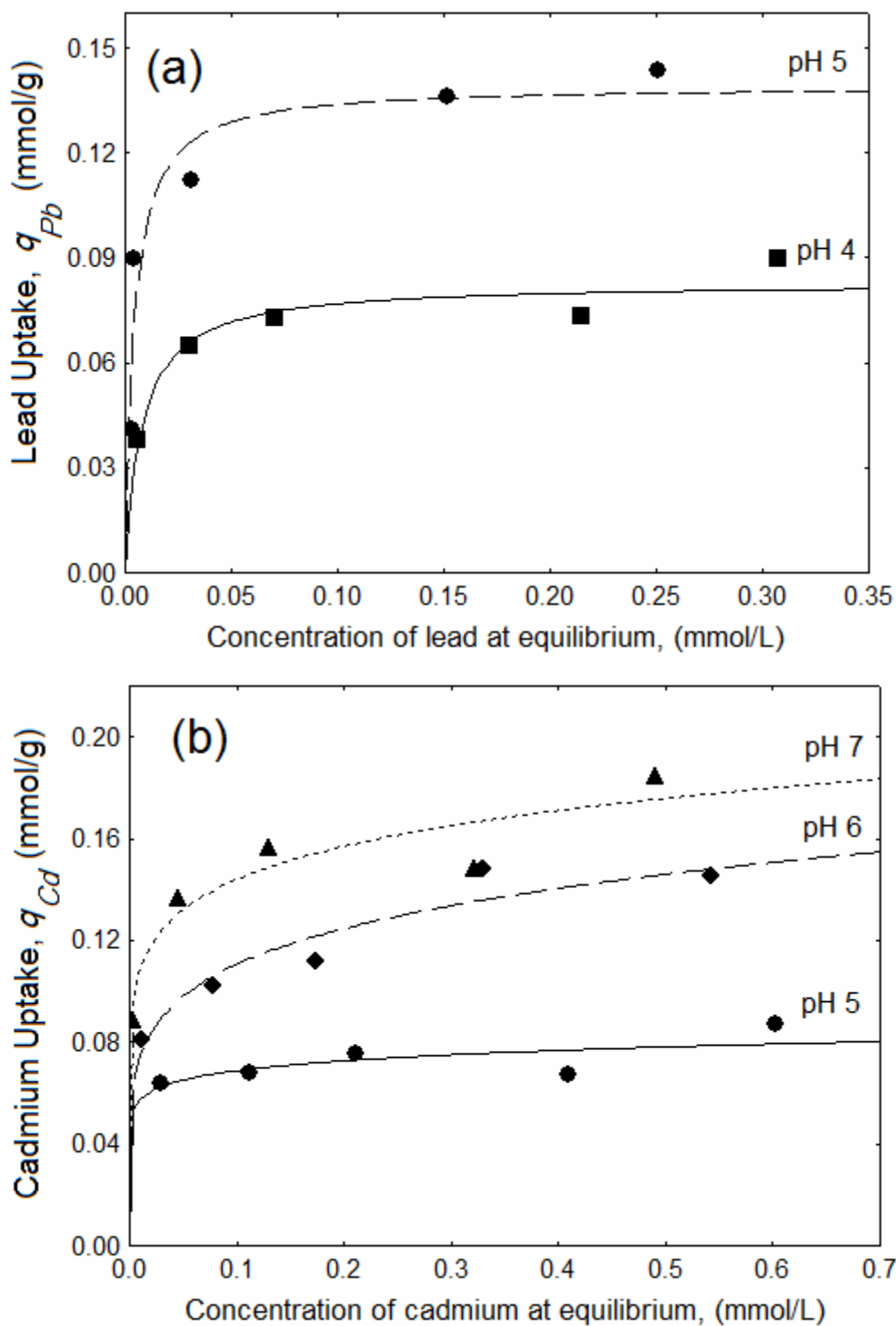
Fig. 2.7 Effect of pH on the adsorption isotherms of (**a**) lead and (**b**) cadmium onto oxidized CNx determined at 25 °C.
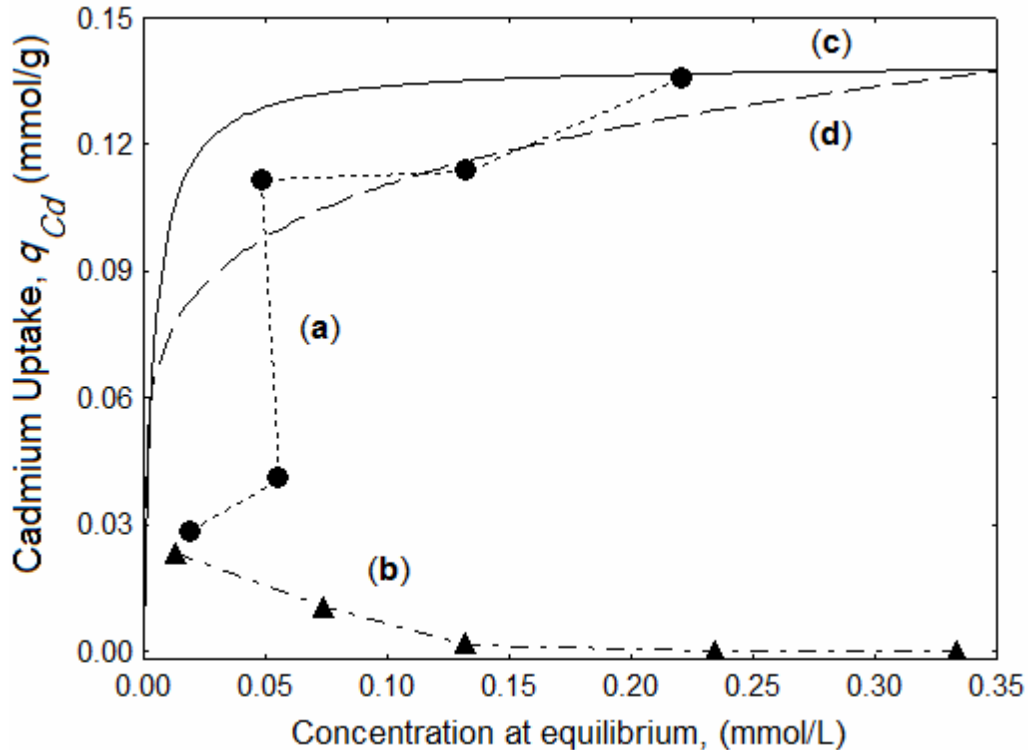
Fig. 2.8 Competition between adsorption of (**a**) lead and (**b**) cadmium onto oxidized CNx at pH 5 and 25 °C. Individual isotherms for (**c**) lead and (**d**) cadmium at pH 5 and 25° C were included.

Li et al., (2003a) reported a similar trend for competitive adsorption of cadmium and lead in solution at pH 5 for oxidized pure-carbon nanotubes. The difference in hydrated radii (r_H) between lead and cadmium is minimal: $r_{H,Pb}$= 4.01 Å, $r_{H,Cd}$= 4.26 Å (Nightingale, 1959), and thus both ions can reach the same adsorption sites mainly on the outer surface, since the interlayer spacing of ox-CNx is not wide enough (3.358 Å as measured by X-ray diffraction) to allow the intraparticle diffusion of these ions. For this reason, the dimension of these contaminants is not a decisive factor in selectivity, although is the chemistry of each ion in solution is important.

The comparison between ox-CNx, oxidized granular activated carbon Filtrasorb® 400 (ox-GAC) and oxidized single wall carbon nanotubes (ox-SWNT) for adsorption of cadmium at pH 6 and 25 °C is presented in Fig. 2.9. The geometry, morphology and chemical surface of each material determines the ease of access

46

to ions to reach the adsorption sites. The adsorption capacity of ox-SWNT was 1.3 times higher than that obtained for ox-CNx. This could be explained because of a higher availability of oxygen-containing groups on ox-SWNT, as revealed by elemental analyses (containing 43% ± 2.3% of oxygen, 0.75% ± 0.1% hydrogen and 56% ± 2.2% carbon). Also their internal and external surface area (66 ± 1 m^2/g) can be easily accessible by ions in solution, while in ox-CNx the only accessible surface area is the external and part of the internal due to their bamboo-type structure. Moreover, ox-CNx had 1.4 times higher adsorption capacity than ox-ACF, mainly due to the amount of oxygen-containing surface groups.
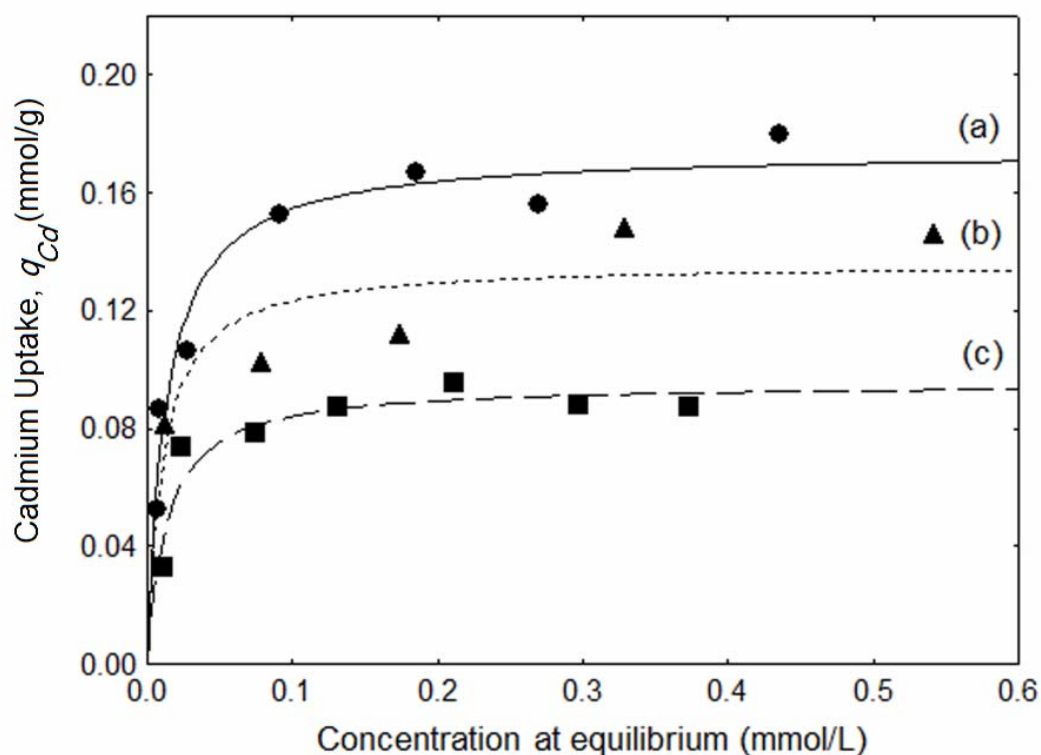
Fig. 2.9 Adsorption isotherms of cadmium in solution at pH 6 and 25 °C, on (**a**) ox-SWNT, (**b**) ox-CNx and (**c**) ox-GAC.

2.3.4 Cadmium Adsorption Kinetic onto Oxidized CNx

The kinetic properties of ox-CNx were compared to powder activated carbon Filtrasorb 400. The kinetic parameters were determined by using the Langmuir adsorption model depicted by the equation 2.1. This relation has been reported previously to calculate the kinetic parameters for organic compounds on activated carbon fiber (Brasquet et al., 1996; Brasquet and Le Cloirec, 1997; Brasquet et al., 1999):

$$\frac{dq}{dt} = K_1 C(q_m - q) - K_2 q \qquad (2.1)$$

Where Q represents the adsorption capacity (mg/g); C, the solution concentration (mg/L); K_1, the adsorption kinetic constant (L/mg-min); K_2, the desorption kinetic constant (L/min); q_m, the maximal surface concentration (mg/g); t, the time (min).

When $t \to 0$, $q \to 0$ and $C \to C_0$, and considering the mass balance, equation 2.1 can be rewritten as follows to obtain the initial kinetic coefficient (γ):

$$\gamma = K_1 q_m = -\frac{V}{C_0 m}\left(\frac{dC}{dt}\right)_{t \to 0} \qquad (2.2)$$

Where C_0 represents the initial concentration (mg/L); V, the solution volume (L); m, the adsorbent weight (g).

The differential term $(dC/dt)_{t \to 0}$ was calculated by using the cadmium concentration decay at 30 s after the beginning of the experiment. Values calculated for γ with the equation 2.2 were 0.77×10^{-3} L/mg-min and 1.45×10^{-3} L/mg-min for ACF-400 and ox-CNx, respectively. For ox-CNx, γ is 1.9 times higher than for ACF-400; thus, the adsorption rate onto ox-CNx was faster during the first 30 s compared to activated carbon, and the equilibrium was reached at about 4 min for ox-CNx (Fig. 2.10).
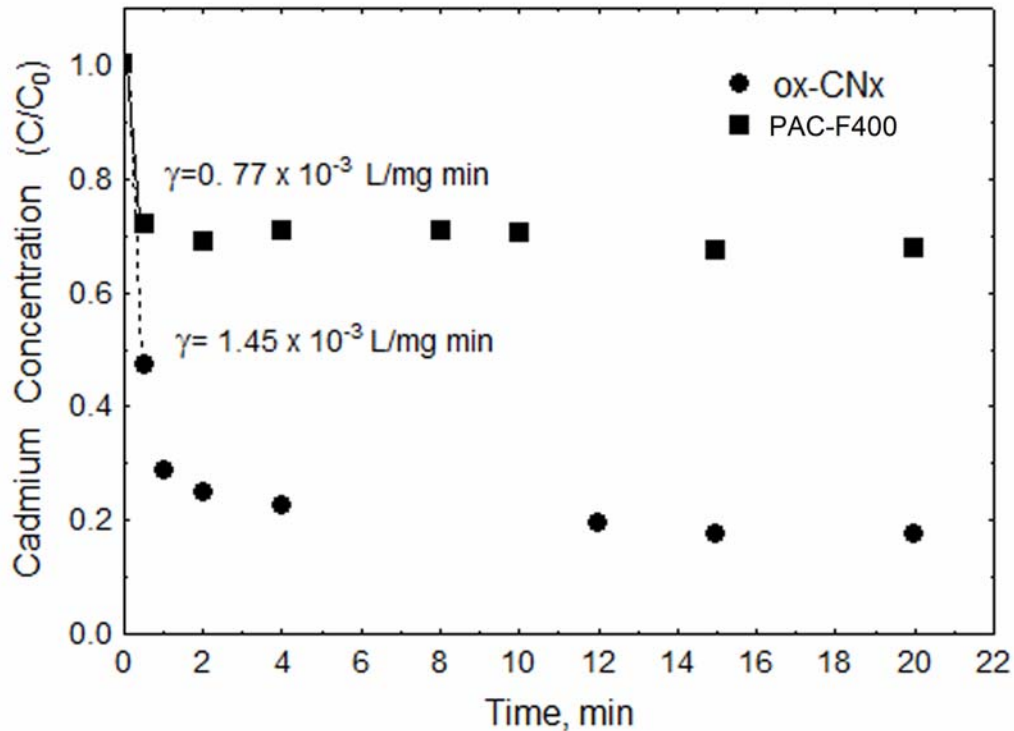
Fig. 2.10 Kinetic experiments with oxidized CNx (circles) and powder activated carbon Filtrasorb 400 (PAC-F400, squares) for cadmium in solution at pH 6 and room temperature.

Several authors have reported the kinetics of adsorption for some cations onto different adsorbents. Wang et al., (2007a) and Li et al., (2005) established that the adsorption equilibrium of lead onto acidified carbon nanotubes was achieved in the first 20 min, with a delay of almost 16 min when compared to cadmium removal on ox-CNx. Lu et al., (2006) reported the adsorption rate for zinc onto purified carbon nanotubes, the equilibrium was obtained between 3 and 5 min for SWNT and MWNT, respectively, and these values are consistent with the ones obtained in this study for cadmium onto ox-CNx. The surface available for adsorption onto ox-CNx is readily exposed to cadmium ions; thus, they do not require diffusion through mesopores and macropores, and hence, the adsorption process is much faster than in powder-activated carbon, where the solute has to diffuse through macro-, meso- and micropores to reach the active sites. This should be considered an

advantage since the use of ox-CNx into adsorption treatment systems will result in faster operative processes.

Indeed, water treatment systems based on nanotechnology, especially on carbon nanostructures, is a research topic that could offer alternatives for solving water pollution problems. For this reason, as a continuation of this study, further study is being developed by our research group to include this scope.

2.4 CONCLUSIONS

Nitric acid-oxidized CNx are highly reactive due to their concentration of acidic oxygenated groups, although their structure is damaged to some extent when they are strongly oxidized; mainly carboxylic groups on the surface of ox-CNx made this material a suitable adsorbent to remove toxic or heavy metals such as cadmium and lead in aqueous solution.

The adsorption capacity of ox-CNx for both metals is about 2 times higher than for oxidized multiwall pure-carbon nanotubes, at pH 5 and 25 °C, according to the data reported in literature. In addition, ox-CNx have higher affinity to adsorb lead than cadmium when both metals are in solution at pH 5 and 25 °C. The surface chemistry and geometry of ox-CNx are key factors for their considerable adsorption capacity; at pH 6 and 25 °C these have 1.4 times higher cadmium adsorption capacity than oxidized activated carbon (ox-GAC), whereas oxidized SWNT have 1.3 times higher adsorption capacity than oxidized CNx (ox-CNx) due to their 1.8 times higher oxygen content. Likewise, the rate of adsorption of cadmium of ox-CNx is determined by their geometry and surface chemistry, which is almost twice that found for activated carbon (PAC-F400). The above features suggest that ox-CNx could become an effective adsorbent of toxic heavy metals present in aqueous solution.

Morphology Effect of Three Different Types of Carbon Nanotubes on Cadmium Adsorption Kinetic

Abstract

Nitrogen-doped multiwall carbon nanotubes (CNx), single-wall carbon nanotubes (SWNT) and multiwall carbon nanotubes (MWNT) were oxidized and their rate to remove cadmium in aqueous solution was determined by batch adsorption kinetic experiments. Similar tests were conducted with non-porous iron oxide nanoparticles (FeOOH) to compare adsorption kinetic. Nanoparticles were mainly characterized by HRTEM, X-ray diffraction, Raman, nitrogen physical adsorption, and their cadmium adsorption isotherms were determined at pH 6. The maximum cadmium adsorption capacity (q_m) was 36.4, 11.9 and 6.4 mg/g for oxidized SWNT, CNx, and MWNT, respectively. The morphology effect on adsorption kinetic was evident in the time to reach equilibrium: about 15, 25 and 180 min. for oxidized CNx, MWNT and SWNT, respectively, and 40 min. for non-porous FeOOH, at an initial cadmium concentration of 4 mg/L and pH 6. Adsorption kinetic data were analyzed by using the pseudo-second order model, an external mass transport model and an intraparticle diffusion model. The intraparticle diffusion model best fitted the experimental data with lower deviations than 5%: the calculated diffusivity coefficients were around 4E-9, 1E-9 and 2.4E-11 cm^2/s for ox-CNx, ox-MWNT and ox-SWNT, respectively, considering individual nanotubes. The slowest equilibrium attained by ox-SWNT might result of their highest concentration of tiny sidewall pores limiting cadmium diffusion. For their adsorption performance, ox-CNx would be a cost-efficient alternative for water treatment systems based on nanotechnology.

3.1 INTRODUCTION

Advanced water treatment systems have included adsorption processes as a key step to reach quality standards of decontamination for several pollutants, activated carbon being the most commonly used adsorbent (Bansal et al., 1988; Radovic, 2001; Bansal and Goyal, 2005). Activated carbon has been used as an all-purpose adsorbent, but future applications of adsorption are limited by the availability of new and better adsorbents (Weber 2002; Yang 2003; Savage and Diallo, 2005; Li et al., 2007; Mauter and Elimelech, 2008; Shannon et al., 2008; Theron et al., 2008). Nanotechnology has made it possible to obtain new forms of carbon, such as carbon nanotubes with cylindrical shape of nanometer size diameter. Single-wall carbon nanotubes (SWNT) and multiwall carbon nanotubes (MWNT) are leading these new carbonaceous nanomaterials, and their unique properties have driven an intensive scientific research for the last two decades (Dresselhaus, 1997).

The structure of SWNT is depicted as a rolled segment of a single graphite layer, called a graphene sheet. MWNT consist of several single-wall carbon nanotubes nested from one to another by approximately 0.34 nm, the interlayer distance of graphite (Dresselhaus et al., 2001). Carbon nanotubes are mostly chemically inert, thus chemical reactions involving the formation of strong covalent or ionic bonds occur preferentially near defect sites and near the nanotube ends (Niyogi et al., 2002; Loiseau et al., 2006; Tománek et al., 2008). Substitutional doping of carbon nanotubes changes their chemical reactivity, as occurs in nitrogen-doped carbon nanotubes (CNx), where nitrogen atoms incorporated into the graphitic lattice disrupt the π cloud and lead to localized electronic states, making the nanotube chemically active. CNx exhibit bamboo-type morphology and their physical and chemical properties are very different, compared to their undoped counterparts (Terrones et al., 2002; 2008; Terrones 2003; Nevidomskyy et al., 2003; Maldonado et al., 2006; Sumpter et al., 2007; Koós et al., 2009).

Besides doping, chemical modification of carbon nanotubes with different functional groups for specific applications is a major growth area nowadays

52

(Duclaux, 2002; Hirsch, 2002; Dyke and Tour, 2004; Tasis et al., 2006; Wang et al., 2009). Attempts to explore potential adsorption applications of modified carbon nanotubes have rendered promising results; different organic and inorganic pollutants present in aqueous solution have been successfully removed. The literature reports studies about adsorption of toxic metal ions in aqueous solution, most of them with acid-oxidized SWNT and MWNT (Li et al., 2002; 2003a; b; c; 2005; 2006; Chen and Wang, 2006; Lu and Chiu, 2006; Lu et al., 2006; Kandah and Meunier, 2007; Rao et al., 2007; Stafiej and Pyrzynska, 2007; Wang et al., 2007 a; c; El-Sheik, 2008; Yang et al., 2009), except for Andrade-Espinosa et al., (2008) and Perez-Aguilar et al., (2010) who are the first to report results for oxidized CNx. Based on adsorption equilibrium experiments, most published data suggest that carbon nanotubes are promising adsorbents due to their advantages over activated carbons, such as higher adsorption capacity, shorter equilibrium time and more efficient regeneration. However, adsorption kinetic data are also required to design adsorption devices with carbon nanotubes (Yang, 2003, Savage and Diallo, 2005; Li et al., 2007; Pan and Xing, 2008).

Kinetic tests are used to determine adsorption rates. Adsorption of a metal ion on a porous material can be described by three main steps: the external mass transfer from the bulk liquid to the solid surface, followed by mass transport of adsorbate into the particle, and finally the instantaneous adsorption of the adsorbate on an active site. The second step determines the rate in porous solids adsorbents; it is referred to as intraparticle diffusion. The external mass transfer and intraparticle diffusion are characterized by a liquid "film" mass transfer coefficient (k_L) and an intraparticle diffusion coefficient (D_s) respectively. Furthermore, two main mechanisms of intraparticle diffusion are often considered: molecular diffusion in the solution in the pores (pore volume diffusion) and diffusion of the solute adsorbed onto the surface of the pores (surface diffusion); both of them can occur independently or simultaneously (Leyva-Ramos and Geankoplis, 1985; Suzuki, 1990; Cooney, 1999; Leyva Ramos et al., 2005; 2007).

Numerous studies of porous adsorbents in liquid phase have underestimated the role of mass transfer in adsorption kinetic, assuming that the rate of adsorption on an active site is the controlling step. This rate is considered to follow first and second-order reactions, and kinetic models have been used to describe rate adsorption processes (McKay and Ho, 1998; Feng-Chin et al., 2009). This is an incorrect assumption because in porous materials a great concentration of adsorption sites are inside the pores; thus intraparticle mass transport should not be neglected (Leyva-Ramos and Geankoplis, 1985).

Research regarding adsorption kinetic of carbon nanotubes is still insufficient. Carbon nanotubes are frequently considered non-porous materials due to their low specific surface and porosity, in consequence some authors only report the time to attain equilibrium in adsorption studies (Li et al., 2002; 2005; Lu and Chiu, 2006; Kandah and Meunier, 2007; Wang et al., 2007 a; Gao et al., 2009). In some cases, adsorption rate data have been analyzed with kinetic models, mainly pseudo-first order and pseudo-second order, ignoring effects of diffusion inside the pores of nanotubes (Li et al., 2003 b; Chen and Wang, 2006; Lu et al., 2006; Chen et al., 2007; Wang et al., 2007 b; Lu and Chiu, 2008; Gao et al., 2008; Kabbashi et al., 2009; Yang et al., 2009). Only a few researchers suggest that diffusion could be a rate-limiting step in the slow attainment of equilibrium (Pillay et al., 2009; Hu et al., 2009); however, properly performed experiments to evaluate kinetic parameters when using CNT have not been reported until now.

Morphology features of carbon nanotubes could play a key role in diffusion of metal ions to adsorption sites, determining the adsorption rate. The objectives of this study are to evaluate kinetic parameters for cadmium adsorption onto oxidized nitrogen-doped carbon nanotubes (ox-CNx), and to compare these results with those for oxidized SWNT (ox-SWNT) and MWNT (ox-MWNT). Data analyses include modeling of the decay concentration curves with a pseudo-second order model and diffusion models. Furthermore, adsorption kinetic with non-porous iron oxide nanoparticles were also studied, in an attempt to understand how morphology influences the overall adsorption kinetic process.

3.2   EXPERIMENTAL

3.2.1   Materials and Oxidation of Carbon Nanotubes

Nitrogen-doped carbon nanotubes were synthesized by chemical vapor deposition according to the method reported by Terrones (2004). Multiwall carbon nanotubes were synthesized in argon atmosphere in a tubular quartz reactor at 800 °C for 30 minutes, by using benzene and ferrocene as precursors. Single-wall carbon nanotubes were commercially available from Elicarb®, reference product P920; the product datasheet reported a purity of at least 70%, average diameter of 0.9-1.7 nm and 700 m^2/g average surface area. These three types of carbon nanotubes were oxidized with nitric acid solution (70%) at 80 ± 3 °C for 5 h, then washed and dried as detailed in Chapter 2 section 2.2.1. Oxidized carbon nanotubes were identified as ox-CNx, ox-MWNT and ox-SWNT.

Iron oxide nanoparticles FeOOH were commercially available from Nanostructured and Amorphous Materials Inc., product reference 7004SZ CAS#: 51274-00-1. These nanoparticles were provided in aqueous solution, and were dried and milled using an agate mortar to a particle size of 90 μm to carry out the experiments.

3.2.2   Characterization of Materials

Morphological analyses were conducted by scanning electron microscopy (SEM) by a UHRSEM FEI XL30 field emission microscope equipped with a STEM detector: operation conditions were described in Chapter 2 section 2.3.2.1. A detailed characterization of the porous structure of carbon nanotubes was carried out by high resolution transmission electron microscopy by a HRTEM FEI TECNAI F30 STWIN G2.

The solid density (ρ_s) of nanoparticles was determined by the helium displacement method using a helium pycnometer (Micromeritics Accupyc 1330). Functional groups attached to carbon nanotubes were identified by Fourier-transformed infrared spectroscopy by attenuated total reflectance (ATR-FTIR) in a Nicolet 6700 FT-IR spectrophotometer, at 1068 scans in the frequency interval of 4000 cm^{-1} to

650 cm^{-1} with resolution of 8 cm^{-1}. The surface functional groups were quantitatively measured by the Boehm's titration method (Boehm 1994) utilizing 0.03 g of sample dispersed in 30 mL of 0.01 M solution of sodium hydroxide, sodium carbonate, or sodium hydrogen carbonate. Each experiment was stirred at 150 rpm in a sealed glass vessel for 48 h at 25 °C. The slurry pH (pH$_{SP}$) was measured by using 0.03 g of sample in 10 mL of deionized water; the experiments were stirred at 150 rpm by 48 h at 25 °C. After this period of time, the pH solution of every sample was measured.

Other techniques were used to complement physical and chemical analyses such as X-ray diffraction, Raman spectra (at 514 nm wavelength laser), BET surface area and pore volume, chemical composition by elemental analyses etc., which are described in Chapter 2 section 2.3.2.

3.2.3 Adsorption Equilibrium Experiments

Analytical grade cadmium nitrate (Cd(NO$_3$)$_2$-4H$_2$O) was used to prepare solutions of known initial concentration. The adsorption capacity of carbon nanotubes and iron oxide nanoparticles was determined by adsorption isotherms at pH 6 and 25 °C, with 0.01 g of sample in 10 mL of solution, at different initial cadmium concentrations. Glass vials containing samples were placed in an incubator and stirred at 150 rpm and 25 °C for 5 days. The solution pH was adjusted daily; samples of the initial and equilibrium solutions were filtrated by polycarbonate membranes of 0.45 μm pore diameter. Cadmium concentrations were determined by atomic absorption spectroscopy (AAS).

3.2.4 Adsorption Kinetic Experiments

A standard batch-stirred tank was used for kinetic experiments (Fig.3.1). The glass adsorber vessel used had 1 L of volume, 0.1 m of internal diameter, and contained 0.5 L of cadmium solution. Four plastic baffles were evenly spaced inside the

vessel to prevent vortex formation as well as to reduce the relative motion between liquid and solid particles. A four-bladed stainless steel impeller of 5 cm of diameter and 1 cm wide, driven by a stainless steel shaft and a variable motor was used to mix the cadmium solution containing adsorbent material.
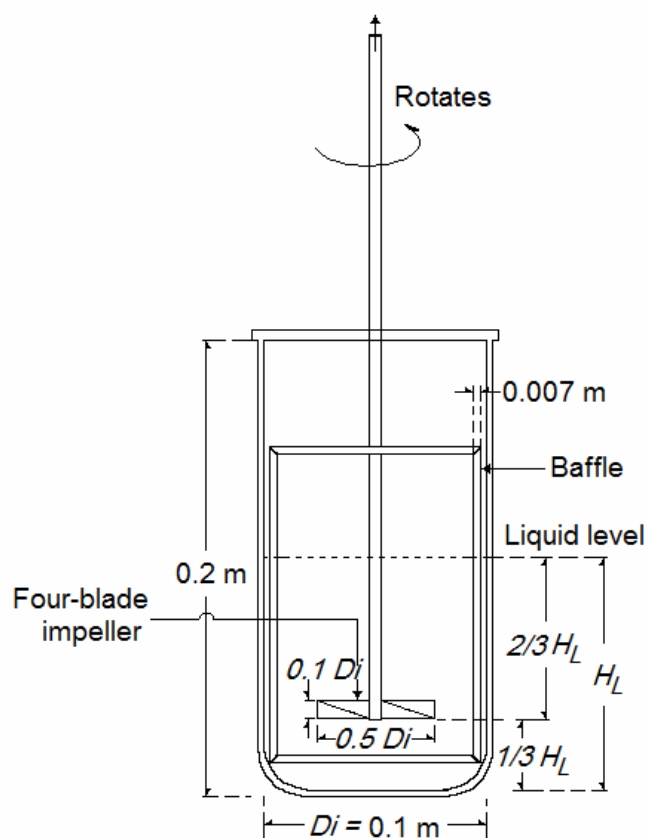
Fig. 3.1   Configuration of stirred vessel for adsorption kinetic experiments.

These experiments were conducted with 0.2 ± 0.01 g of sample at 25 ± 2 °C, 4.5 ± 0.5 mg/L of cadmium initial concentration, pH 6 ± 0.1, at 200 ± 5 rpm. In due course the effect of initial concentration of cadmium was studied by using 9 ± 1 and 18 ± 1 mg/L of cadmium. The shaking rate was increased from 200 to 250 and 300 rpm. Samples of 3 mL were taken by using a calibrated micropipette and immediately filtered with polycarbonate membranes of 0.45 µm of pore diameter. The total volume withdrawn from the vessel was less than 5%. Sampling was more frequent during the first ten minutes.

3.2.5 Modeling of Adsorption Kinetic Data

Cadmium adsorption rate on carbon nanotubes considers different mass transfer processes as illustrated in Fig.3.2. One or a combination of them can determine the overall adsorption rate.
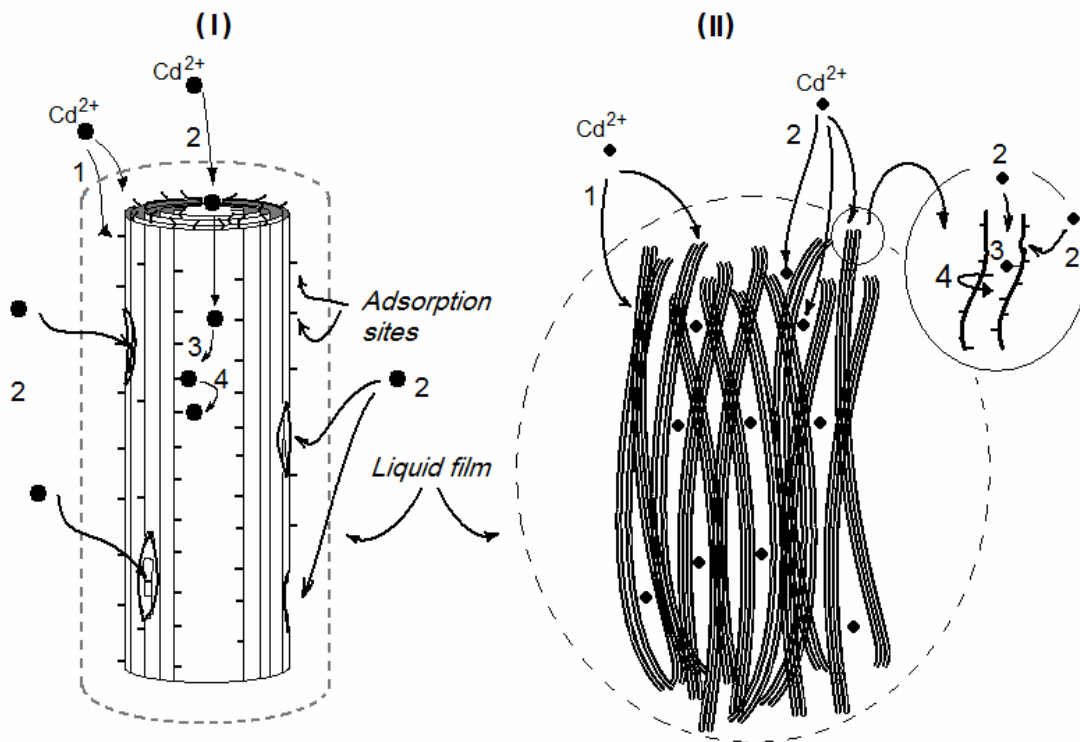
Fig. 3.2 Mass transport processes on cadmium adsorption by carbon nanotubes. (I) Adsorption on a carbon nanotube includes: (1) external mass transport, (2) pore volume diffusion through axial and/or radial direction, (3) adsorption, and (4) surface diffusion. (II) Adsorption on aggregates of carbon nanotubes, where pore volume diffusion also includes the space between nanotubes.

Kinetic tests in a finite volume batch system were conducted to determine cadmium adsorption rates onto different types of oxidized carbon nanotubes. The experimental cadmium concentration data, expressed in dimensionless form according to equation 3.1, was plotted against time to obtain the dimensionless concentration decay curve.

$$\varphi_A = \frac{C_A}{C_{A_0}}$$
(3.1)

Where:

φ_A = dimensionless concentration of cadmium in solution

C_A = Cadmium concentration in solution at time t, (mg/L)

C_{A_0}= Initial cadmium concentration in solution, (mg/L)

Experimental adsorption kinetic data were fitted by the following models:

a) Kinetic model: it was assumed that the adsorption reaction of cadmium onto the active adsorption sites was the limiting step. A pseudo-second order model was selected to compare our findings with similar results reported in the literature.

b) Film diffusion model: External mass transfer of cadmium from bulk solution through the boundary layer around a single nanoparticle was the limiting rate adsorption step, assuming a homogeneous dispersion of nanoparticles in solution and most adsorption sites locate at the outer surface of nanoparticles.

c) Intraparticle diffusion model: This model only considers pore volume diffusion as the rate limiting step. Considering cylindrical shape pore volume diffusion can occur in axial and/or radial direction. Two cases were analyzed: firstly homogeneous dispersion of single nanoparticles in the solution, assuming cadmium adsorption at the outer surface beside radial diffusion through pores created on sidewall nanotubes by chemical oxidation. In the second case, it was assumed that nanotubes in the solution formed aggregates with roughly spherical shape; hence diffusion through all available space occurred (holes or space between tubes in the aggregate besides radial diffusion through pores along sidewall of nanotubes). Both cases are depicted in Fig. 3.2.

3.2.5.1   Pseudo-second Order Kinetic Model

The generic adsorption mechanism which describes the interaction between ionic species and a carbonaceous surface is usually named adsorption pseudo-reaction. This process can be considered as a network of parallel-consecutive adsorption

reactions with the ionic species and the active sites as reagents and the adsorbed species as products (Natale et al., 2009). It was assumed that the adsorption reaction of cadmium onto an active site is the limiting rate step; which follows a pseudo-second order chemisorptions kinetic rate. This model is represented by the following equation (Blanchard et al., 1984):

$$\frac{dq_t}{dt} = k_2 \left(q_e - q_t \right)^2 \tag{3.2}$$

Where q_e and q_t are the sorption capacity at equilibrium and at time t, respectively, and k_2 is the constant rate of pseudo-second order sorption. For the boundary conditions $t=0$ to $t=t$ and $q_t=0$ to $q_t=q_t$, the integrated form of equation (3.2) becomes:

$$\frac{1}{(q_e - q_t)} = \frac{1}{q_e} + k_2 t \tag{3.3}$$

This is the integrated rate law for a pseudo-second order reaction. It can be arranged in linear form as follows:

$$\frac{t}{q_t} = \frac{1}{k_2 q_e^2} + \frac{1}{q_e} t \tag{3.4}$$

Where h can be regarded as the initial sorption rate as $q_t / t \rightarrow 0$, hence:

$$h = k_2 q_e^2 \tag{3.5}$$

Thus equation 3.5 can be written as:

$$\frac{t}{q_t} = \frac{1}{h} + \frac{1}{q_e} t \tag{3.6}$$

If pseudo-second order kinetic is applicable, the plot of t/q_t against t (from equation 3.6) should give a linear relationship: q_e, k_2 and h can be determined from the slope and intercept to the origin of the plot.

3.2.5.2   External Mass Transfer Model

The external mass transfer model considers that ionic diffusion through a stagnant film of liquid surrounding the adsorbent particle is the only controlling adsorption

process. Mass transfer through the film liquid was modeled with the rate law (Cooney 1999):

$$\frac{dq}{dt} = k_L S(C_A - C_S)$$ (3.7)

C_A is the cadmium concentration in the bulk solution, C_S is the cadmium concentration adsorbed on the surface of the adsorbent nanoparticle, S is the surface area of adsorbent nanoparticles (expressed as equations 3.8 for cylindrical nanoparticles and 3.9 for spherical nanoparticles)

$$S = \frac{4m}{d_p \rho_s (1-\varepsilon)}$$ (3.8)

$$S = \frac{6m}{d_p \rho_s (1-\varepsilon)}$$ (3.9)

Combining these expressions with equation 3.7, considering the surface area (S_V) of the adsorbent as $\frac{4m}{d_p}$ for cylindrical nanoparticles and $\frac{6m}{d_p}$ for spherical nanoparticles, the resultant equation is:

$$\frac{dq}{dt} = \frac{k_L S_V (C_{Ai} - C_{Si})}{\rho_s (1-\varepsilon)}$$ (3.10)

Where:

C_{Ai} = bulk cadmium concentration at time i (g/cm^3)

C_{Si} = cadmium concentration on the surface of the adsorbent nanoparticle at time i (g/cm^3)

q_i = average mass of cadmium per mass of adsorbent nanoparticle at time i

dt = time difference (s)

C_{Si} is calculated from the Langmuir isotherm with equation 3.11 and C_{Ai} is calculated from the mass balance with equation 3.12:

$$C_s = \frac{q}{b}\left(\frac{1}{q_m - q}\right)$$ (3.11)

$$C_A = C_0 - \frac{m}{V} q$$ (3.12)

Equations 3.10 to 3.12 were solved numerically by the PDESOL v.2.0 software to determine the mass transfer coefficient (k_L) that best fits the experimental data.

3.2.5.3   Intraparticle Diffusion Model

The adsorption rate of cadmium in aqueous solution onto carbon nanotubes and iron oxide nanoparticles was analyzed with an intraparticle diffusion model, considering pore volume diffusion. The model was derived by mass balances of cadmium in the liquid solution and in the nanoparticles surface. The mass balance for cadmium in solution is represented by equation 3.13: the left side accounts for the cadmium concentration decay in solution, and the right side represents the mass transport of cadmium from the bulk solution to the outer surface of the nanoparticle. The initial condition is given by equation 3.14 (Leyva-Ramos et al., 2007; Leyva-Ramos and Geankoplis, 1985).

$$V\frac{dC_A}{dt} = -mSk_L\left(C_A - C_{A,R}\right) \tag{3.13}$$

$$t = 0, \quad C_A = C_{A0} \tag{3.14}$$

In equation 3.14, S represents the external surface per unit mass of nanoparticles; it was calculated with equation 3.8 for carbon nanotubes (cylindrical) or with equation 3.9 for iron oxide nanoparticles (spherical), previously described in section 3.3.5.2:

The mass balance for cadmium adsorption on a differential element of the adsorbent is expressed by equation 3.15 for nanotubes, considering radial diffusion, and by equation 3.16 for iron oxide nanoparticles. The initial and boundary conditions are given by equations 3.17 to 3.19.

$$\varepsilon_p\frac{\partial C_{A,r}}{\partial t} + \rho_p\frac{\partial q}{\partial t} = \frac{1}{r}\frac{\partial}{\partial r}\left[r\left(D_{e,p}\frac{\partial C_{A,r}}{\partial r}\right)\right] \tag{3.15}$$

$$\varepsilon_p\frac{\partial C_{A,r}}{\partial t} + \rho_p\frac{\partial q}{\partial t} = \frac{1}{r^2}\frac{\partial}{\partial r}\left[r^2\left(D_{e,p}\frac{\partial C_{A,r}}{\partial r}\right)\right] \tag{3.16}$$

$$C_{A,r} = 0 \quad t = 0, \quad 0 \leq r \leq R \tag{3.17}$$

$$\left.\frac{\partial C_{A,r}}{\partial r}\right|_{r=0} = 0 \tag{3.18}$$

$$D_{e,p} \left. \frac{\partial C_{A,r}}{\partial r} \right|_{r=R} = k_L \left(C_A - C_{A,R} \right) \tag{3.19}$$

The apparent density (ρ_p) and the void fraction of porosity (ε_p) of the adsorbent nanoparticles were estimated with the following equations:

$$\rho_p = \frac{\rho_s}{1 + V_\rho \rho_s} \tag{3.20}$$

$$\varepsilon_p = \frac{V_\rho}{V_\rho + \frac{1}{\rho_s}} \tag{3.21}$$

It was assumed that cadmium in solution inside the pores ($C_{A,r}$) was in equilibrium with that on the pores surface (q) because the adsorption occurs instantaneously at an active site. This equilibrium relationship can be represented with the adsorption isotherm model by using the Langmuir isotherm for all cases:

$$q = \frac{q_m K C}{1 + K C} \tag{3.22}$$

Equations of this model were solved numerically by using the PDESOL v.2.0 software. The effective pore volume diffusivity, $D_{e,p}$, was evaluated by matching the experimental concentration decay data with the predicted concentration decay from the model. The value of $D_{e,p}$ that best fits the experimental data, according to the following objective function, is considered the effective pore volume diffusivity coefficient:

$$\sum \left(\varnothing_{exp} - \varnothing_{pred} \right)^2 \tag{3.23}$$

3.3 RESULTS AND DISCUSSION

3.3.1 Chemical Modification and Physicochemical Characterization of Carbon Nanotubes and Iron Oxide Nanoparticles

Bundles of aligned pristine multiwall carbon nanotubes (MWNT and CNx) were kept close together by Van der Waals forces (Fig.3.3a). On the other side, SWNT were agglomerated forming entangled nets of nanotubes (Fig.3.3b). These agglomerates were almost spherical with a wide distribution of diameters in the

range of 1 to 100 μm. According to literature, SWNT are grouped in 2D nanocrystals with 10 to 100 aligned nanotubes and separated by a distance of approximately 3.354 Å (Dresselhaus et al., 2001). Carbon nanotubes in bundles were exfoliated after nitric acid oxidation (Fig.3.3c) because the attached oxygen functional groups had surface repulsion forces between dipoles. In consequence, the π-conjugation of the graphene sheet was reduced overcoming the Van der Waals forces (Ago et al., 1999).

Proximal dimensions of 500 μm in length and 60 to 90 nm of external diameter were observed for oxidized MWNT (ox-MWNT), while oxidized CNx (ox-CNx) were 70 to 80 μm in length and 40 to 60 nm of external diameter. The length of a single oxidized SWNT (ox-SWNT) was impossible to determine because it was difficult to observe both end caps; their external diameter was in the range of 1 to 3 nm.

Additional effects of nitric acid oxidation were the dissolution of amorphous carbon and catalyst particles, the erosion of the tips in ox-CNx (Fig.3.3d), the mechanical distortion of the most internal cylindrical planes in ox-MWNT (Fig.3.3e), probably as a result of decreasing the cohesive energy of the tubes yielding to their partial destruction (Duclaux, 2002), as well as pore creation along the sidewall of carbon nanotubes. For the case of FeOOH, these nanoparticles formed irregular agglomerates with diameters in a wide range from 1 to 10 μm (Fig.3.3f).

The morphological features and changes observed for nitric acid oxidized carbon nanotubes have been previously reported by several authors, who suggest that defects like pentagons, heptagons, vacancies or dopant atoms (as nitrogen), located mainly at the tips and sidewalls, are the most reactive sites to attach oxygen functional groups to the nanotube structures (Ago et al.,1999; Hirsch, 2002; Ovejero et al., 2006; Tasis et al., 2006). These covalently bonded atoms pull the reactive C atom out of the base plane, reducing the curvature strain of nanotubes and creating holes and pores. Prolonged periods of oxidation lead to the shortening and destruction of the nanotubes (Hirsch, 2002; Niyogi et al., 2002; Zhang et al., 2003).
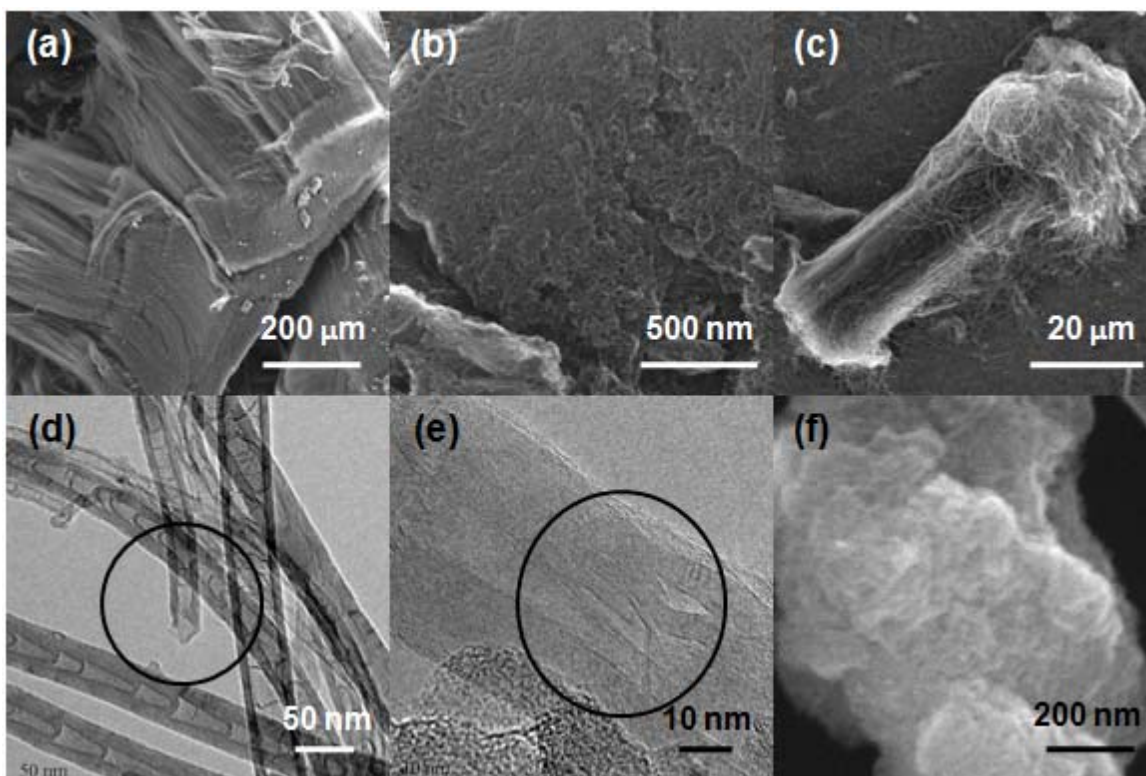
Fig. 3.3 SEM images of used nanoparticles in adsorption kinetic experiments. (a) Bundles of pristine aligned multiwall carbon nanotubes, (b) entangled ropes of single-wall carbon nanotubes; (c) exfoliated bundles of oxidized nitrogen-doped carbon nanotubes; (d) catalyst free and eroded tip of an oxidized nitrogen-doped carbon nanotube; (e) partial destruction of an oxidized multiwall carbon nanotube; (f) agglomerate of iron oxide nanoparticles.

The surface defects besides the oxygen-containing groups attached to nanotubes can be viewed as intercalated species in the lattice, as occurs in graphite intercalation compounds (GIC), where entire planes of atoms or molecules can be hosted between the carbon layers (Dresselhaus et al., 2001; Duclaux, 2002; Niyogi et al., 2002). Intercalated species on nanotubes lead to expansion of their interplanar as well as their inter-nanotube spacing that can be measured by X-ray diffraction (XRD) (Lambin et al., 2006; Kondratyuk and Yates, 2007).

Comparison of XRD-pattern diffraction showed the expansion of space between graphene layers, after pristine nanotubes were oxidized. Changes in the interplanar distance are registered in Table 3.1 and showed in Fig. 3.4.

Table 3.1 Spacing between graphene layers in carbon nanotubes determined by X-ray diffraction

	Interlayer distance, d (nm)		
	Pristine nanotubes	*Oxidized nanotubes*	*Cadmium exhausted oxidized nanotubes*
SWNT	0.3440	0.3550	0.3528
MWNT	0.3334	0.3394	0.3373
CNx	0.3406	0.3448	0.3345
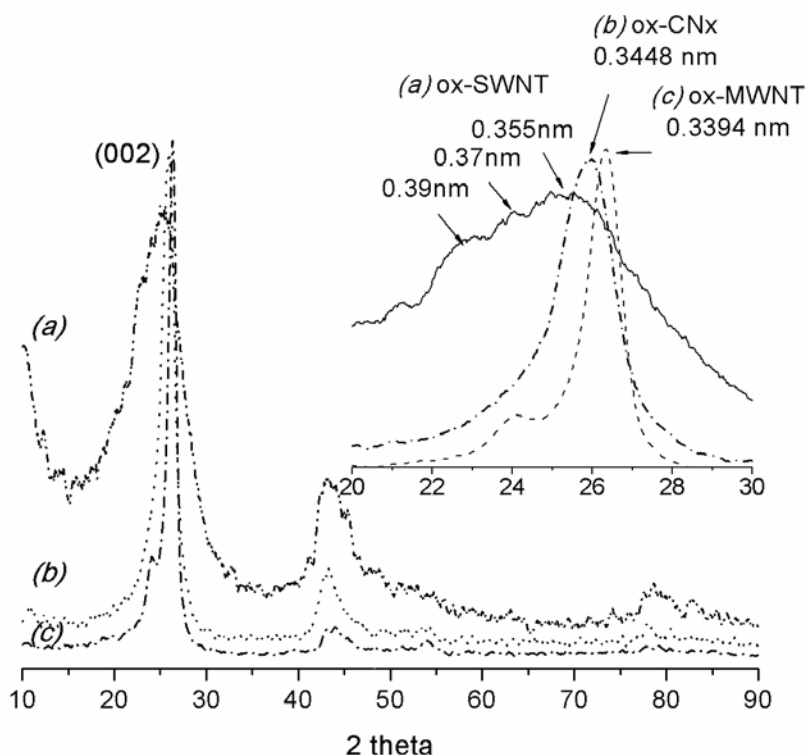
Fig. 3.4   XRD patterns show the interlayer spacing between graphene layers for oxidized carbon nanotubes: (a) single-wall nanotubes, ox-SWNT, (b) nitrogen-doped nanotubes, ox-CNx, and (c) multiwall nanotubes, ox-MWNT.

The interlayer spacing observed for ox-SWNT followed a wide distribution with a maximum value near to 0.355 nm, followed by ox-CNx with 0.3448 nm and ox-MWNT with 0.3394 nm. In similar form Duclaux (2002) reported the expansion of the inter-nanotube spacing of SWNT after being immersed in nitric acid (70%) for 2 h, due to insertion of NO_3^- ions (crystal size diameter of 0.269 nm) in the interstitial sites, following the exfoliation of nanotubes after prolonged exposition. The same author also reported intercalation of ionic species between the graphite shells of nitric acid oxidized MWNT; at oxidation periods longer than 12 h, these ions induced the mechanical distortion and/or partial or complete destruction of the cylindrical planes (Duclaux, 2002), in agreement with micrographs reported herein for ox-MWNT.
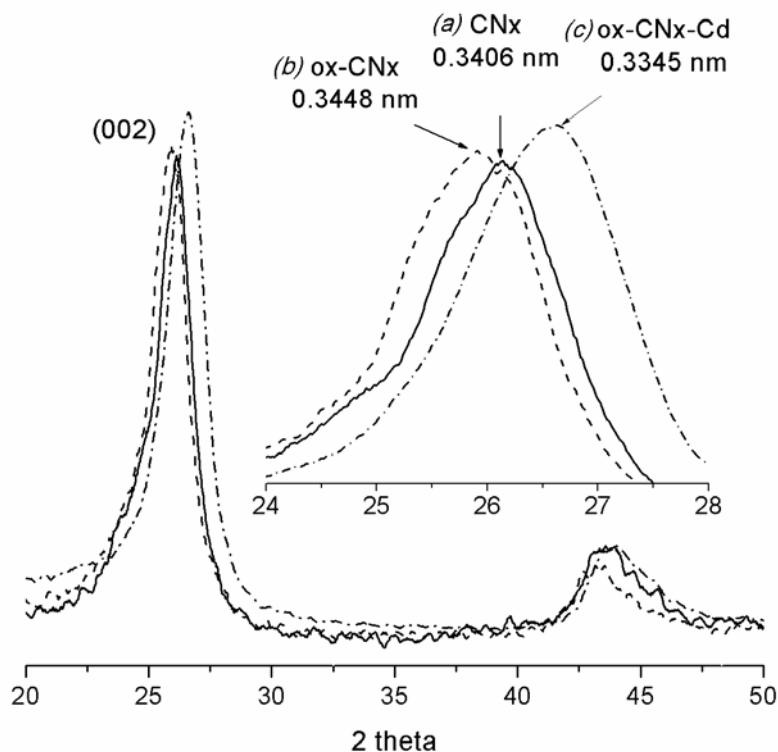
Fig. 3.5 XRD patterns show shifting of the plane (002) corresponding to the interlayer spacing between graphene layers, for (a) pristine nitrogen-doped carbon nanotubes, CNx, (b) oxidized nitrogen-doped carbon nanotubes, ox-CNx, and (c) cadmium exhausted ox-CNx.

Furthermore, the interlayer spacing showed a contraction after oxidized nanotubes adsorbed cadmium. The contraction of interlayer spacing in cadmium exhausted oxidized nanotubes could result by the reduction of the repulsive forces between negative dipoles of oxygen functional groups, after these were occupied by positively charged cadmium ions. All cadmium-exhausted nanotube samples showed similar patterns to those presented in Fig. 3.5, corresponding to ox-CNx.

XRD pattern of iron oxide nanoparticles showed a highly crystalline structure corresponding mainly to hematite (89-0597 JCPDS). A second phase was lepidocrocite (03-0079 JCPDS) an instable hydrated iron oxide that oxidizes to iron oxide in air atmosphere.
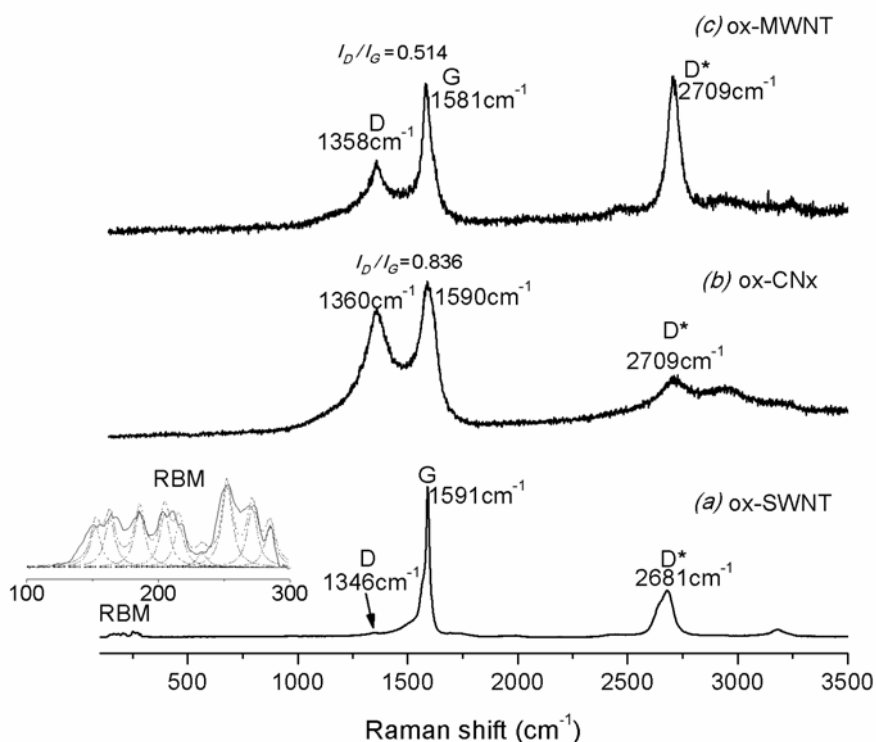
Fig. 3.6 RAMAN spectra obtained with 514 nm laser line, for oxidized carbon nanotubes: (a) single-wall nanotubes, ox-SWNT, (b) nitrogen-doped nanotubes, ox-CNx, and (c) multiwall nanotubes, ox-MWNT.

Raman spectra obtained at 514 nm (Fig. 3.6) showed the graphite band (G-band) from 1580 to 1590 cm^{-1}, the disorder band (D-band) from 1340 to 1360 cm^{-1}, the

second order D-band (D*-band) from 2680 to 2700 cm^{-1} (Liu et al., 2004), and the characteristic radial breathing mode (RBM) associated to the diameter of SWNT in the range of 130 to 280 cm^{-1}. Analyses of RBM by Lorentzian curves indicate diameters of ox-SWNT of 0.9 to 1.5 nm, which is in agreement with values, 1 to 3 nm, reported in the literature (Kim et al., 2008; Dresselhaus et al., 2001).

The relative intensity between D and G bands (I_D/I_G ratio) is sensitive to the defect density in multiwall carbon nanotubes (Antunes et al., 2007; Zhang et al., 2004). An increase of I_D/I_G ratio from 0.365 to 0.514 and 0.769 to 0.836 was determined for ox-MWNT and ox-CNx, respectively, in relation to pristine nanotubes.

The morphology of oxidized carbon nanotubes was associated with their surface area and pore volume, determined by nitrogen adsorption. Thus, long entangled ox-SWNT had the highest BET surface area and DFT pore volume, 812 m^2/g and 0.532 cm^3/g, respectively, followed by ox-CNx with 74 m^2/g and 0.29 cm^3/g, and ox-MWNT with 38 m^2/g and 0.07 cm^3/g. Non-porous features of iron oxide nanoparticles were evident by their lowest value of surface area (1.13 m^2/g) and pore volume (0.0021 cm^3/g). The surface area and pore volume of ox-MWNT reported herein are lower than those values reported in the literature, ranging from 60 to 300 m^2/g and 0.25 to 0.45 cm^3/g, respectively (Lu et al., 2006; Gao et al., 2008; Lu and Chiu, 2008; Gao et al., 2009; Hu et al., 2009). Meanwhile the surface area and pore volume of ox-SWNT were higher than those obtained by Lu et al., (2006); 420 cm^2/g and 0.43 cm^3/g, respectively.

In addition, a wide polidispersity was observed for oxidized multiwall nanotubes (Fig.3.7), showing maximum pore size diameters around 120 and 150 nm for ox-MWNT and ox-CNx, respectively. That means that mesopores between nanotube agglomerates were more significant than their internal tubular cavity, with a proximal diameter of nearly 10 nm as was observed by micrographs. Furthermore, the hysteresis loop of the nitrogen adsorption isotherms for ox-CNx and ox-MWNT was type H3 according to the IUPAC classification, proper of aggregates of particles containing slit-shaped pores. For the case of ox-SWNT, their entanglement offered an open network of mesopores with a narrow pore size

distribution from 3 to 10 nm. Also, their hysteresis loop type H2 suggested a more complex pore structure, with interconnected networks of pores of different size and shape (Rouquerol et al., 1999). For the case of iron oxide nanoparticles, a hysteresis loop type H3 suggested their agglomeration; a wide polidispersity was also observed with a maximum pore size diameter of about 120 nm.
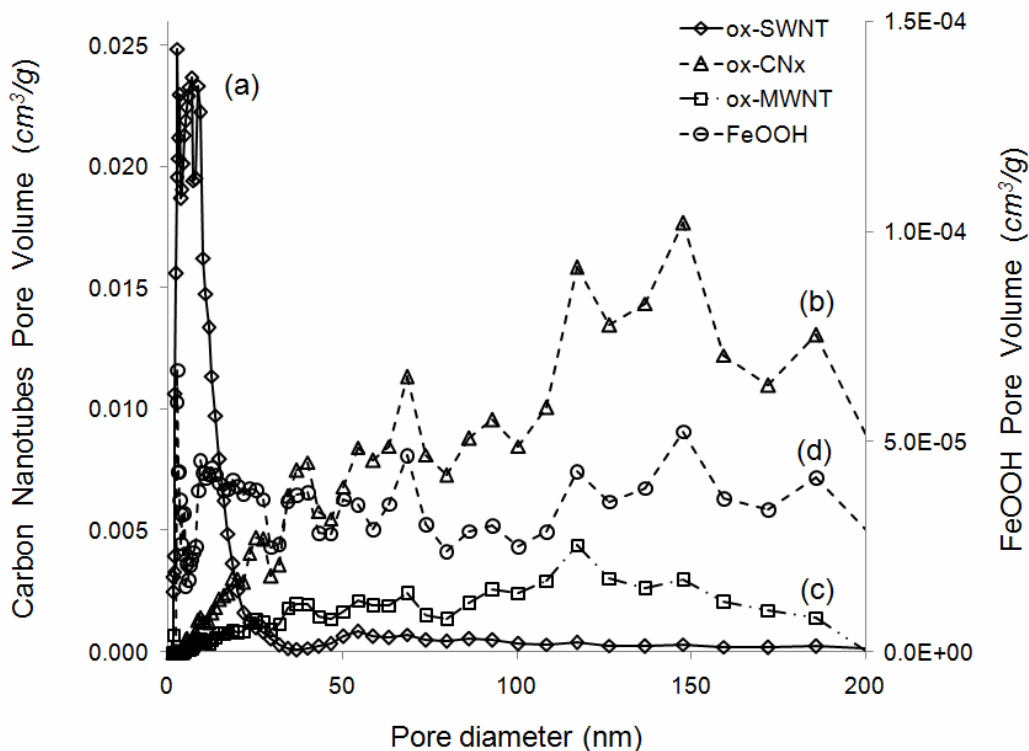
Fig. 3.7 Pore size distribution of (a) ox-SWNT; (b) ox-CNx; (c) ox-MWNT; and (d) iron oxide nanoparticles.

Chemical characterization of oxidized carbon nanotubes by elemental analyses showed an important increment in oxygen content as the carbon content was reduced, the hydrogen content was also increased probably as result of carboxylic group attachment, while the nitrogen content remained almost constant in ox-CNx. Iron catalyst particles remained as ash after sample decomposition. Table 3.2 shows that the oxygen content in ox-SWNT was 2.3 and 1.1 times higher than in ox-CNx and ox-MWNT, respectively, while oxygen in ox-MWNT was 2 times higher

than in ox-CNx. The hydrogen content in CNx was 5 and 6.5 times higher than in ox-SWNT and ox-MWNT, respectively, and the nitrogen content was 10 times higher in ox-CNx than in ox-SWNT and ox-MWNT.

Table 3.2 Chemical composition of nitric acid oxidized carbon nanotubes

	% C	% N	% H	% Ash	% O (by difference)
ox-SWNT	47.1 ± 8	0.1 ± 0.01	1.8 ± 0.6	2.7	47.4 ± 7.1
ox-MWNT	53.5 ± 5	0.1 ± 0.01	1.4 ± 1.0	2.8	42.3 ± 6.1
ox-CNx	66.7 ± 7	1.0 ± 0.1	9.1 ± 0.2	2.4	20.8 ± 7.2

Differences between oxidation degree observed for carbon nanotubes could be related to their diameter and morphology: ox-SWNT had the highest oxygen content but smallest diameter and highest curvature, which enhanced pyramidalization of sp^2 carbon framework and their reactivity to overcome geometry strain through addition reactions (Hirsch 2002; Niyogi et al., 2002). On the other side, ox-MWNT had two times higher oxygen content than ox-CNx. Probably bamboo-type morphology of ox-CNx may determine a low attachment of oxygen-containing groups inside their tubular spacing, in contrast to continuous tubular spacing in ox-MWNT.

Under nitric acid oxidation, bonds of carbon nanotubes could follow several reactions, for example the formation of quinones which further evolve to different oxygen acidic groups, such as phenolic, lactonic and carboxylic groups. The attached oxygenated groups change the surface chemistry of carbon nanotubes, in particular their wetting and adsorption behavior (Niyogi et al., 2002; B'eguin et al., 2006). The acid character and identity of the surface-attached groups were measured for oxidized carbon nanotubes and iron oxide nanoparticles by titration of total acidic sites (TAS): the obtained values of 0.972, 0.246, 0.155 and 0.109 mmol/g followed the trend ox-SWNT > ox-CNx > ox-MWNT > FeOOH,

respectively. The highest TAS concentration observed for ox-SWNT was in agreement with the oxygen content reported in the Table 3.2. However, in opposition to oxygen content, TAS concentration was 37% lower in ox-MWNT than in ox-CNx, probably due to a higher concentration of neutral quinone groups in ox-MWNT (Niyogi et al., 2002). Further characterization of attached acidic sites (Fig. 3.8) indicated that ox-CNx had 2.7 times higher concentration of carboxylic groups than in ox-MWNT, in agreement with higher hydrogen content for ox-CNx reported in the Table 3.2. Furthermore, ox-MWNT had almost two times higher concentration of phenolic and lactonic groups than ox-CNx.
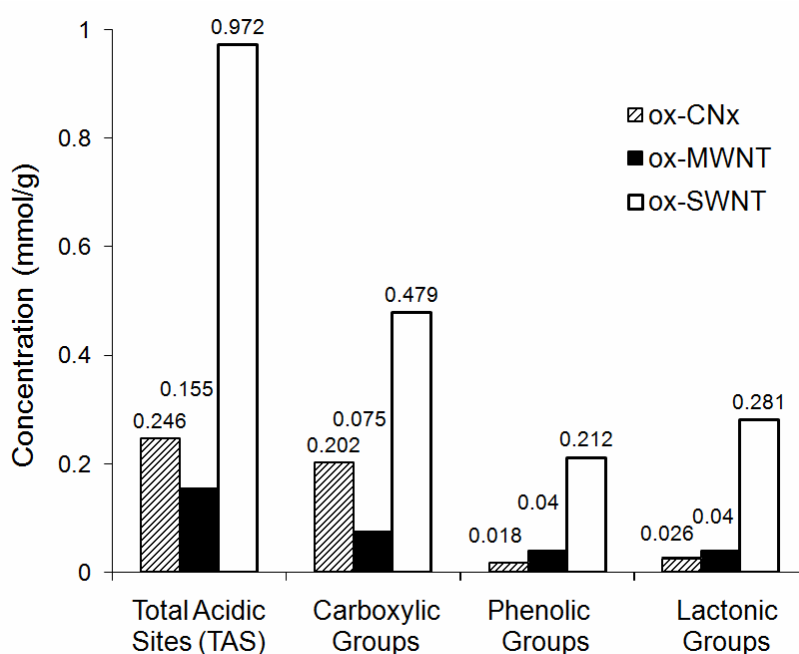
Fig. 3.8 Oxygen acidic groups reported as total acidic sites (TAS), carboxylic, phenolic and lactonic groups attached onto oxidized carbon nanotubes, determined by titration.

The slurry pH which is related to the concentration of acidic surface functional groups was 4.0, 4.6 and 5.3, for ox-SWNT, ox-CNx, and ox-MWNT respectively. These values were comparable to those reported previously, ranging from 3 to 7 for oxidized MWNT (Chen et al., 2007; Gao et al., 2009; Hu et al., 2009; Pillay et al., 2009). Moreover, the slurry pH of FeOOH was 5.6; it was lower than the

reported value of 7.8, for a sorbent based on hydrated iron oxide (Zeng et al., 2008) and iron oxide nanoparticles (Baalousha, 2009).
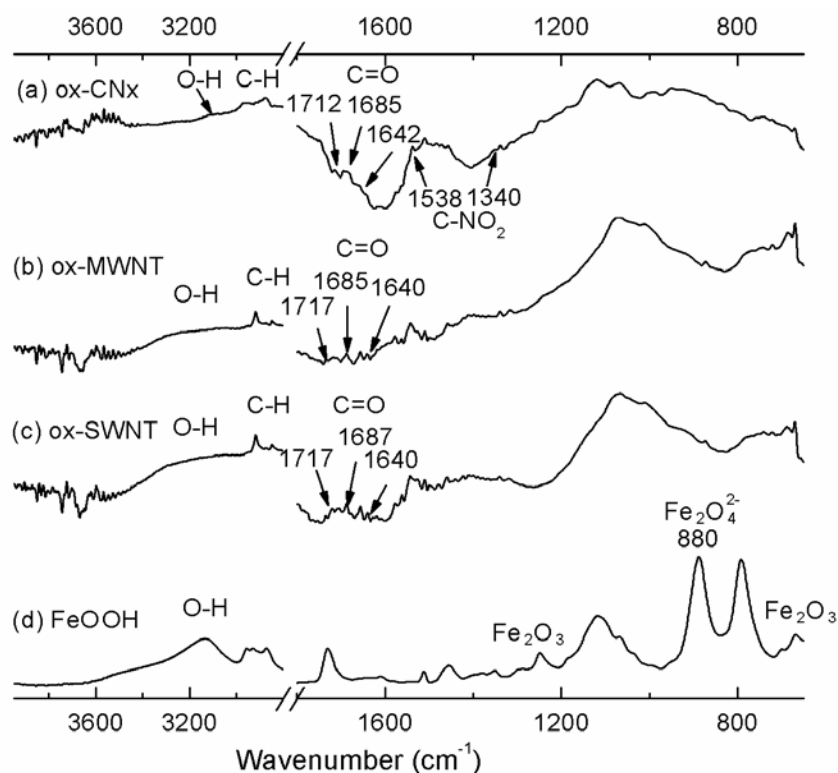
Fig. 3.9 FTIR spectra of (a) oxidized nitrogen-doped carbon nanotubes, ox-CNx; (b) oxidized multiwall carbon nanotubes, ox-MWNT; (c) oxidized single-wall carbon nanotubes, ox-SWNT; and (d) iron oxide nanoparticles, FeOOH, obtained by attenuated total reflectance (ATR).

Chemical characterization by infrared spectroscopy (Fig. 3.9) showed broad features from 3400 cm^{-1} to 3000 cm^{-1} by the stretching of the bonding -OH in carboxylic and hydroxyl groups (Misra et al., 2007). Signals near 1710 cm^{-1} and 1685 cm^{-1} were of carbonyl vibrations in carboxyl bonding, a weak band about 1640 cm^{-1} of quinones, and the broad band from 1200 to 1000 cm^{-1} was attributed to single-bonded oxygen atoms such as phenols and lactones. Two weak signals related to the nitro group were observed at 1538 and 1340 cm^{-1} for oxidized CNx (Zawadski, 1980; Wade, 1993). Similar spectra have been reported for oxidized multiwall carbon nanotubes; characteristic peaks were assigned to carboxylic,

carbonyl, and hydroxyl groups (Wang et al., 2007; Gao et al., 2008; Lu and Chiu 2008; Gao et al., 2009; Hu et al., 2009).

The FTIR spectrum of iron oxide nanoparticles showed a strong band in the range of 3200 to 3000 cm^{-1} attributed to stretching of the hydroxyl bonding –OH of hydrous iron oxide. Bands approximately to 1340 and 725 cm^{-1} were attributed to hematite (Fe_2O_3), and a broad band about 880 cm^{-1} was assigned to ferrate ion ($Fe_2O_4^{2-}$) (Nyquist and Kagel, 2000).

Acidic oxygen-containing groups improved wetting of oxidized carbon nanotubes in aqueous solution, and provided nucleophilic sites to which metallic ligands could be adsorbed.

3.3.2 Cadmium Adsorption

Adsorption experiments were carried out at pH 6, above the slurry pH of oxidized carbon nanotubes and iron oxide nanoparticles. Because the surface was negatively charged, positive cadmium ions were adsorbed at the tips and along the side-walls of oxidized carbon nanotubes, as was revealed by HRTEM images (Fig. 3.10a) and corroborated by mapping surface analysis (Fig. 3.10b).
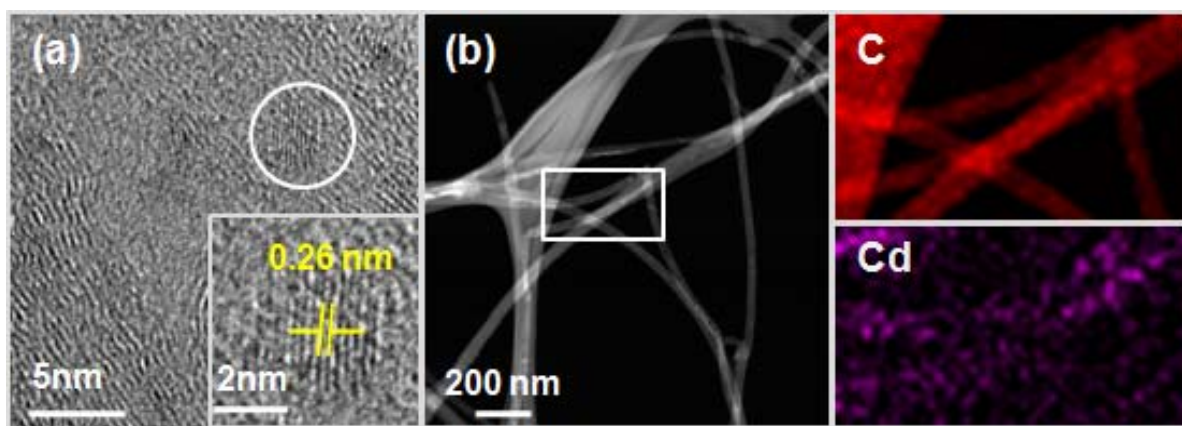
Fig. 3.10 (a) HRTEM image of oxidized CNx reveal a structure of cadmium, the inset shows its interlayer spacing (about 0.26 nm); (b) STEM image shows a surface mapping analysis for ox-CNx to corroborate the presence of cadmium (shown in purple), carbon is shown in red.

The Langmuir model was used to fit the experimental data of adsorption equilibrium; the isotherm parameters for each adsorbent are presented in Table 3.3, and the corresponding cadmium adsorption isotherms are shown on Fig.3.11. As discussed previously, the acidic sites concentration determined the maximum adsorption capacity (q_m), which followed a similar trend to the concentration of acidic sites and carboxylic groups: ox-SWNT >ox-CNx >ox-MWNT. q_m was 3 and 5.7 times higher than for ox-CNx and ox-MWNT, respectively,and it was 3.3 times higher than FeOOH.

The highest cadmium adsorption capacity of ox-SWNT was a result of their physicochemical properties as discussed previously, such as high oxidized surface area, pore volume and concentration of acidic groups. As a consequence the slurry pH of ox-SWNT was lower than for ox-CNx and ox-MWNT. Oxidized CNx and FeOOH had similar q_m, 1.9 times higher than for ox-MWNT; however parameter b, which is related to the adsorption intensity, was 24 and 36 times higher for ox-CNx and ox-MWNT, respectively, compared to that associated with FeOOH.

Table 3.3 Langmuir isotherm parameters determined for cadmium adsorption onto oxidized carbon nanotubes and iron oxide nanoparticles, at pH 6 and 25 °C

	q_m (mg/g)	b (L/mg)	[a]R^2
ox-SWNT	36.406	0.3287	0.9580
ox-MWNT	6.409	0.7568	0.9650
[b]ox-CNx	13.920	0.1497	0.9969
[c]ox-CNx (pH 6)	11.995	0.5117	0.9323
FeOOH	11.464	0.0211	0.9490

[a]*Correlation coefficient for this table*

[b]*Adsorption isotherm parameters obtained at initial pH 6*

[c]*Adsorption isotherm parameters obtained at constant pH 6*

Despite the different experimental conditions, available results from literature for cadmium adsorbed onto nitric acid oxidized MWNT are in close agreement with the results obtained in this study. Li et al., (2003c) reported a value of 5.1 mg/g at pH 5, and recently Gao et al., (2009) reported a value of about 3.6 mg/g at pH 6.5, and 2.9 mg/g at final pH of 4.5 (Gao et al., 2008).
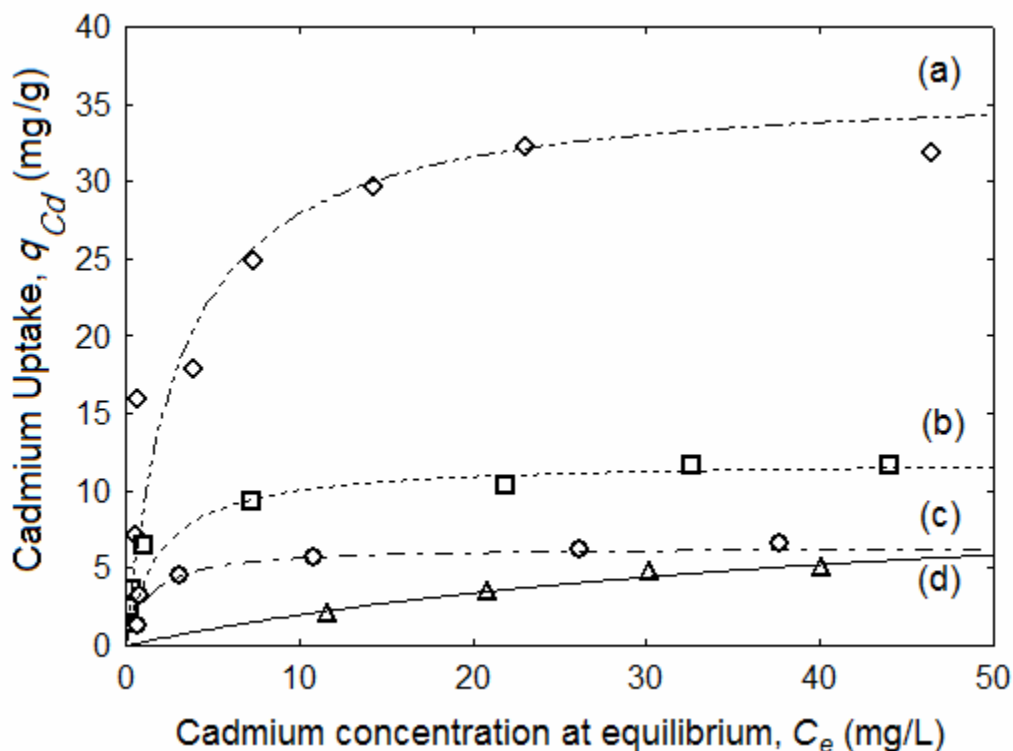
Fig. 3.11 Cadmium adsorption isotherms at pH 6 and 25 °C adjusted by Langmuir model. (a) Oxidized single-wall carbon nanotubes, ox-SWNT; (b) oxidized nitrogen-doped carbon nanotubes, ox-CNx; (c) oxidized multiwall carbon nanotubes, ox-MWNT; (d) iron oxide nanoparticles, FeOOH.

3.3.3 Cadmium Adsorption Kinetic onto Oxidized Carbon Nanotubes

Besides adsorption capacity, adsorption kinetic parameters would be necessary to design adsorption processes based on carbon nanotubes. Morphology of carbon nanotubes may determine adsorption kinetic, and eventually the adsorption

process cost. Assessment of the morphology effect was performed through adsorption kinetic experiments under the conditions presented in Table 3.4.

Table 3.4 Experimental conditions for batch adsorption kinetic tests

Run #	Adsorbent	C_{A0} (mg/L)	pH	Shaking rate v (rpm)	Time of experiment t (min)
1	ox-CNx	4.14	-[a]	150	120
2		4.12	-[a]	150	40
3		4.14	-[a]	200	40
4		9.65	-[a]	200	40
5		19.29	-[a]	200	40
6		4.19	6±0.1	200	40
7		9.28	6±0.1	200	40
8		18.52	6±0.1	200	40
9	ox-MWNT	4.17	-[a]	200	40
10		4.33	6±0.1	200	60
11		4.90	6±0.1	250	70
12	ox-SWNT	4.13	-[a]	200	60
13		4.17	6±0.1	200	71
14		4.74	6±0.1	350	100
15	FeOOH	4.04	-[a]	200	60
16		4.22	6±0.1	200	60

[a] initial pH 6 without control

Morphology effects on adsorption kinetic were evidenced: a shaking rate of 200 rpm was enough to maintain ox-CNx homogeneously suspended, attaining equilibrium in less than 40 minutes as determined by Run 1. Also ox-MWNT attained equilibrium in less than 40 minutes, but their low concentration of oxygen acidic groups resulted in a higher agglomeration; in this case a shaking rate of 250 rpm was required to obtain a homogeneous suspension (Run 11). Meanwhile ox-

SWNT were homogeneously suspended by using a shaking rate of 350 rpm, and the equilibrium was reached in no less than 100 minutes (Run 14).

The slower adsorption rate for ox-SWNT could be due to cadmium diffusion through spacing between entangled nanotubes, the pores along the sidewall created by oxidation as well as their internal tubular space: open tips were wide enough (0.9 to 1.5 nm, Fig 3.12a) for cadmium ions with hydrated radii of 0.426 nm (Nightingale 1959) to diffuse inside the nanotubes. In contrast, a faster diffusion occurred in ox-MWNT and ox-CNx because of some closed tips (Fig. 3.12b) and internal sections (Fig.3.12c), respectively.
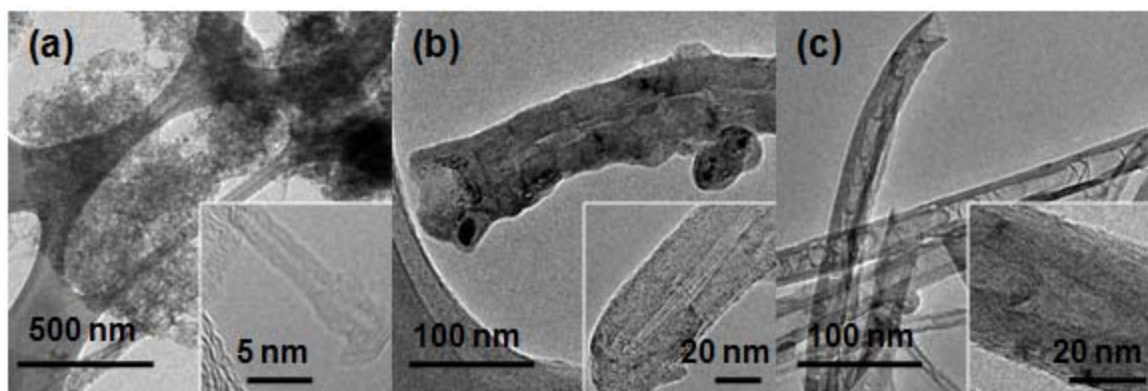
Fig. 3.12 HRTEM Micrographs of tips and internal tubular section of (a) oxidized single-wall carbon nanotubes, ox-SWNT; (b) oxidized multiwall carbon nanotubes, ox-MWNT; and (c) oxidized nitrogen-doped carbon nanotubes, ox-CNx.

Based on the previous observations, morphological properties and diffusion are closely related, and their impact on the operational cost of processes involving carbon nanotubes should be considered. The following sections include a detailed discussion of the obtained experimental kinetic data analyzed with the pseudo-second order, an external mass diffusion and intraparticle diffusion models.

3.3.3.1 Analysis of Adsorption Kinetic Data with the Pseudo-second Order Model

The pseudo-second order model has been used to analyze the adsorption data of metal ions on carbon nanotubes. This model assumes that the cadmium adsorption reaction is the limiting rate step (Li et al., 2003b; Chen and Wang, 2006; Lu et al., 2006; Chen et al., 2007; Wang et al., 2007b; Lu and Chiu, 2008; Gao et al., 2008; Kabbashi et al., 2009; Yang et al., 2009).

The plot of t/q_t against t gave a linear relationship with a correlation factor (R^2) higher than 0.9 as observed in figures (A1 to A5) reported in Appendix A. The kinetic parameters called adsorption capacity at equilibrium (q_e), a constant rate of pseudo-second order (k_2) and an initial adsorption rate (h), were determined from the slope and intercept to the ordinate of the plot (Table 3.5). Also, the half-life of adsorption process ($t = t_{0.5}$) defined as the time needed to attain an adsorption $q_t = 0.5\, q_e$, was calculated (Wu et al., 2009):

$$t_{0.5} = \frac{1}{k_2 q_e} \tag{3.24}$$

Comparing k_2 for ox-MWNT (Runs 9 to 11) with data from literature it can be deduced that the values reported herein were more than 25 times smaller than those reported by Gao et al., (2008), 4.8528 g/mg-min, obtained at C_{A0} of 2 mg/L and pH 6.5. These differences could be due to the physicochemical properties of oxidized MWNT, and to the configuration of the adsorption kinetic systems used to conduct the experiments in each case. In relation to cadmium adsorption onto other adsorbents, for example k_2 for ox-MWNT was 34 times smaller than that obtained for peanuts husks carbon at pH 6, 4.495 g/mg-min (Ricordel et al., 2001), while k_2 for ox-SWNT was 6.5 times smaller than the reported for sugar beet pulp, 0.0996 g/mg-min at pH 5.5 (Reddad et al., 2002), and 2.4 times smaller than the reported for lichen *Ramalina fraxinea* biomass, 0.037 g/mg-min at pH 6 (Tay et al., 2009).

Table 3.5 Pseudo-second order parameters for adsorption kinetic of cadmium onto oxidized carbon nanotubes and iron oxide nanoparticles

Run #	Adsorbent	C_{A0} (mg/L)	q_e (mg/g)	k_2 (g/ mg-min)	h (mg/ min-g)	$t_{0.5}$ (min)	R^2	%E q_e
1	ox-CNx[a,c]	4.14	4.67	0.160	3.50	1.34	0.998	17
2	ox-CNx[a,c]	4.12	4.46	0.148	2.96	1.51	0.999	13
3	ox-CNx[a,d]	4.14	4.26	0.371	6.71	0.63	0.998	9
4	ox-CNx[a,d]	9.65	7.94	0.212	13.3	0.59	0.999	16
5	ox-CNx[a,d]	19.29	11.76	0.185	25.6	0.46	0.997	18
6	ox-CNx[b,d]	4.19	6.10	0.219	8.13	0.75	0.999	4
7	ox-CNx[b,d]	9.28	9.52	0.187	16.9	0.56	0.999	6
8	ox-CNx[b,d]	18.52	11.76	0.195	27.0	0.44	0.999	10
9	ox-MWNT[a,d]	4.17	4.76	0.124	2.80	1.69	0.999	10
10	ox-MWNT[b,d]	4.33	4.72	0.131	2.91	1.62	0.998	10
11	ox-MWNT[b,e]	4.90	5.13	0.175	4.61	1.11	0.998	11
12	ox-SWNT[a,d]	4.13	7.58	0.0218	1.25	6.06	0.978	8
13	ox-SWNT[b,d]	4.17	9.35	0.0154	1.35	6.95	0.988	12
14	ox-SWNT[b,f]	4.74	11.36	0.0086	1.11	10.2	0.993	19
15	FeOOH[a,d]	4.04	1.46	0.111	0.24	6.17	0.999	43
16	FeOOH[b,d]	4.22	1.51	0.134	0.31	4.96	0.999	43

[a] initial pH 6 without control; [b] pH 6 ; [c] 150 rpm; [d] 200 rpm; [e] 250 rpm; [f] 350 rpm

As can be seen from Table 3.5, the initial adsorption rates (h) for runs 3 to 5 and 6 to 8 increased between two and four times with an increase in the initial cadmium concentration (C_{A0}), which can be attributed to the increase in the driving force of the mass transfer; as a consequence $t_{0.5}$ was approximately 10% to 40% shorter at the higher initial cadmium concentration. When controlling the solution pH at 6 a higher concentration of active sites was available for cadmium adsorption, as it was observed from the distribution charge for ox-CNx (Perez-Aguilar et al., 2010); hence adsorbed cadmium at equilibrium (q_e) was about 20% higher for ox-CNx

(runs 3 and 6, and 4 and 7) and for ox-SWNT (runs 12 and 13), while a minimum effect was observed for ox-MWNT and FeOOH, probably as a result of their lower adsorption capacity. As a result of a faster shaking rate, k_2 and h increased about 2.4 and 1.4 times in ox-CNx (runs 2 and 3) and ox-MWNT (runs 10 and 11), respectively. Thus the adsorption process was shaking rate dependent because according to theory at a faster speed the liquid film surrounding multiwall nanotubes became narrower, and the external transport of cadmium was faster. However, for ox-SWNT, k_2 and h decreased about 45% and 20% at a faster speed (runs 13 and 14), suggesting that the external mass transport was not a key factor for cadmium adsorption on these nanotubes.
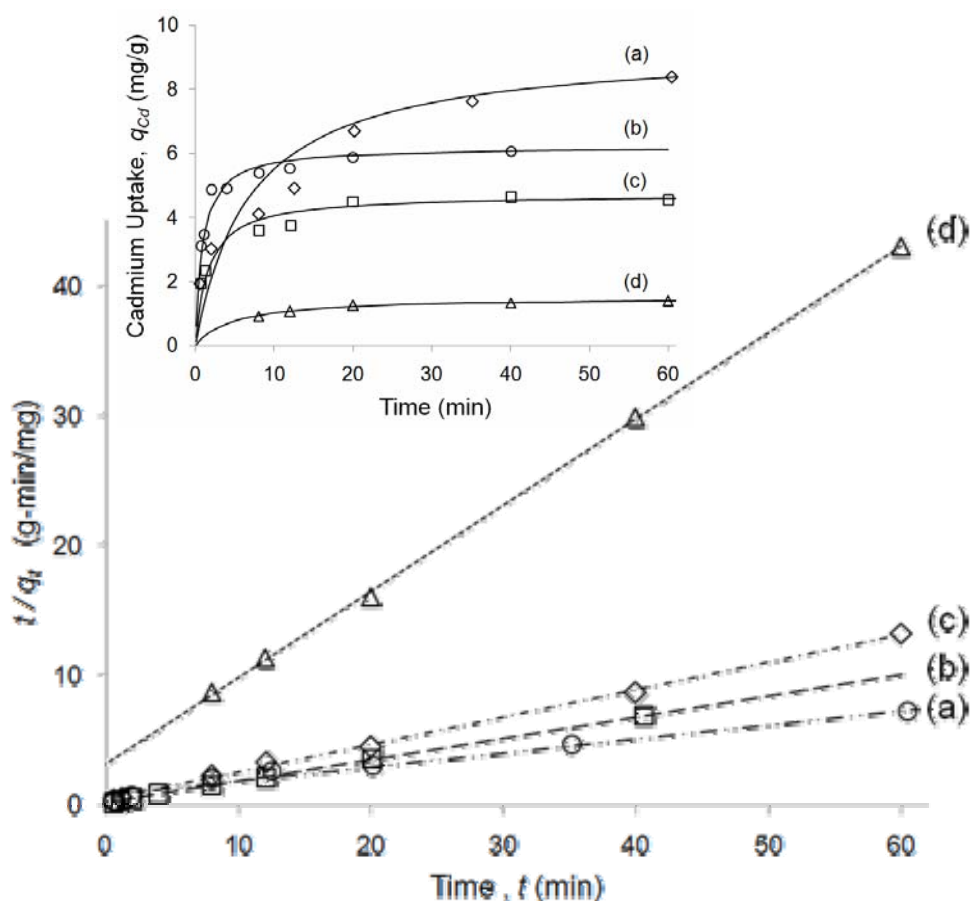
Fig. 3.13 Cadmium adsorption rate onto (a) ox-SWNT, run 13; (b) ox-CNx, run 6; (c) ox-MWNT, run 10; and (d) FeOOH, run 16, fitted by the pseudo-second order model. Data obtained at C_{A0} 4 mg/L, m/V=0.4 g/L, pH 6 ± 0.1, 25 °C, 200 rpm. Inlet shows cadmium uptake curves predicted with model parameters.

The experimental adsorption kinetic data fitted by the pseudo-second order model, obtained for the different nanoparticles studied can be compared in Fig. 3.13. For ox-CNx k_2 was 1.7 times higher than for ox-MWNT and FeOOH, and 14 times higher than for ox-SWNT. Moreover, h for ox-CNx was 2.8, 6 and 26 times higher than ox-MWNT, ox-SWNT and FeOOH, respectively.

For engineering design the relationship between the operating time and amount adsorbed is the most useful. The half-life of the adsorption process ($t_{0.5}$) and/or the time required to attain 95% of the adsorption capacity at equilibrium ($t_{0.95}$, $q_t=0.95q_e$) might be adopted (Wu et al., 2009). Fig. 3.14 shows data obtained for $t_{0.5}$, around 1, 2, 5 and 7 min for ox-CNx, ox-MWNT, FeOOH and ox-SWNT, respectively; thus a more significant difference was observed at $t_{0.95}$: 14, 30, 120 and 90 min in the same order.
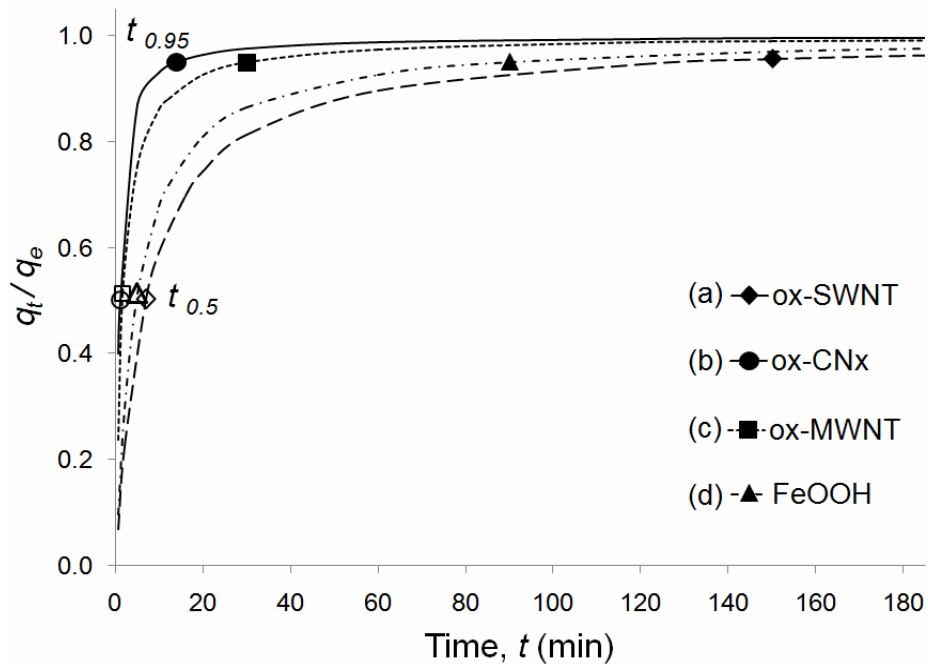
Fig. 3.14 Curves for approximation to equilibrium (lines) predicted by the pseudo-second order model, showing the half-life adsorption time $t_{0.5}$ (empty symbols), and the time to attain 0.95 of adsorption $t_{0.95}$ (full symbols), for cadmium adsorption onto (a) ox-SWNT (run 13); (b) ox-CNx (run 6); (c) ox-MWNT (run 10); and (d) FeOOH (run 16).

The observed trend could be determined by the concentration of acidic groups at each adsorbent; ox-SWNT had the highest concentration, and also the highest surface area and pore volume; thus a longer time to reach equilibrium was needed. However non-porous iron oxide had the lowest concentration of acidic sites and also the lowest specific surface and pore volume. If adsorption had been the limiting rate step, non-porous iron nanoparticles might have reached equilibrium faster than carbon nanotubes. Instead, adsorption rate for FeOOH was slower than ox-CNx and ox-MWNT but faster than ox-SWNT, suggesting that cadmium could have undergone a mechanism of intraparticle diffusion through micropores caused by agglomeration of iron oxide nanoparticles. Hence, the intraparticle diffusion effect was greater in highly entangled ox-SWNT.

3.3.3.2 Analysis of Adsorption Kinetic Data with an External Mass Transfer Model

The adsorbent particle can be visualized as having a stagnant "film" of liquid of thickness δ surrounding it (Fig 3.2). The mass transfer resistance of this film is proportional to δ/D_i^0: the ionic diffusivity of cadmium in water D_i^0= 1.23E-5 cm^2/s, calculated with equation 3.30 according to Newman (1973). Values for z_1 =2 and z_2=1, the charge of cadmium and nitrate ions, respectively, and diffusion coefficients for cadmium D_1^0= 7.2E-6 cm^2/s (Dobos, 1994) and nitrate D_2^0 =1.9E-5 cm^2/s (Newman, 1973) were used. Controlling the speed of mixing can accelerate the external mass transfer because of the reduction of the film thickness (Cooney, 1999).

$$D_i^0 = \frac{|z_1| + |z_2|}{\frac{|z_2|}{D_1^0} + \frac{|z_1|}{D_2^0}}$$

(3.25)

Experimental adsorption kinetic data were fitted to the external mass transfer model considering single nanotubes and properties listed in Table 3.6. Table 3.7 presents results for the theoretical mass transfer coefficient ($k_{L,theo}$) and percentage of deviation between the predicted curves and the experimental data.

Table 3.6 Physical properties of single nanoparticles to predict concentration decay curves by using the external mass transfer model

Adsorbent	d_{outer} (cm)	ρ_s (g/cm³)	V_p (cm³/g)	ρ_p (g/cm³)	p
ox-SWNT	1.5E-7	2.13	3.1E-3	2.12	6.1E-3
ox-MWNT	7E-6	2.17	3.6E-2	2.02	7.2E-2
ox-CNx	5E-6	2.24	1.7E-1	1.61	2.8E-1
FeOOH	1E-6	2.20	6.5E-4	2.20	1.4E-3

Table 3.7 External mass-transfer parameters for adsorption kinetic of cadmium onto oxidized carbon nanotubes and iron oxide nanoparticles

#	Adsorbent	C_{A0} (mg/L)	$k_{L,exp}$ (cm/s)	$k_{L,theo}$ (cm/s)	t_e (min)	% D
1	ox-CNx[a,c]	4.14	6.5E-6	2.5E-2	11.4	2.4
2	ox-CNx[a,c]	4.12	4.8E-6	2.8E-2	12.0	1.9
3	ox-CNx[a,d]	4.14	4.3E-5	3.6E-2	12.3	1.5
4	ox-CNx[a,d]	9.65	1.9E-4	6.8E-2	3.4	1.7
5	ox-CNx[a,d]	19.3	3.6E-4	8.3E-2	1.2	0.5
6	ox-CNx[b,d]	4.19	1.3E-5	8.7E-2	7.0	8.2
7	ox-CNx[b,d]	9.28	1.1E-5	8E-2	3.4	2.7
8	ox-CNx[b,d]	18.5	7.3E-6	5.3E-2	1.8	1.7
9	ox-MWNT[a,d]	4.17	3.7E-6	5.8E-2	13.8	3.9
10	ox-MWNT[b,d]	4.33	5.9E-6	9.8E-2	7.2	4.1
11	ox-MWNT[b,e]	4.90	4.3E-6	8.7E-2	7.8	3.3
12	ox-SWNT[a,d]	4.13	1.2E-6	4E-4	124	18.0
13	ox-SWNT[b,d]	4.17	1.1E-6	5E-4	98	7.7
14	ox-SWNT[b,f]	4.74	2.4E-7	6E-4	80	2.4
15	FeOOH[a,d]	4.04	1.5E-7	2.6E-4	41	0.2
16	FeOOH[b,d]	4.22	2E-7	3.4E-4	45	0.8

[a] initial pH 6 without control; [b] pH 6 ; [c] 150 rpm; [d] 200 rpm; [e] 250 rpm; [f] 350 rpm

The external mass transfer model did not adjust well over the entire experimental data for carbon nanotubes (Fig. 3.15a, b, c); the prediction of a deep first stage resulted in an underestimation of the time to reach equilibrium. Also, experimental data depicted a slower second stage suggesting the influence of intraparticle diffusion on cadmium adsorption rate. In general, predicted concentration decay curves showed deviations from experimental data higher than 5% for ox-SWNT but lower than 5% for ox-CNx and ox-MWNT, as well as 1% for FeOOH.
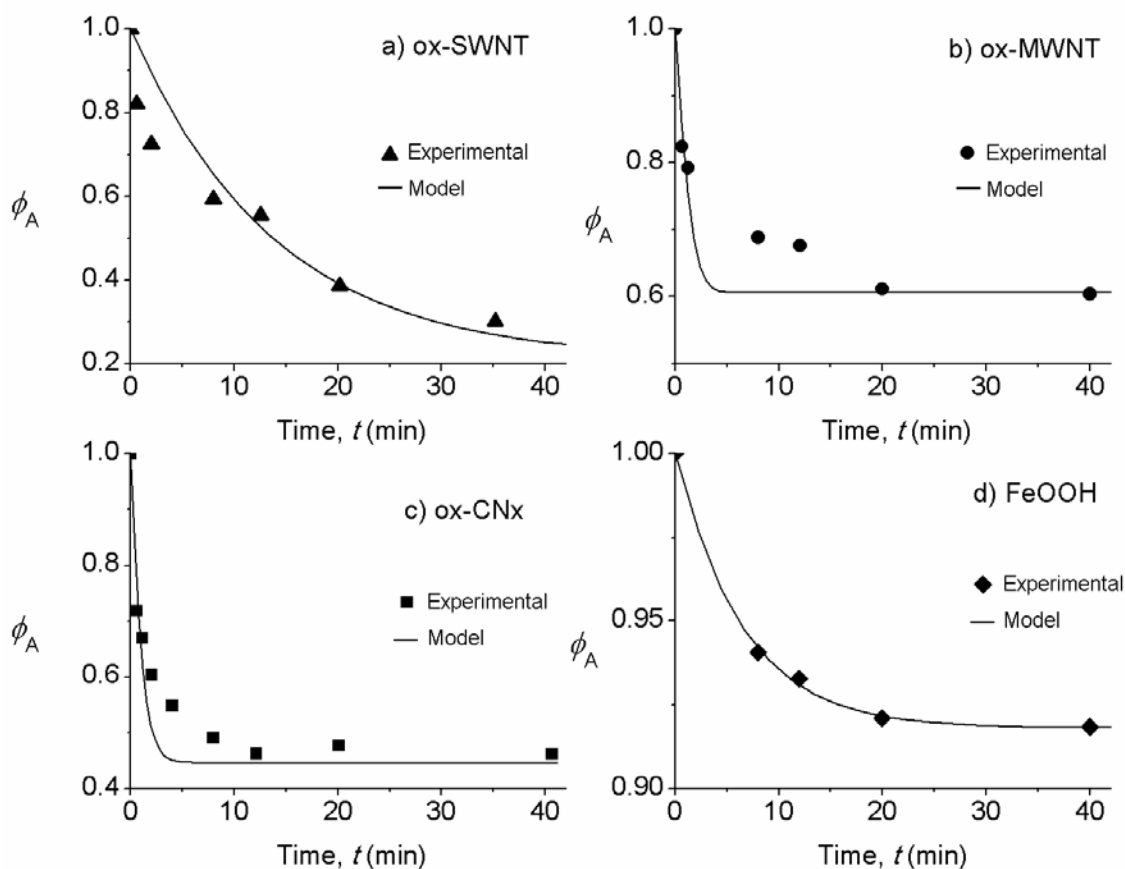
Fig. 3.15 Concentration decay curves for cadmium adsorption onto (a) ox-SWNT, run 13; (b) ox-CNx, run 6; (c) ox-MWNT, run 10; and (d) FeOOH, run 16, predicted by the external mass transfer model at C_{A0} 4 mg/L, pH 6 ± 0.1, 25 °C and 200 rpm. Symbols and lines represent the experimental data and the predicted curves, respectively.

In addition, theoretical values for k_L were far higher than the experimental ones: around 4000, 17000, 300 and 1700 times, for ox-CNx, ox-MWNT, ox-SWNT and FeOOH, respectively. Such high values could result from the nanometric dimensions of the adsorbents, as equation 3.10 shows, where the term $\frac{m}{d_p}$ replaces S_V:

$$dq = \frac{mk_L(C_{Ai}-C_{Si})}{d_p\rho_s(1-\varepsilon)}\, dt \qquad (3.10)$$

This equation also shows the influence of initial concentration on k_L, as observed from experiments 3, 4 and 5 at initial pH 6, for ox-CNx (Fig.B1b, Appendix B). Experimental k_L increased around four and eight times when C_{A0} increased from 4 to 9 and 19 mg/L, suggesting a fast occupation of the external adsorption sites at the tips and along the outside walls of nanotubes. These results agree with those reported by Allen et al., (1997): intraparticle diffusion becomes negligible as initial concentration increases. However, k_L decreased about 20% and 40% for the same increasing of C_{A0} in experiments 6, 7 and 8, performed at pH 6 (Fig. B2, Appendix B). This suggests that under controlled pH a slower occupation of the external sites might occur, since a high concentration of internal adsorption sites could be available and diffusion might happen to reach these sites.

Results obtained for the different nanoparticles showed that controlling the pH had a positive effect on theoretical k_L, in relation to those outcomes obtained at uncontrolled pH: k_L increased to about 2.4, 1.7, 1.25 and 1.32 times for ox-CNx (runs 3, 6), ox-MWNT (runs 9, 10), ox-SWNT (runs 12, 13) and FeOOH (runs 15, 16), respectively, because a higher concentration of active sites became available. Higher shaking speed reduced the thickness of the external film, thus increasing theoretical k_L around 1.3, 1.1 and 1.2 times for ox-CNx (runs 2, 3), ox-MWNT (runs 10, 11) and ox-SWNT (runs 13, 14), respectively. The obtained k_L for nanotubes showed the highest value for ox-CNx, 4.55E-2 cm^2/h, 2 and 12 times higher than that for ox-MWNT, 2.13E-2 cm^2/h and for ox-SWNT, 3.93E-3 cm^2/h, respectively, at C_{A0} 4 mg/L, pH 6 and 200 rpm. This difference could be due to a larger exposed

surface for ox-CNx, near 1E-3 cm^2, than 6E-4 and 2.5E-6 cm^2 for ox-MWNT and ox-SWNT, correspondingly. These values were far smaller than k_L, 54 cm/h, reported for cadmium adsorption onto activated carbon at pH 8 and particle size of 0.4 mm (Leyva Ramos et al., 2005).

The previously discussed results suggest that intraparticle diffusivity could play an important role in the cadmium adsorption rate onto carbon nanotubes, in contrast with results for macroscopic size adsorbents, as those reported by Allen et al., (1997) for cadmium and copper onto peat and lignite, for which external mass transfer controlled the adsorption rate.

3.3.3.3 Analysis of Adsorption Kinetic Data with an Intraparticle Diffusion Model

The intraparticle diffusion model was applied considering the physical properties listed in Table 3.8. The outer diameter for agglomerate nanoparticles were considered based on microscopic analysis (average of 40 agglomerates, standard deviation around 200, 110 and 30 μm for ox-MWNT, ox-SWNT and ox-CNx, respectively).

Table 3.8 Physical properties of nanoparticles considered for the intraparticle diffusion model

Adsorbent	d_{outer} (μm)	d_{pore} (cm)	ρ_s (g/cm^3)	V_p (cm^3/g)	ρ_p (g/cm^3)	p
ox-SWNT[a]	3E-3	1.5E-7	2.13	3E-3	2.12	0.006
ox-SWNT[b]	350	7E-7	2.13	3E-1	1.23	0.421
ox-MWNT[a]	7E-2	3E-7	2.17	7E-4	2.17	0.002
ox-MWNT[b]	400	1.2E-5	2.17	4E-3	1.8	0.178
ox-CNx[a]	5E-2	4E-7	2.24	3E-5	2.2	7E-5
ox-CNx[b]	90	1.5E-5	2.24	2E-1	1.6	0.302
FeOOH[a]	1E-2	2.5E-7	2.2	6E-5	2.2	1E-4
FeOOH[b]	10	2.5E-5	2.2	2E-3	2.2	0.005

[a] physical properties considering a single nanoparticle

[b] physical properties considering agglomerates of nanoparticles

Table 3.9 Intraparticle diffusion model parameters for adsorption kinetic of cadmium onto single oxidized carbon nanotubes and iron oxide nanoparticles

Run #	Adsorbent	C_{A0} (mg/L)	k_L (cm/s)	$D_{e,p}$ (cm^2/s)	% D	t_e (min)	τ
1	ox-CNx[a,c]	4.14	6.5E-6	3.4E-9	1.5	18	78
2	ox-CNx[a,c]	4.12	4.8E-6	3.6E-9	1.6	18	74
3	ox-CNx[a,d]	4.14	4.3E-5	4E-9	1.5	16	67
4	ox-CNx[a,d]	9.65	1.9E-4	6.3E-9	0.9	6	43
5	ox-CNx[a,d]	19.29	3.6E-4	2.9E-8	0.7	2	9
6	ox-CNx[b,d]	4.19	1.3E-5	4.2E-9	3.0	16	63
7	ox-CNx[b,d]	9.28	1.1E-5	1.2E-8	1.9	4	23
8	ox-CNx[b,d]	18.52	7.3E-6	8.1E-8	1.7	2	5
9	ox-MWNT[a,d]	4.17	3.7E-6	9.9E-10	2.2	26	86
10	ox-MWNT[b,d]	4.33	5.9E-6	1.1E-9	3.2	23	98
11	ox-MWNT[b,e]	4.90	4.3E-6	1.3E-9	1.6	18	79
12	ox-SWNT[a,d]	4.13	1.2E-6	1E-11	5	440	32E3
13	ox-SWNT[b,d]	4.17	1.1E-6	2.4E-11	7.7	183	13E3
14	ox-SWNT[b,f]	4.74	2.4E-7	1.3E-10	3.3	82	2.5E3
15	FeOOH[a,d]	4.04	1.5E-7	4.1E-9	0.2	43	4
16	FeOOH[b,d]	4.22	2E-7	1.3E-8	0.8	41	4

[a] initial pH 6 without control; [b] pH 6 ; [c] 150 rpm; [d] 200 rpm; [e] 250 rpm; [f] 350 rpm

Table 3.10 Intraparticle diffusion model parameters for adsorption kinetic of cadmium onto agglomerates of carbon nanotubes and iron oxide nanoparticles

Run #	Adsorbent	C_{A0} (mg/L)	k_L (cm/s)	$D_{e,p}$ (cm^2/s)	% D	t_e (min)	τ
6	ox-CNx	4.19	1.3E-5	3.1E-5	4	19	0.14
10	ox-MWNT	4.33	6E-6	2E-4	4	30	0.01
13	ox-SWNT	4.17	1E-6	4.5E-5	8	118	0.11
16	FeOOH	4.22	2E-7	1.1E-6	0.1	42	0.01

Tables 3.9 and 3.10 present intraparticle diffusion coefficient (D_{ep}) and deviation percentage obtained for predicted concentration decay curves. Compared to the external mass transfer model, the intraparticle diffusion model better adjusted the experimental kinetic data, as can be seen from the obtained deviation percentage and figures in Appendix C (C1 to C5). The sensitivity of the model was tested by using $D_{e,p}$ of 0.5 and 2 times higher than those best fitted the experimental data. These tested values for $D_{e,p}$ resulted in deviations of 3.5% and 2.1%, respectively (Fig.C1 Appendix C).

The intraparticle diffusivities ($D_{e,p}$) obtained for single nanoparticles were around 4E-9, 1E-9, 2.4E-11 and 1.3E-8 cm^2/s for ox-CNx, ox-MWNT, ox-SWNT and FeOOH, respectively, all of them smaller than the bulk diffusivity for cadmium in water, 1.23E-5 cm^2/s. Results for $D_{e,p}$ and experimental k_L suggested that intraparticle diffusion could be a key factor in the overall cadmium adsorption rate. Although increasing initial C_{A0} resulted in greater values for k_L and $D_{e,p}$ at uncontrolled pH 6 (runs 3 to 5), smaller k_L and larger $D_{e,p}$ were obtained when C_{A0} increased at constant pH (runs 6 to 8); hence more active sites available inside ox-CNx might induce cadmium diffusion. The effect of controlling pH resulted in similar responses: k_L decreased 70% and 10% while $D_{e,p}$ went up 6% and 2.4 times for ox-CNx (runs 3, 6) and ox-SWNT (runs 12, 13), correspondingly. However k_L and $D_{e,p}$ increased 60% and 8% respectively for ox-MWNT (runs 9,10), probably because more active sites were available on the external surface. Faster speed reduced k_L 70% and 80% while $D_{e,p}$ increased 20% and 5.4 times for ox-MWNT (runs 10,11) and for ox-SWNT (runs 13, 14), respectively.

The found tendency for $D_{e,p}$ for single nanotubes was ox-CNx > ox-MWNT > ox-SWNT, in correspondence to pore size trend but contrasting to pore volume and porosity, for which ox-SWNT > ox-MWNT > ox-CNx. These features in addition to their greater length and probably highest concentration of sidewall pores might explain the slowest transport through ox-SWNT compared to that of ox-MWNT and ox-CNx. Hence tendency to reach equilibrium was: ox-SWNT > ox-MWNT > ox-CNx.

High ratio *L/D* and flexibility of carbon nanotubes resulted in agglomerates unlike cylindrical morphology, which might influence mass transport processes. Concentration decay curves predicted by the intraparticle model for agglomerates nanoparticles showed that equilibrium was attained at about 19, 30 and 118 minutes for ox-CNx, ox-MWNT and ox-SWNT, respectively (Fig. 3.16).
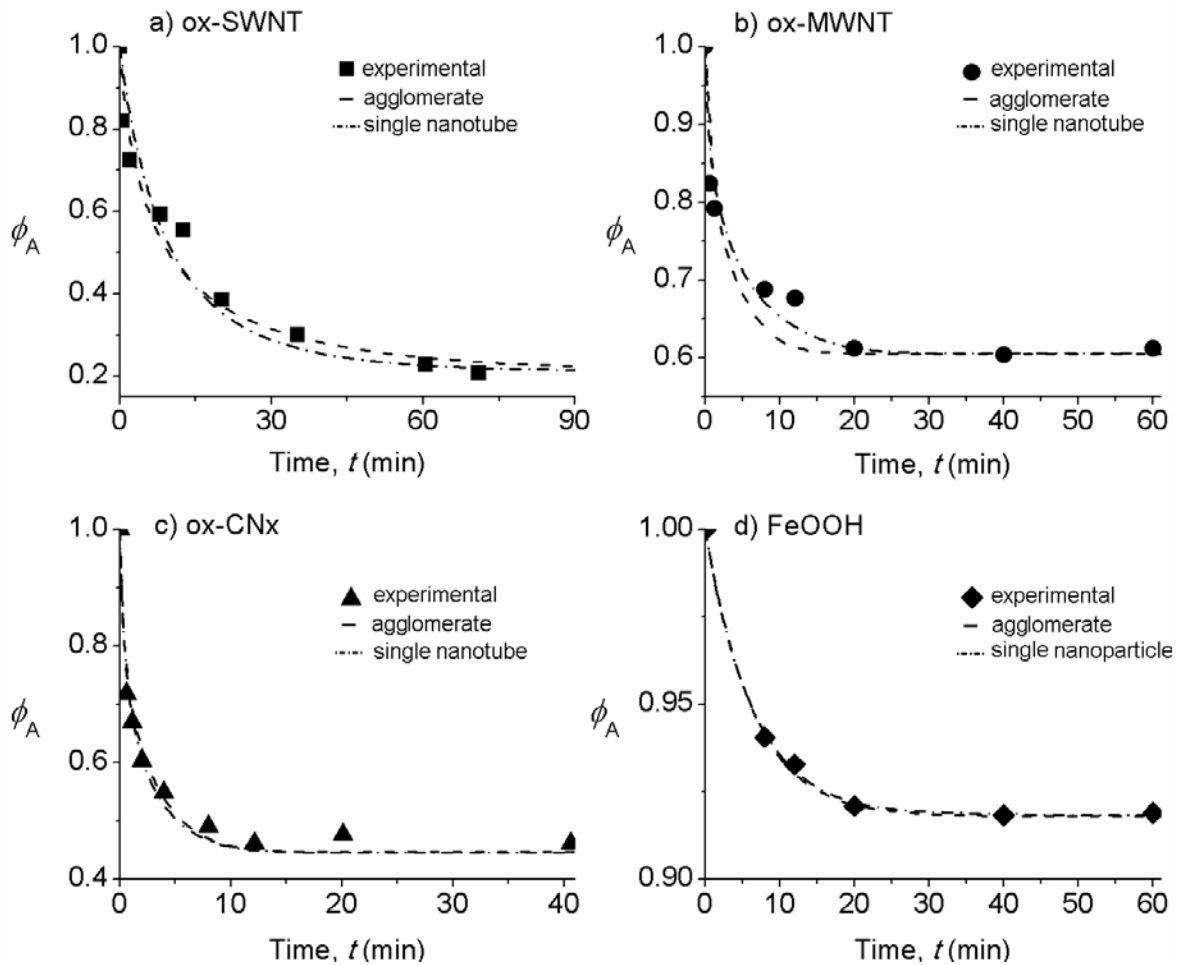
Fig. 3.16 Concentration decay curves predicted by the intraparticle diffusion model, for cadmium adsorption onto (a) ox-SWNT, run 13; (b) ox-CNx, run 6; (c) ox-MWNT, run 10; and (d) FeOOH, run 16. Symbols represent experimental data and the lines the model considering single or agglomerates of nanoparticles.

Predicted concentration decay curves for single nanoparticles and agglomerates apparently did not show significant differences. However, the intraparticle diffusivities ($D_{e,p}$) obtained for agglomerate nanotubes were 3.1E-5, 4.5E-5, and 2E-4 cm^2/s for ox-CNx, ox-SWNT and ox-MWNT, respectively. These values for $D_{e,p}$ were 2.5, 3.7 and 16 times higher than the bulk diffusivity for cadmium in water (1.23E-5 cm^2/s), which is not possible because pores limited cadmium transfer to adsorption sites, thus $D_{e,p}$ should be lower than $D°_{Cd}$. Therefore, modeling cadmium adsorption kinetic on agglomerates nanotubes by using the intraparticle diffusion model may need different assumptions or even a different configuration of the adsorption kinetic experiments, in example the rotating basket adsorber.

The cadmium adsorption process onto carbon nanotubes involved both mechanisms: at the initial stage of the adsorption, the transport through the external film controlled the process. However, the intraparticle diffusion rate was slower than the film diffusion, and therefore the overall mass transport process could be mainly controlled by intraparticle diffusion. Both mass transfer mechanisms were related to the modified Sherwood number ($N_{Sh'}$) according to equation 3.26.

$$N_{Sh'} = \frac{k_L d_p}{D_{e,p}}$$

(3.26)

The obtained $N_{Sh'}$ were 0.0075, 0.028 and 0.35 for ox-SWNT, ox-MWNT and ox-CNx, respectively, or $1/N_{Sh'}$ 133, 36 and 3, correspondingly. This means that intraparticle diffusion was more important than external mass transport in single nanotubes. The pore size tendency observed for single nanotubes was ox-CNx > ox-MWNT > ox-SWNT, suggesting a high binding energy toward adsorbing molecules in the nanotube interior and/or through the smallest pores of ox-SWNT, because closeness of the surrounding sidewalls maximizes the attractive interaction favoring diffusion inside the pores (Kondratyuk and Yates, 2007). It is also difficult for the adsorbate to diffuse through the longest and highly entangled ox-SWNT to reach internal active sites (B'eguin et al., 2006), resulting in a slower kinetic process than for multiwall nanotubes.

Unusually high values of tortuosity (see Table 3.9) were obtained for single carbon nanotubes: 63, 98 and 13000 for ox-CNx, ox-MWNT and ox-SWNT, respectively. Values in the range of 2 to 10 have been reported for adsorption of inorganic or organic species onto carbonaceous materials (Leyva-Ramos and Geankoplis, 1985; Leyva-Ramos et al., 2005; 2007). However, it is important to mention that a tortuosity of 6700 was reported for adsorption of acid blue 25 onto peat (Hui et al., 2003). The high values obtained for τ in the present study may be related to roughness due to tiny pores on the sidewall of nanotubes which limit cadmium diffusion.

Adsorbents of nanometric dimensions would have different adsorption kinetic behavior than those of macroscopic size: smaller diffusivities and faster times to reach equilibrium can be expected for nanoadsorbents. This can be deduced since diffusivities for single carbon nanotubes obtained in this research were smaller than those reported for cadmium adsorption onto bone char 5.3E-7 cm^2/s at pH 5 (Cheung et al., 2001), and 2.5E-6 cm^2/h onto activated carbon Filtrasorb 400 at pH 8 (Leyva-Ramos et al., 2005). As a consequence of smaller diffusivities, the equilibrium was attained in 16, 23 and 180 min for single ox-CNx, ox-MWNT and ox-SWNT, respectively, which were far faster than those reported for activated carbon (around 35 h) and for bone char (more than 10 h).

Thus, ox-CNx had the fastest kinetic and ox-SWNT the slowest, in agreement with trends reported by the pseudo-second order and the external mass transfer model. Moreover, the intraparticle diffusion model includes more physical parameters resulting in a better fitting of the experimental data. Thus, for an analysis of adsorption kinetic of carbon nanotubes, it is recommended to use an intraparticle diffusion model. Also, it is important to mention the limitations of the intraparticle diffusion model applied in this research: it only considers radial diffusion and does not include properties of fluids in nanometric dimensions.

At present, the cost of carbon nanotubes is still high for a real application in water treatment, but it will be more accessible because higher production and lower cost have been observed in recent years. The actual price per gram ranges from 60 to

380 USD for SWNT, from 0.2 to 0.4 USD for MWNT (Nanostructured and Amorphous Materials, Thomas Swan, Arkema, Bayer Material Sciences, Nanocarb Lab, Carbon Solutions, Apex Nanomaterials), and is less than 5 USD to produce one gram of CNx.

Considering the results obtained in this study ox-CNx represents an attractive option for future applications in adsorption systems, due to their physicochemical features and faster adsorption kinetic in relation with ox-SWNT and ox-MWNT, in addition to their lower cost in relation to ox-SWNT.

Finally, many techniques can be employed to treat polluted water with heavy metals. Selection of the most suitable treatment depends on its technical applicability, plant simplicity and cost-effectiveness (Kurniawan et al., 2006), and in the near future, systems based on nanotechnology would offer a cost-effective alternative to solving water pollution problems.

3.4   CONCLUSIONS

Nitric acid oxidation of three different types of carbon nanotubes attaches acidic oxygenated groups to their surface. Morphology as well as doping of carbon nanotubes determines the extent of the surface modification: SWNT are the most reactive followed by CNx and MWNT. Ox-SWNT have the highest concentration of total acidic sites and in consequence their cadmium adsorption capacity is about three and six times higher than that for ox-CNx and ox-MWNT, respectively. In contrast, ox-SWNT present the slowest adsorption rate because of the intraparticle diffusion effect through longer nanotubes which are highly entangled.

Fitting of adsorption kinetic data by using the pseudo-second order model showed that the operating time to adsorb 95% of cadmium ($t_{0.95}$) is about 14, 30, 120 and 90 minutes for ox-CNx, ox-MWNT, ox-SWNT and non-porous FeOOH respectively. The longest time period to attain equilibrium in ox-SWNT suggests intraparticle diffusion in the adsorption mechanism. The external mass transfer model did not fit well the experimental data. Theoretical k_L calculated by the external mass transport

is about 4000, 17000, 300 and 1700 times higher for ox-CNx, ox-MWNT, ox-SWNT and non-porous FeOOH, in relation to the experimental k_L obtained at an initial cadmium concentration of 4 mg/L, pH 6 and 200 rpm; thus external mass transfer is not the rate-limiting step.

The intraparticle diffusion model better fitted the experimental kinetic data than the external mass transfer model, mainly in the slow stage. The obtained D_{ep} were lower than the bulk diffusivity of cadmium in water only for modeling single nanotubes: 2.4E-11, 4.2E-9 and 1.1E-9 cm^2/s, for ox-SWNT, ox-CNx and ox-MWNT, respectively, at initial cadmium concentration of 4 mg/L, pH 6 and 200 rpm, suggesting that intraparticle diffusion could be the rate limiting step. The tortuosity is higher than 10 for all cases suggesting that tiny pores restrain cadmium diffusion to adsorption sites as well as limitations of the model.

The best fitting of predicted decay concentration curves to the experimental data resulted by using the intraparticle diffusion model, because more variables were included. Even high values for tortuosities might indicate the high complexity of adsorption through single carbon nanotubes.

CHAPTER 4

Carbon Nanotube-Based Composites for Adsorption of Toxic Metals from Aqueous Solution

Abstract

Composites of oxidized nitrogen-doped multiwall carbon nanotubes (ox-CNx) supported on polyurethane were prepared at ambient conditions. Carbon nanotubes loads of 1% to 7% by weight were synthesized, with or without carboxylated SBR as an additive, in order to obtain a composite with the highest cadmium adsorption capacity. Since the obtained composites were designed to be used in water treatment systems, their morphological and physicochemical properties were evaluated by several techniques, which include acidic sites concentration and cadmium adsorption capacity. The best obtained composites had a nanotube loading of 2.5% (composite C1) and 1% plus 5% SBR (composite C3). The maximum cadmium adsorption capacity, q_m, of C1 and C3 was 0.016 and 0.22 mg/g, respectively. Dynamic adsorption tests were conducted in bed-packed columns with C1 and C3; a cadmium solution of 0.3 mg/L at pH 6 was fed at 3 BV/h. About 7 BV were processed before bed saturation. The bed adsorption capacity of the composite C3 was 5.4 μg/ g, two times higher than for the composite C1. Consecutive cycles of adsorption-desorption suggested that the obtained composites are a safe support for carbon nanotubes and their application in water treatment. Further research is required to support ox-CNx or other carbon nanoparticles in a safe way to preserve their adsorptive properties.

4.1   INTRODUCTION

Nanoscience development has prompted a technological revolution. Less than twenty years of active research in different knowledge areas has resulted in the rapid growth of consumer products containing engineered nanoparticles (ENP), that is, manufactured particles with at least one dimension below 100 nm. Among others, ENP include carbon-based materials (fullerenes, nanotubes and fibers), for which a wide variety of products and processes are being investigated (Terrones 2003; 2004; Terrones et al., 2008).

Promising applications for carbon nanotubes would include devices for water decontamination systems, such as membranes and filters, since their small and uniform pore sizes constitute an advantage over activated and porous carbons, traditionally used in water purification (Srivastava et al., 2004; Savage and Diallo, 2005; Noy et al., 2007; Mauter and Elimelech, 2008; Pan and Xing, 2008; Theron et al., 2008). Although nanotube-based filters are still far from commercial products and their development could take several years (Endo et al., 2008), general advances in adsorption have shown that carbon nanotubes of different types (single wall, multiwall, nitrogen-doped, etc) have a higher adsorption capacity than activated carbon to adsorb a wide variety of toxic pollutants present in aqueous solution (Li et al., 2002; 2003 a; b; c; 2005; 2006; 2007; Liu et al., 2004; Chen and Wu, 2004; Chen and Wang, 2006; Kandah and Meunier, 2007; Stafiej and Pyrzynska, 2007; Wang et al., 2007 a; b; c; Andrade-Espinosa et al., 2008; El-Sheik, 2008; Gao et al., 2008; 2009; Lu and Chiu, 2006; 2008; Hu et al., 2009; Perez-Aguilar et al., 2010; Pillay et al., 2009; Yang et al., 2009).

At the same time, increasing concern over the potential release of ENP has motivated the investigation of the health and environmental impact of these nanomaterials. Once a nanoparticle is introduced into the water environment, there are many processes that might affect their fate, including partitioning to sediment and suspended particulate material, biological and/or abiotic degradation

96

(Hassellöv et al., 2008; Tiede et al., 2008; 2009; Tsai and Pui, 2009). Moreover, the use of nanoparticles in the treatment of water is likely to result in direct emissions to surface and groundwater or soil; hence it is almost inevitable that humans will be exposed to ENP (Boxall et al., 2007).

Preventing human health repercussions from the release of carbon nanotubes to the environment should motivate a search for a safe way to support carbon nanotubes before their use in water treatment systems. Additional benefits would be an economic cost process through the large-scale application of nanotubes and their regeneration and use during several cycles (Weber, 2002; Savage and Diallo, 2005; Shannon et al., 2008).

Polymeric matrices are an alternative to the effective support of carbon nanotubes. In fact, composite reinforcement with these materials is one of the most investigated areas nowadays (Tománek et al., 2008). The main challenge for integration of carbon nanotubes to the polymer is to achieve a uniform dispersion, since high aspect ratios combined with high flexibilities increase the possibility of nanotube entanglement and close packing (Vaisman et al., 2006).

A wide variety of polymeric materials have been used to prepare composites with carbon nanotubes; however, for application as filter media, chemical and mechanical resistance is required. Polyurethane foams have these features as well as a tortuous open cell structure that physically retains small particles (Billmeyer, 1984; Evans 1993).

Granular activated carbon has been supported in polyurethane foams to be used as filters for the purification of air streams; moreover, this type of filters is already used in many air filtering systems (Pinto et al., 2004; 2006). A first attempt to support carbon nanotubes in a polymeric matrix to use the obtained composite as adsorbent of organic pollutants in liquid phase was reported by Salipira et al. (2007). The composites were prepared with polyurethane, cyclodextrin and oxidized MWNT at loadings from 1% to 5% by weight, and tested to remove *p-*

nitrophenol and trichloroethylene from aqueous solution; the obtained efficiencies were higher than 95%.

So far, there are no reports regarding the support of carbon nanotubes to adsorb inorganic pollutants from aqueous solutions. The objective of this study is to support ox-CNx in polyurethane to evaluate their adsorption performance in bed-packed columns through cycles of adsorption-desorption. Oxidized nitrogen-doped carbon nanotubes (ox-CNx) were selected to be supported, because they showed higher cadmium adsorption capacity than oxidized multiwall carbon nanotubes (ox-MWNT) and faster adsorption kinetics than oxidized single-wall carbon nanotubes (ox-SWNT) and ox-MWNT.

4.2   EXPERIMENTAL

4.2.1   Materials and Synthesis of Carbon Nanotube-Based Composites

Nitrogen-doped carbon nanotubes (CNx) synthesized by chemical vapor deposition were oxidized with nitric acid solution as previously detailed (Perez-Aguilar et al., 2010). Then, oxidized nanotubes (ox-CNx) were supported in polyurethane foam through a one-step reaction at ambient conditions: 1 g of 4,4'-methylene-bis(phenylisocyanate) (MDI, from Bayer Company) was mixed with deionized water (1% w/w) and dimethyl-amine (1% w/w) as a catalyst in a glass vessel; about 20 seconds later ox-CNx were added in continuous mixing. The composite was cured for 24 h at room temperature and then washed with deionized water and dried at 60 °C for 48 h before its use.

In addition, some samples were prepared with carboxylated styrene-butadiene rubber (SBR at 5% w/w) as additive. Previous tests (not reported here) showed that a composite with 5% in SBR had higher cadmium adsorption capacity than those prepared with polyethylene-glycol (PEG) or carboxylated polyacrylic-acid (PAA).

From several obtained composites at different nanotube loadings, the more relevant results are reported here, which correspond to composites with nanotube

loadings of 2.5% and 5% by weight, identified as C1 and C2, respectively, and one containing SBR and a nanotube loading of 1% by weight identified as C3. Also the polymeric matrices were tested; these were identified as PU and PU-SBR, respectively.

4.2.2 Characterization of Carbon Nanotube-Based Composites

The morphology of the obtained composites was observed by scanning electron microscopy (SEM) by a UHRSEM FEI XL30 field emission microscope operating at 10 kV. The composite cross-sections were attained by brittle fracture in liquid nitrogen, and then spraying gold particles on their surface was carried out before analysis. Physicochemical characterization of the composites included BET surface area by nitrogen adsorption with a Micromeritics ASAP 2010 analyzer. The solid density (ρ_s) was determined by the helium displacement method using a helium pycnometer Micromeritics Accupyc 1330.

The probable interaction between nanotubes and polyurethane was analyzed by infrared spectroscopy by attenuated total reflectance (ATR-FTIR) in a Nicolet 6700 FT-IR spectrophotometer, at 28 scans in the frequency interval of 4000cm^{-1} to 650cm^{-1} with resolution of 4 cm^{-1}. Also Raman spectra were collected in the range of 100 cm^{-1} to 3500 cm^{-1}, by using an inVia Raman Renishaw system at 632.8 nm wavelength excitation, 0.39 mW laser intensity and 30 s time exposures. Thermo-gravimetric analyses (TGA) were performed by a Thermo Cahn model VersaTherm instrument: samples were heated from 30 °C to 600 °C at a heating rate of 10 °C/min in nitrogen atmosphere (12 mL/min). The thermal properties of the composites were determined with a Perkin-Elmer instrument by differential scanning calorimetry with two successive cycles of cooling-heating from 25 °C to -150 °C, then to 220 °C, at a rate of 10 °C /min.

The total acidic sites concentration of the composites was quantitatively measured by the Boehm's titration method as follows: 0.03 g of sample were immersed in 30 mL of 0.01 M sodium hydroxide solution and stirred at 25 °C in a sealed vessel for 7 days. After this time, the suspensions were filtrated and aliquots were titrated

with 0.01 M hydrochloric acid. The concentration of acidic sites was calculated as the difference between the initial and final concentration of base solution.

The point of zero charge (PZC) of the composites was determined by titration as previously described in Chapter 2, by using samples of 0.03 g in 29 mL of 0.05 M sodium chloride solution, the total volume was adjusted to 30 mL with 0.01 M hydrochloric acid or sodium hydroxide solutions to reach a final pH in the range of 2 to 10.

4.2.3 Adsorption Equilibrium Experiments

The cadmium adsorption capacity of the obtained composites was determined by equilibrium experiments following the procedure described in Chapters 2 and 3, by using samples of 0.03 g in 30 mL of solutions at pH 6 and 25 °C. Then dynamic adsorption tests were performed in polycarbonate columns coated with Teflon, with an internal diameter of 2.5 cm. Before being packed the composites (3 g to 6 g) were fragmented into particles of about 1 mm in diameter and immersed in deionized hot water to eliminate the air in their pores. The cadmium initial concentration at the inlet was 0.3 ± 0.1 mg/L at pH 6 and was pumped at 3 BV/h. Samples at the effluent were collected by an automatic fraction collector and then their cadmium concentration was determined by atomic absorption spectrometry (AAS). The cadmium retained by the composite was calculated by using the equation 4.4:

$$q_e = \frac{\sum_{i=1}^{n} (C_0 - C_i)V_i}{m}$$

(4.4)

Two consecutive cycles of adsorption-desorption were conducted, with a rinse step between each process to neutralize the pH of the composite.

4.3   RESULTS AND DISCUSSION

4.3.1 Synthesis and Characterization of Carbon Nanotube-Based Composites

Oxidized nitrogen-doped carbon nanotubes (ox-CNx) supported in polyurethane showed approximate dimensions of 40 nm in outer diameter and 70 μm in length, as determined by SEM. Agglomerates of nanotubes were disaggregated mainly at their tips, as a result of surface oxygenated groups attached during acidic oxidation (Fig. 4.1a). On the other side, polyurethane foam showed its characteristic macroporous open cell structure (Fig.4.1b), created by the evolution of carbon dioxide bubbles as the foam sets into a rigid structure (Evans, 1993); furthermore, the morphology of the surface was regular and smooth.

The surface oxygenated groups of carbon nanotubes favored their dispersion into the polymeric mixture to obtain the composites with polyurethane. However, the matrix enclosed the nanotubes and the surface of the obtained composites became roughness and irregular (Fig. 4.1c). As a consequence, a major reduction in the foaming and flexibility of the structure of the composites was observed when increasing the nanotube loading: the composite C1 with 2.5% nanotubes loading showed lower flexibility than the one observed for PU, while the composite C2 with 5% nanotube loading showed a stiff structure with few macropores.

Higher magnifications of the surface fracture of the composites showed that carbon nanotubes were pulled out from the polymeric matrix, suggesting weak interaction in the interface and that nanotubes might be physically bonded to the matrix (Fig. 4.1d, e). Nevertheless, just some tips of carbon nanotubes were exposed as could be observed from the image of the outer surface of the composite C2 (Fig. 4.1e inset).

In addition, SBR changed the morphology of the composite C3, which showed segregated granular sections from the additive while dispersion of carbon nanotubes was heterogeneous (Fig.4.1f). This effect might occur as a result of

poor interaction between the carboxylic groups in SBR chains and those on the surface of nanotubes.
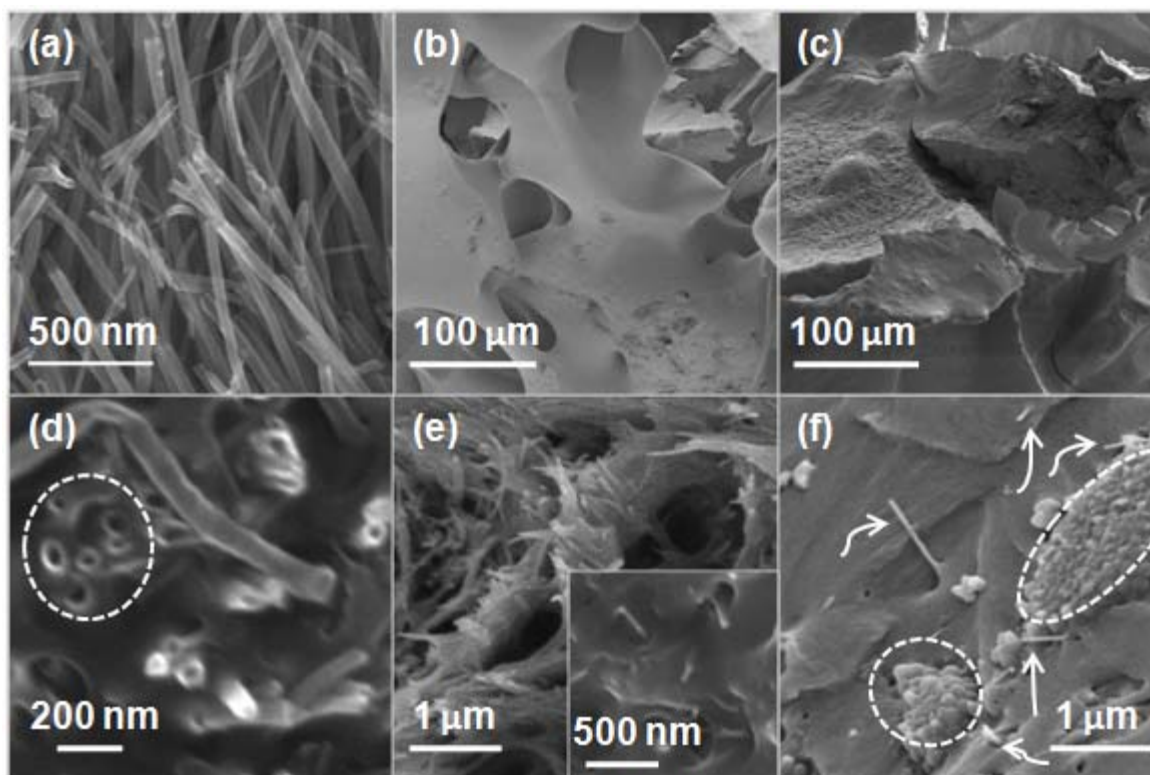
Fig. 4.1   SEM images show (a) oxidized nitrogen-doped carbon nanotubes (ox-CNx) before being supported; surface fracture of (b) polyurethane foam matrix; (c) the composite C1 with nanotube load of 2.5%; (d) holes caused by the extraction of carbon nanotubes (dotted circles) in the composite C1; (e) the composite C2 with nanotube load of 5%, and outer surface of the composite (inset); (f) segregated sections of SBR (dotted circles) and carbon nanotubes (arrows) in the composite C3 with nanotube loading of 1% plus 5% SBR.

Polyurethane is composed of long flexible "soft" segments alternating with "hard" urethane-based segments. The group urethane (-NHCOO-) is formed through the reaction of a diisocyanate and a glycol. In some cases excess isocyanate (NCO) groups are present in the polymer mixture, reacting with water to produce carbon dioxide, which through inflation create the foamy material, that at the same time

reacts with the active hydrogen of the ureas to form biuret crosslinks as the general reactions shows (Billmeyer 1984; Rubner 1986; Evans 1993):

$$RNCO + H_2O \rightarrow [RNHCOOH] \rightarrow RNH_2 + CO_2^{\uparrow} \qquad (4.1)$$

$$R'NCO + RNH_2 \rightarrow RNH(CO)NHR' \qquad (4.2)$$

For an overall reaction:

$$2\ RNCO + H_2O \rightarrow RNH(CO)NHR + CO_2 \qquad (4.3)$$
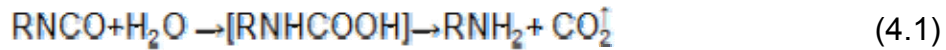
The modification of the foam structure by nanotubes could occur during polymerization: after addition of nanotubes the viscosity of the mixture increased quickly due to chemical interactions between surface groups of nanotubes and polymer chains. In similar form as the equations 4.2 and 4.3 describe, the excess NCO groups probably react with active hydrogen of carboxylic groups on the surface of ox-CNx, leading to linkage formation. This reaction is well known to occur with carbon black, frequently used as filler to improve mechanical properties of polyurethane-based products, and with activated carbon supported into polyurethane foams (Evans, 1993; Pinto et al., 2004; 2006), it was also suggested by Salipira et al., (2007) for reaction between polyurethane and oxidized MWNT. Besides formation of linkage with isocyanate group, carboxylic groups of carbon nanotubes could form hydrogen bonds with polyurethane chains, improving the dispersion of nanotubes in the polymeric matrix (Lachman et al., 2009).

The addition of carboxylated SBR to the polymeric mixture prior to carbon nanotube, could produce a reaction between hydrogen of carboxylic groups in SBR with isocyanate groups of polyurethane; thus chemical interactions between nanotubes and polyurethane might be reduced. Moreover, some carboxylic groups of SBR might remain free to act as adsorption sites.

As a result of chemical interaction between nanotubes and polyurethane, generation of CO_2 was insufficient for bubbles growing and foaming. In addition,

CO_2 absorption by nanotubes could also occur (Evans, 1993). The effect of nanotubes on polyurethane foaming was evident by the reduction in the specific surface of the composites, as determined by nitrogen physisorption. However, this technique was not the most appropriate because the results were below the detection limit of the instrument. The BET surface of the obtained composites is reported in Table 4.1, as well as the results obtained for density, which showed a direct trend with the nanotube load. The trend observed for these data was in agreement with those observations made by Pinto et al., (2006), who reported the reduction in the BET surface of activated carbon particles (about 2mm in diameter) supported in polyurethane foams, from 1065 m^2/g to 860 m^2/g: this reduction might be explained because most of the surface area of activated carbon is inside the mesopores and micropores, where big polymer chains had no access.

Table 4.1   BET surface area and density of oxidized nanotubes, polyurethane matrix and obtained nanotube-based composites determined by nitrogen adsorption at 77 K and by helium displacement, respectively.

Sample	S_{BET} (m^2/g)	ρ (g/cm^3)
ox-CNx	74.0	2.24
PU	0.727	1.00
C1	0.143	1.16
C2	0.044	1.23
C3	0.115	1.05

Morphology is a key factor to explain the dispersion of fillers in a polymeric matrix and, in consequence, the performance of the obtained composite. One-dimensional carbon nanotubes can contact polymer chains along a line leading to enhanced particle interaction, but as nanotubes are packed into two-dimensional rope-like aggregates, the surface contact is enhanced. In contrast, three-dimensional particle of activated carbon touch at a point with the polymer chains;

hence, the effect of interfacial contact is lower and could permit higher loading of particles (Schaefer and Justice, 2007).

Characterization of the obtained composites by several techniques revealed different aspects of interaction between nanotubes and polyurethane. X-ray diffraction spectra (Fig.4.2) showed the occurrence of only a broad band amorphous centered at about 20° (2θ) for polymer matrices (PU and PU-SBR), as well as the composites. A separated phase due to carbon nanotubes was observed around 26° in the composites C1 and C2, but in C3 due to the nanotube load (1%) it was below the detection limit of the instrument.
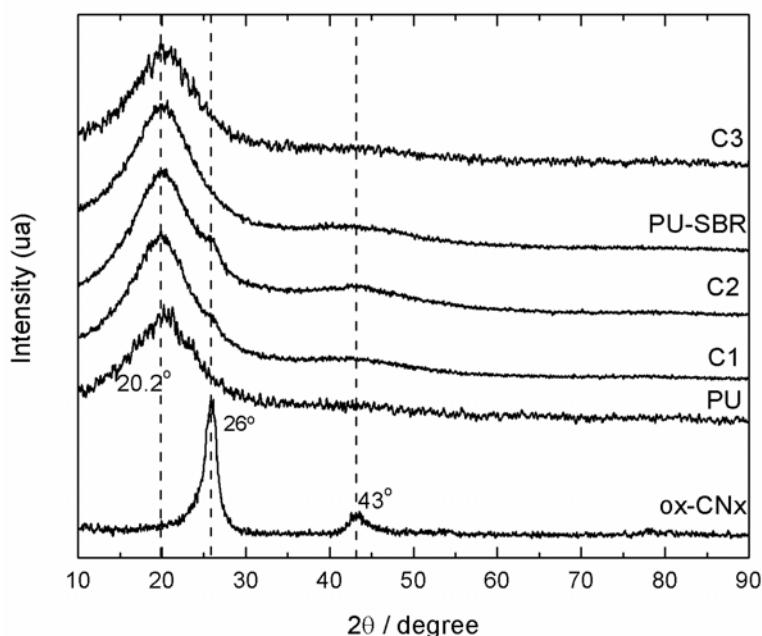
Fig. 4.2 XRD spectra for nitric acid oxidized carbon nanotubes, ox-CNx, polyurethane matrix (PU and additive containing PU-SBR), and obtained composites with nanotube load of 2.5% (C1), 5% (C2), and 1% (C3).

FTIR spectra provide more information about interaction between chemical groups of the matrix and the nanotube surface (Fig. 4.3). It is possible to say that polymerization of isocyanate groups was completed because the band in 2240 cm^{-1} was absent in the spectra of the composites (Xiong et al., 2006). Also, the broad band from 3600 to 3200 cm^{-1} corresponding to carboxylic groups in ox-CNx was absent in the spectra of the composites. Instead, a band of medium intensity was

observed with peaks at 3340 cm^{-1} and 3300 cm^{-1} due to N-H stretching of urea and amide bondings, respectively. Moreover, carbonyl bonding in urethane (1729 cm^{-1}) and urea (1659 cm^{-1}) observed in the spectra of composites (Rubner, 1986; Bassi et al., 2003; Xiong et al., 2006; Jung et al., 2007) might indicate the interaction of polymer chains with nanotubes.
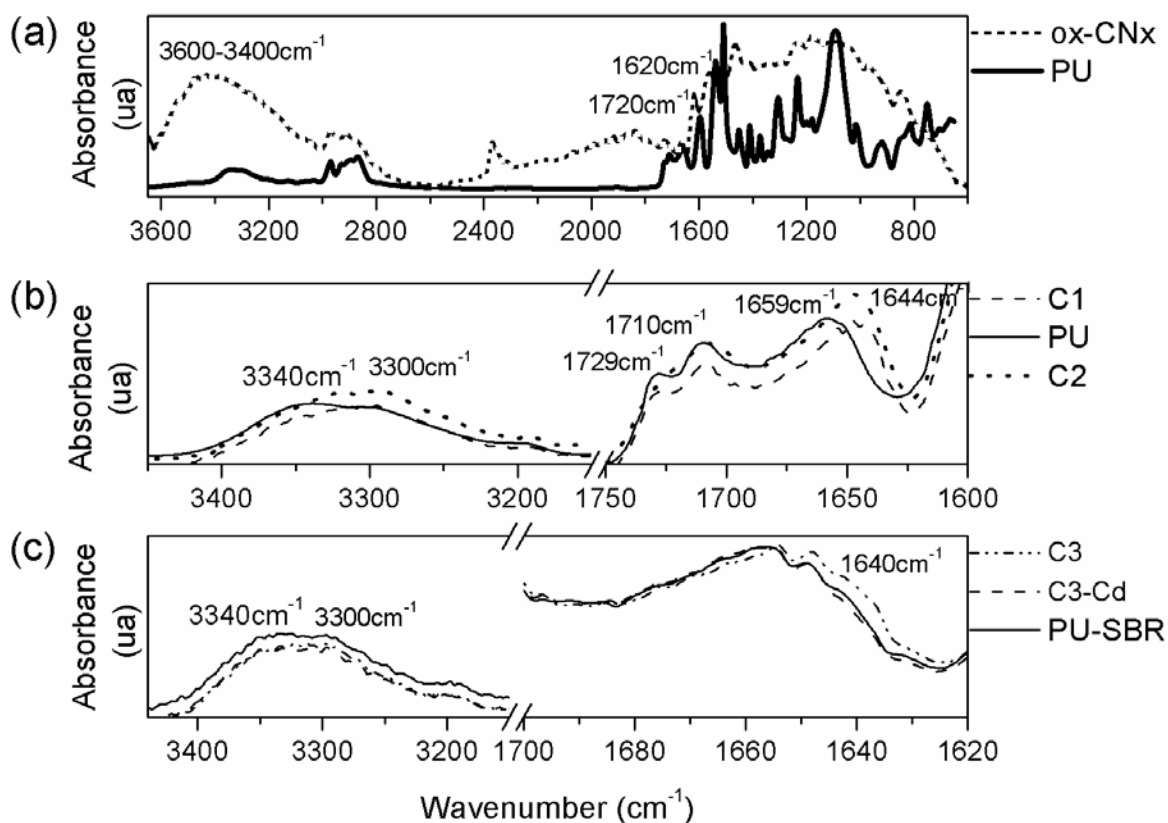
Fig. 4.3 FTIR spectra obtained by attenuated total reflectance (ATR) for (**a**) oxidized carbon nanotubes (ox-CNx) and polyurethane matrix (PU), (**b**) PU and obtained composites with nanotube load of 2.5% (C1) and 5% (C2), and (**c**) PU-SBR matrix and obtained composite with nanotube load of 1% (C3); C3-Cd is the spectra for cadmium adsorbed onto composite C3.

Comparison between spectra of cadmium exhausted composite C3 (C3-Cd) with those obtained for C3 and for PU-SBR, showed that intensity of bands in 1710 cm^{-1} and 1640 cm^{-1} decreased in the C3-Cd spectra until they overlapped with the PU-

106

SBR, suggesting the presence of carboxylic sites on nanotubes available for cadmium adsorption.
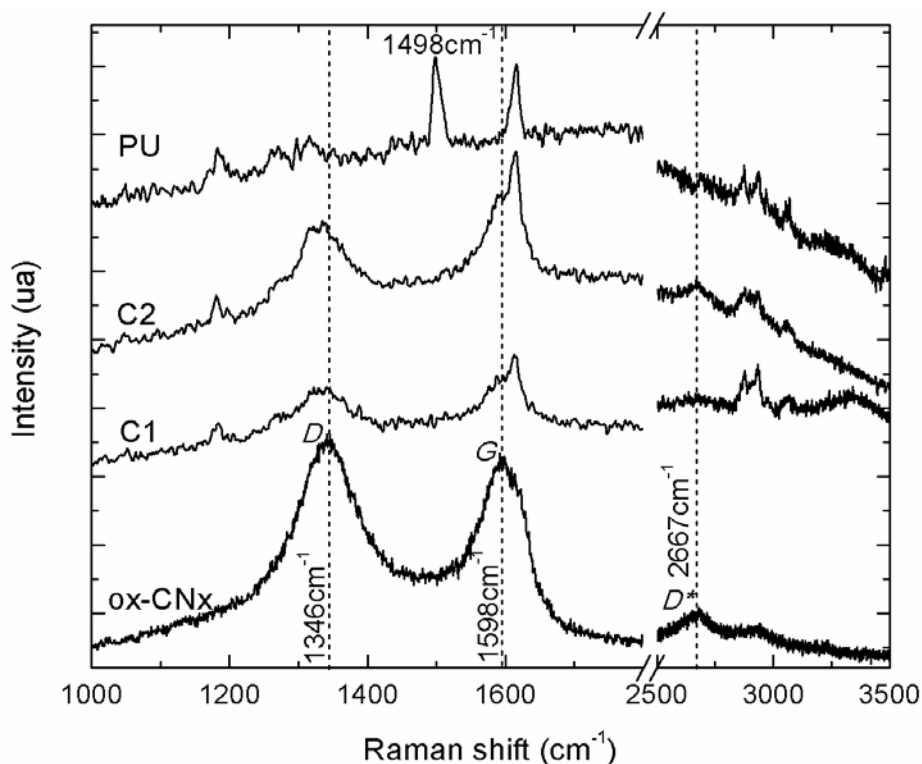
Fig. 4.4 Raman spectra at 632.8 nm excitation wavelength of oxidized nanotubes (ox-CNx), polyurethane matrix (PU) and the obtained composites with nanotube load of 2.5% (C1) and 5% (C2).

Raman spectra of the composites (Fig.4.4) showed a broad fluorescent background caused by extensive disordering of amorphous segments of polyurethane; this effect decreased at higher loading carbon nanotubes. A Raman feature of carbon-carbon double bond of the conjugated backbone is found around 1498 cm^{-1} (Rubner, 1986); this feature was evidenced only in PU and PU-SBR spectra but disappeared in those for the composites, indicating a probable interaction between the nanotubes and the matrix. Moreover, characteristic D and G bands of carbon nanotubes were observed at 1346 cm^{-1} and 1598 cm^{-1}, respectively. These bands were observed as shoulders in the spectra for composites, which were overlapped by polyurethane bands near 1330 cm^{-1} and

1610 cm^{-1}. This means that supported nanotubes were exposed in a certain way, and that is why they appeared in the spectra.

Thermal gravimetric analysis (TGA) was performed to determine the thermal stability of the obtained composites. The thermograms are presented in Fig. 4.5. Both series of composites showed different behavior in thermal stability. In comparison with PU matrix, composites C1 and C2 showed a shift toward lower temperature decomposition. In addition, derivative thermal curves showed that decomposition of PU matrix occurred at a maximal degradation rate of about 270 °C. Meanwhile thermal decomposition of composites occurred in two steps: the first one with a maximal degradation rate of about 210 °C, and the second one near 255 °C and 260 °C for C1 and C2, respectively. These steps were 15 °C and 10 °C lower than for the PU matrix. In contrast, composite C3 decomposed at a higher temperature in relation to PU-SBR matrix. Two stages were observed: the first about 205°C and 210 °C and the second nearly 250 °C and 255 °C for PU-SBR and C3, respectively. This behavior was in agreement with values reported for polyurethane composites with a multiwall carbon nanotube load of 5%: their thermal stability was improved in about 6 °C probably as a result of linkage between nanotubes and polymer chains (Jung et al., 2006; Xiong et al., 2006; Salipira et al., 2007).

Thermal decomposition of polyurethane-carbon nanotube composites in two steps might occur due to long amorphous and short crystalline segments of polyurethane chains, respectively (Jung et al., 2006). For the case of the composite containing additive, the maximal degradation rate was shifted to lower temperatures because of a dilution effect as well as the chemical structure of SBR, where the carbon-carbon double bond of butadiene is of low thermal resistance (Billmeyer, 1984). However, the stronger structure of carbon nanotubes had a reinforcement effect in the composites as observed by the increase in their temperature of degradation.
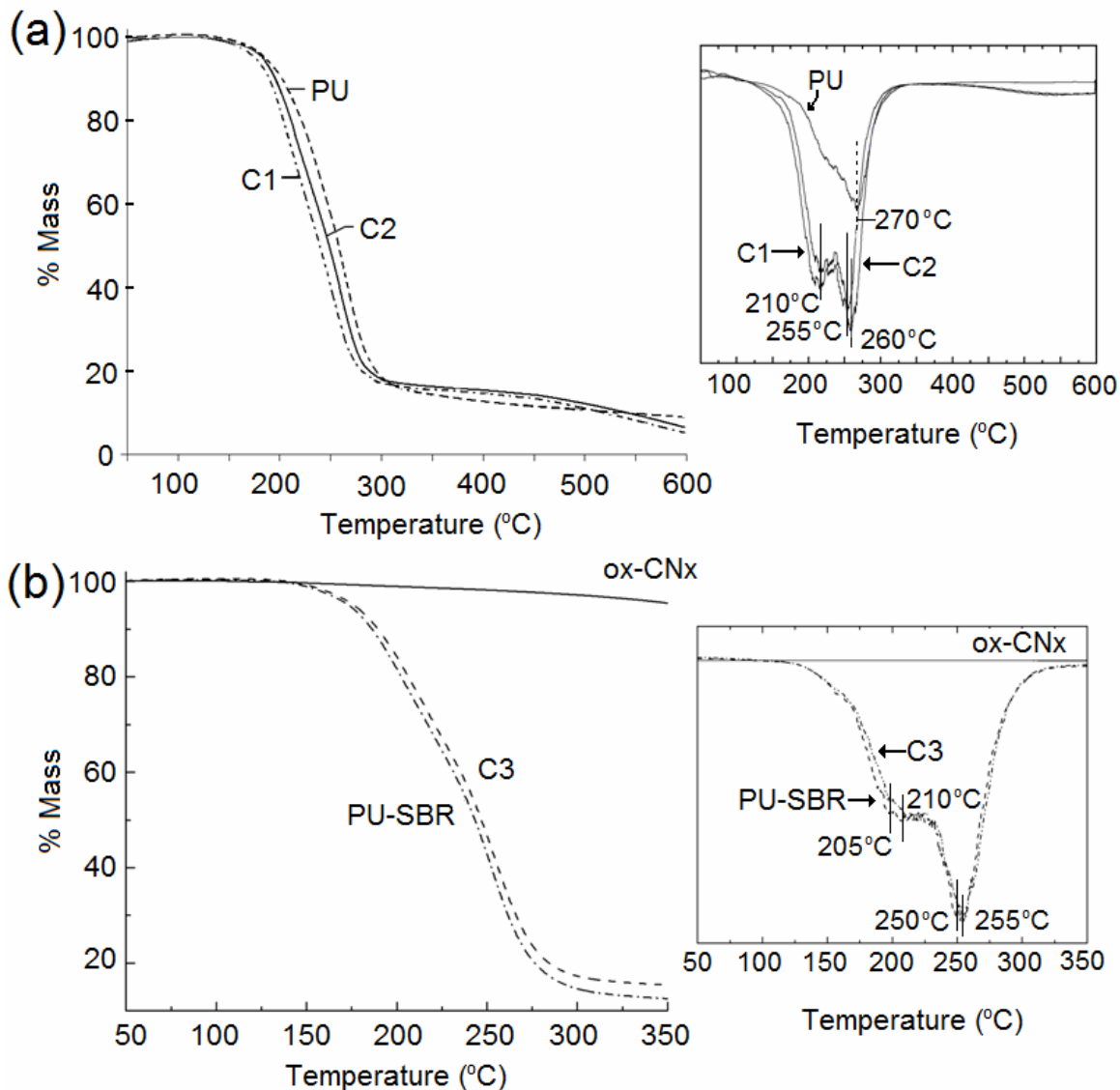
Fig. 4.5 Thermograms for (a) polyurethane matrix, PU and composites C1 and C2 with nanotube loads of 2.5% and 5%, respectively; and (b) PU-SBR matrix, oxidized nanotubes (ox-CNx) and composite with a nanotube load of 1% (C3). Insets show DTA analyses for each sample.

The effect of interaction between polyurethane chains and surface groups of nanotubes also might be observed from results of differential scanning calorimetry (DSC). Results reported in Table 4.2 confirmed the interaction between carbon nanotubes and polymer chains, probably a reinforcement effect due to hydrogen bonding between hard segments of polyurethane with nanotubes, and the

109

entanglement of long polymer chains wrapping the nanotubes. Since T_m is related to the disappearance of a polymer crystalline phase at the melting point, it means that order segments of the sample gain mobility with energy increasing while physical properties changes (Billmeyer, 1984). T_m of composites increased about 5.5 °C and 2.6 °C for C1 and C2 respectively in relation to PU, suggesting better interfacial contact at smaller loads of nanotubes, indicating a better dispersion. For the case of the composite C3 and the matrix PU-SBR, T_m values were considerably lower than those without additive due to SBR, but even a reinforcing effect was caused by the nanotubes because T_m increased 4.1 °C.

In contrast, T_g is related to the mobility of the backbone in polyurethane; it decreased 2.4 °C and 2.1 °C for C1 and C2, respectively, in relation to PU, and only 0.5 °C for C3 in relation to PU-SBR. Likewise, this tendency could be due to the nanotube load, but the smallest effect in T_g shown for C3 suggested a poor interaction between SBR segments and nanotube surfaces. The observed trends were in agreement with those reported in the literature. For example, a significant increase in the T_g from 5.7 °C to 21.6 °C at 5% of nanotubes loading was reported by Xiong et al., (2008); this behavior was attributed to the existence of crosslinking nanotubes inside the matrix where the chain mobility becomes difficult under such conditions.

Table 4.2 Glass transition temperature (T_g) and melting temperature (T_m) of the obtained composites determined by differential scanning calorimetry (DSC)

Sample	T_g (°C)	T_m (°C)
PU	-56.8	64.7
C1	-59.3	70.2
C2	-58.9	67.3
PU-SBR	-58.6	36.5
C3	-59.1	40.6

As a result of the interaction between nanotubes and polyurethane, the total acidic sites concentration (SAT) of the obtained composites decreased significantly in relation to that for ox-CNx. SAT concentration of 0.046, 0.041 and 0.056 mmol/g for C1, C2 and C3, respectively, were far below 0.246 mmol/g, for ox-CNx. Besides, SAT for PU and PU-SBR were 0.076 and 0.038 mmol/g, respectively. SAT concentration of PU was nearly two times higher than C1 and C2. In contrast SAT concentration of C3 was 1.5 times higher than PU-SBR, a differential which suggested that the additive reduced the interaction between nanotubes and polyurethane chains.

Carbon nanotubes shifted the pH at the point of zero charge (pH_{PZC}) of the composites toward lower values in contrast with the polyurethane matrix, from 7.4 to 5 for PU and C1, and from 5.7 to 5 for PU-SBR and C3. These properties govern the behavior of the obtained composites in the adsorption of metal ions in aqueous solution.

4.3.2 Adsorption Behavior of Carbon Nanotube-Based Composites

4.3.2.1 Cadmium Adsorption Capacity of Carbon Nanotube-Based Composites

The cadmium adsorption capacity of the obtained carbon nanotube-based composites was determined at pH 6 and 25 °C. The polyurethane matrix was also tested to find out its adsorption properties. The Langmuir model was used to fit the experimental adsorption data: the isotherm parameters for each sample are presented in Table 4.3, and the adsorption isotherms are reported on Fig.4.6. The maximum cadmium adsorption capacity, q_m, of the obtained composites was far below than the one for the unsupported nanotubes. Even the polyurethane matrix had 8, 50 and 6 times higher cadmium adsorption capacity than the composites C1, C2 and C3, respectively. This trend was in agreement with SAT concentration.

Table 4.3 Langmuir isotherm parameters determined for cadmium adsorption onto nanotube-based composites, at pH 6 and 25 °C

	q_m (mg/g)	b (L/mg)	[a]R^2
[c]ox-CNx	11.995	0.512	0.932
PU	1.24	0.121	0.984
C1	0.163	0.107	0.979
C2	0.024	0.356	0.969
C3	0.218	0.038	0.987

[a]*Correlation coefficient for this data*
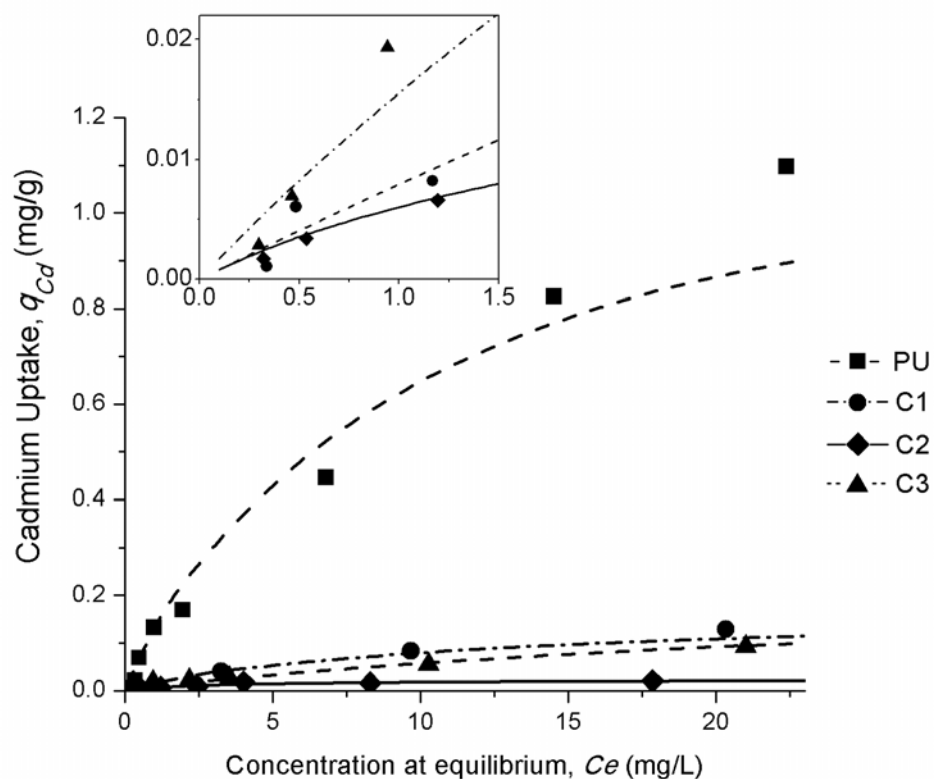
Fig. 4.6 Cadmium adsorption isotherms at pH 6 and 25 °C adjusted by Langmuir model, determined for polyurethane matrix (PU) and composites with nanotube load of 2.5% (C1), 5% (C2) and 1%+SBR (C3). The inset shows isotherms at low concentration.

4.3.2.2 Cadmium Adsorption Tests in Packed Column with Carbon Nanotube-Based Composites

Based in the results of adsorption at equilibrium, composites C1 and C3 were packed in columns to evaluate their performance in an approaching scenario for their intended application. Fixed-bed adsorption systems have been widely used to treat drinking water as well as wastewater to remove hazardous components. The information obtained from column tests is usually represented by breakthrough curves, plotting the percentage of the adsorbate outlet and inlet concentrations against the service time of the column (Cooney, 1999; Ko et al., 2001).

The slope and position of the breakthrough curves is determined mainly by the mass-transfer coefficient and the bed adsorption capacity, respectively (Cooney, 1999). In this study the bed adsorption capacity was calculated by using overall mass balances on the column from the area above the breakthrough curve.

On the basis of the approximate assumption that the S-shaped breakthrough curve is symmetrical at about 50% breakpoint, the bed capacity is normally found by the equation:

$$q_e = \frac{c_0 Q t^*}{m}$$

(4.5)

Where t^* corresponds to the time at which the effluent concentration is one-half of the feed concentration, that means the service time at 50% breakthrough (Ko et al., 2001).

Two empty bed contact times (EBCT) were tested to select the operation time at which better bed adsorption capacity was obtained. From these results an EBCT of 20 min was selected for experiments of adsorption and desorption. The experimental conditions for each experiment are reported in Table 4.4, and the results regarding volume processed of cadmium solution, cadmium mass balances and bed adsorption capacity are reported in Table 4.5. The breakthrough curves obtained for these experiments are presented in Fig. 4.8 and 4.9.

Table 4.4 Experimental conditions for dynamic adsorption tests in bed-packed columns with composites C1 and C3, for cadmium adsorption in aqueous solution

	Mass packed (g)	Bed Volume (cm^3)	Influent flow rate, Q (cm^3/min)	EBCT (min)	Influent Cd concentration (mg/L)
Composite C3, loading nanotubes 1% + SBR					
Run 1	3.46	33.9	3.4	10	0.238
Run 2	3.46	33.9	1.7	20	0.178
Run 3	3.46	33.9	1.7	20	0.343
Run 4	3.46	33.9	1.7	20	0.307
Run 5	3.46	33.9	1.7	20	0.313
Composite C1, loading nanotubes 2.5%					
Run 6	6.0	45.7	2.3	20	0.438
Run 7	6.0	45.7	2.3	20	0.261

Table 4.5 Dynamic adsorption tests for composites C3 and C1 until bed saturation. Influent cadmium solution at pH 6 and room temperature (22 ± 3 °C)

	Volume Passed (BV)	Cadmium mass balance			Bed adsorption capacity
		Influent (µg)	Effluent (µg)	Adsorbed (µg)	Experimental q (µg/g)
Composite C3, loading nanotubes 1% + SBR					
Run 1	5	40	24	16	4.7
Run 2	6.4	38	23	15	3.5
Run 3	8.4	97	67	30	6.1
Run 4	7.4	77	51	26	5.4
Run 5	6.4	68	44	24	5.4
Composite C1, loading nanotubes 2.5%					
Run 6	4.9	114	68	46	3.4
Run 7	6.8	63	44	19	2.3

The bed adsorption capacity calculated from column tests showed a discrepancy with the one calculated at equilibrium, since experimental data followed an inflexion trend or s-shape at low concentration as can be seen in the inset of Fig. 4.6. Breakthrough curves for runs 1 and 2 showed saturation of C3 after 5 and 6.4 bed volumes passed (BV), respectively, in other words a 30% longer life when the EBCT increased 10 minutes (Fig. 4.7). The lower slope of the breakthrough curve for run 2 might indicate a better contact between the solution and the composite. Ideally longer residence time could permit the adsorbate to diffuse deeper into the adsorbent particle thus utilizing a higher fraction of the bed adsorption capacity (Basmadjian, 1997; Cooney, 1999). However, the bed adsorption capacity was different between both runs because they were conducted under different experimental conditions.
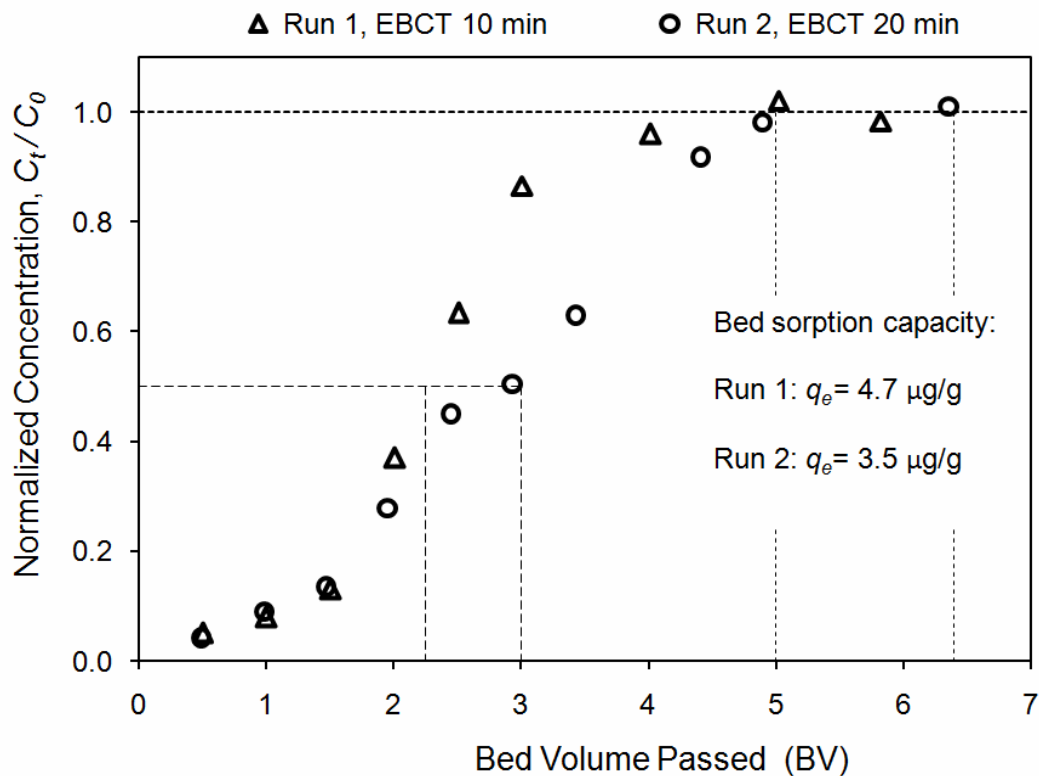
Fig. 4.7 Cadmium breakthrough curves obtained for composite C3 at EBCT of 10 min (Run 1) and 20 min (Run 2). Initial concentration of 0.238 and 0.178 mg/L, respectively, at pH 6 and room temperature.

Experiments of consecutive cycles of adsorption-desorption showed that it was possible to regenerate exhausted composites while keeping their adsorption capacity (Fig. 4.8). This behavior suggested that the composites developed in this research can be used in packed columns without liberating carbon nanotubes to the effluent. It means that nanotubes were well supported by the polymeric matrix due to physical and chemical interactions, as the characterization results previously showed.
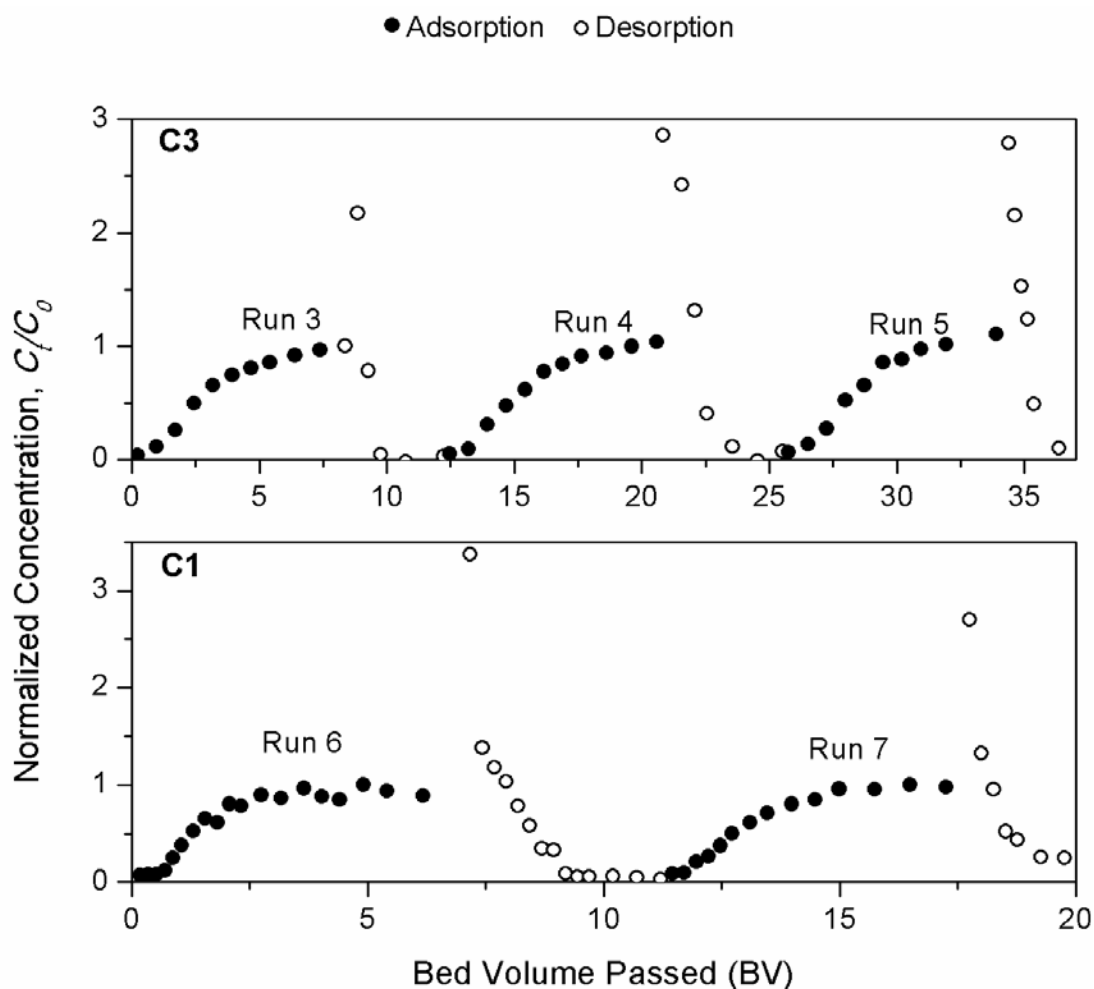
Fig. 4.8 Consecutive Cd^{2+} breakthrough curves and adsorption/desorption processes using nanotube-based composites packed in a column. Composites C1 and C3 with nanotube load of 2.5% and 1% + SBR, respectively. Cadmium influent at 0.3 ± 0.1 mg/L, pH 6, room temperature and 3 BV/h.

At first glimpse, the composite C3 had higher bed adsorption capacity and processed more volume solution than composite C1, before bed saturation. However, in a closer comparison between both composites, for example in runs 4 and 7 that used an influent cadmium concentration at 0.307 and 0.261 mg/L at 3 BV/h, the processed volumes were 7.4 and 6.8 BV respectively, almost the same. Nevertheless, the bed adsorption capacity for C3 was two times higher than for C1. This behavior is related to the stronger interactions in composite C1 than in composite C3 due to the additive SBR, which was helpful in making weaker interactions between polymer chains and carbon nanotubes. The contribution of the polymeric matrix to adsorption should not be neglected, as the SAT concentration and adsorption at equilibrium suggested.

The results obtained in this study suggested that composite C3 has some advantages over composite C1; besides its higher adsorption capacity, the economical cost due to lower carbon nanotube loading is the most expensive component in the composite. An estimation of the cost of the obtained nanotube-based composites, considering the cost of polymers as approximately 9 USD/Kg and 4500 USD/Kg for ox-CNx, is of 117, 225 and 47 USD/Kg, for C1, C2 and C3, respectively, or 137, 276 and 50 USD/m^3, in the same order. The cost followed a direct trend with carbon nanotube loading.

Certainly, more studies will be necessary to increase the carbon nanotube loading and to solve the supporting of these nanoparticles in composites before their application in water treatment. Preventing nanotube liberation into the environment and preserving the adsorptive capacities of carbon nanotubes in the composites should be the main objectives. Moreover, it is fundamental to understand the morphology of carbon nanotubes to develop nanotube-based adsorbents: aggregation of nanotubes, interfacial contact and chemical interaction with polymeric matrix are phenomena involved in the reduction of active sites for adsorption. Based on the results reported herein our perspective suggests alternative strategies, for example, to form large aggregates of nanotubes before

supporting them in the matrix in order to reduce contact surface and interfacial bonding. This measure could preserve active sites for adsorption.

4.4   CONCLUSIONS

Oxidized nitrogen-doped carbon nanotubes (ox-CNx) were effectively supported in a polyurethane matrix. Oxygenated groups such as carboxylic groups on the surface of nanotubes favor their dispersion onto the matrix, although physical and chemical interactions with polymer chains occur, and in consequence these groups were unable to act as adsorption sites for metal ions in aqueous solution. Several composites were obtained with nanotube loads of 2.5% (C1), 5% (C2) and 1% (C3). Nanotube loading higher than 2.5% increases the hardness of the composite.

Characterization of the nanotube-based composites by several techniques suggests the chemical interaction between surface oxygenated groups in the nanotubes and the polymer chains. As a consequence, the availability of surface adsorption sites in the supported nanotubes decreases significantly. The total acidic site concentrations of ox-CNx are 0.25 mmol/g, while for C1, C2 and C3, they are 0.05, 0.04 and 0.06 mmol/g, respectively. Besides, the cadmium adsorption capacity of ox-CNx is 11.9 mg/g and decreases to 0.16, 0.02 and 0.22 mg/g for C1, C2 and C3, respectively.

Adsorption dynamic tests performed with composites C1 and C3 in bed-packed columns, at residence time of 20 min, influent concentrations of 0.3 ±0.1 mg/L at pH 6 and 3 BV/h, are able to process about 7 BV. Even the bed adsorption capacity for C3 is 5.4 μg/g, two times higher than for C1. The advantages of composite C3 over C1 are, besides higher bed adsorption capacity, lower production cost due to the smaller nanotube loads.

Three and two consecutive cycles of adsorption-desorption tests in packed columns for C3 and C1, respectively, showed that the bed adsorption capacity

remains, suggesting that nanotubes are well supported in the polymeric matrix. The configuration of carbon nanotube-based composite could prevent the liberation of nanotubes into the environment, and allow their safe application in water treatment systems. Indeed more studies are necessary to support carbon nanostructures in polymeric matrices while preserving their adsorption capacity. Moreover, it is thought that this research has contributed to the development of nanostructure composites and their use in the water treatment field.

CHAPTER 5

General Discussion, Final Conclusions and Perspectives for Future Research

5.1   GENERAL DISCUSSION

Research and development of nanotechnology-based devices for water treatment systems can offer alternatives for solving water pollution caused by toxic heavy metals. Carbon nanotubes (CNT) are key elements in nanotechnology; their physical and chemical properties can offer advantages if are applied in water purification systems.

Early studies performed with oxidized MWNT and SWNT showed that these nanoparticles have higher adsorption capacities than activated carbons to remove toxic metals. Present research reports that oxidized CNx (ox-CNx) are also capable of adsorbing toxic metals from aqueous solution. Carboxylic groups on the surface of oxidized CNT contribute in great part to the maximum adsorption capacity for cadmium and lead in aqueous solution; FTIR spectroscopy showed the characteristic bands for carboxylic group around 1720 cm^{-1} and from 3600 cm^{-1} to 3300 cm^{-1}. The oxygen-containing surface groups attached to ox-CNx shifted the point of zero charge (pH$_{PZC}$) from pH 6.6 to pH 3.1 for ox-CNx (Fig. 2.6). The low pH$_{PZC}$ of ox-CNx means that at the pH of natural waters, their surface is negatively charged and can adsorb positively charged species, such as toxic metals. Adsorption isotherms determined at different pH values showed increasing adsorption capacity observed for cadmium and lead when the pH increased: this effect was related to the higher concentration of available carboxylic groups. The Langmuir model fitted well to experimental equilibrium data for lead adsorption, and the maximum adsorption capacities (q_m) were 0.083 mmol/g and 0.139 mmol/g at pH values 4 and 5, respectively. The experimental data for adsorption of

cadmium were better depicted by the Freundlich model: the values for parameter K were 0.083 mmol-L/g, 0.165 mmol-L/g and 0.192 mmol/L-g at pH 5, 6 and 7, respectively. ox-CNx had 1.8 times higher cadmium adsorption capacity at pH 5. The mechanism of adsorption of cationic species in aqueous solution can occur by electrostatic interactions and formation of complexes with carboxylic groups. Exhausted ox-CNx with metal ions can be regenerated and reutilized since more than 90% of the mass of both adsorbed metals was desorbed. The ox-CNx had higher affinity toward adsorption of lead than for cadmium, when both metals were in solution at pH 5 and 25 °C. At low concentration of both metals, there is enough concentration of acidic sites for adsorption of lead and cadmium, but as the concentration of both metals in solution increased, lead was preferentially adsorbed instead of cadmium. The dimension of these contaminants was not a decisive factor in selectivity, although the chemistry of each ion in solution was important, since their hydrated radii (r_H) was similar for both ions: $r_{H,Pb}$= 4.01 Å, $r_{H,Cd}$= 4.26 Å, thus both ions could reach the same adsorption sites mainly onto the outer surface. In relation to other carbonaceous adsorbents, cadmium adsorption capacity at pH 6 and 25 °C for ox-SWNT was 1.3 times higher than for ox-CNx, because the former had 1.8 times higher concentration of oxygenated groups. On the other hand, q_m for ox-CNx was 1.4 times higher than oxidized activated carbon Filtrasorb® 400 (ox-ACF).

Adsorption kinetic for CNT remains largely unexplored because nanotubes frequently are considered non-porous materials. In this study, cadmium adsorption kinetic was evaluated for three different types of carbon nanotubes (CNx, SWNT and MWNT). Dimensions of about 500 μm in length and 60 to 90 nm of external diameter were observed for ox-MWNT, and for ox-CNx 70 to 80 μm in length and 40 to 60 nm of external diameter. Ox-SWNT formed highly entangled structures and had an external diameter from 1 to 3 nm. Morphology and chemical structure determined the extent of the surface modification: SWNT were the most reactive nanotubes followed by CNx and MWNT. Ox-SWNT had the highest concentration of total acidic sites. These features determined the surface chemistry of nanotubes and their slurry pH, which is related to the concentration of acidic surface functional

groups: it was 4.0, 4.6 and 5.3, for ox-SWNT, ox-CNx, and ox-MWNT respectively. In consequence the cadmium adsorption capacity for ox-SWNT was about three and six times higher than that for ox-CNx and ox-MWNT, respectively. However, ox-SWNT showed the lowest adsorption rate as a result of intraparticle diffusion through longer and more highly entangled nanotubes.

The pseudo second order model assumed that the cadmium adsorption reaction was the rate limiting step. This model fitted to the experimental data with a correlation factor (R^2) higher than 0.9. However, the trend followed by the time to reach equilibrium was as follows: ox-SWNT> FeOOH> ox-MWN > ox-CNx, nevertheless FeOOH had the smallest TAS concentration and porosity, thus their adsorption rate might be faster than ox-MWNT and ox-CNx. This behavior suggested that diffusion effects could determine the trend followed by these nanoparticles.

Fitting of cadmium adsorption kinetic data with the external mass transfer model reported much higher theoretical coefficients (k_L) than those calculated with the experimental data: about 4000, 17000 and 300 times for ox-CNx, ox-MWNT, ox-SWNT, thus external mass transfer was not the rate-limiting step. The intraparticle diffusion model had the best adjustment to experimental data; the obtained diffusivities (D_{ep}) were 2.4E-11, 1.1E-9 and 4.2E-9 cm^2/s for ox-SWNT, ox-MWNT and ox-CNx, respectively, considered as single nanotubes, at initial cadmium concentration C_{A0} 4 mg/L, pH 6 and 200 rpm, suggesting that intraparticle diffusion could be the rate limiting step. The tortuosity was higher than 10 for all cases, suggestinf tiny sidewall pores may limit diffusion of cadmium to reach internal adsorption sites; even, it can result of limitations of the model. For their physicochemical features, ox-CNx would be a cost-efficient alternative for adsorption technologies for water treatment systems based on nanotechnology.

Carbon nanotubes could have different adsorption kinetic from those carbonaceous materials of macroscopic size, such as activated carbon. Smaller diffusivities and faster times to reach equilibrium can be expected for nanoadsorbents. As a consequence of small diffusivities the equilibrium was

attained in 20, 30 and 120 min for agglomerates of ox-CNx, ox-MWNT and ox-SWNT, respectively, which was much faster than that reported for activated carbon, around 35 h.

Supporting carbon nanotubes before their use in water treatment systems would prevent their release to the environment. The ox-CNx were effectively supported in a polyurethane matrix. Several composites were obtained with nanotube loadings of 2.5% (C1), 5% (C2) and 1% (C3). Loadings higher than 2.5% increased the stiffness of the obtained composites. Since the polymeric matrix enclosed the nanotubes, the surface of the obtained composites became rough.

Chemical interactions between isocyanate groups (NCO) could react with active hydrogen of carboxylic groups on the surface of ox-CNx, leading to formation of linkages. Also, these carboxylic groups of carbon nanotubes could form hydrogen bonds with polyurethane chains, improving the dispersion of nanotubes in the polymeric matrix. Chemical interactions between nanotubes and polyurethane prevented the generation of CO_2 and foaming of the composites. The addition of carboxylated SBR to the polymeric mixture prior to carbon nanotubes, could produce a reaction between hydrogen of carboxylic groups in SBR with isocyanate groups of polyurethane, thus chemical interactions between nanotubes and polyurethane might be reduced. Moreover, some carboxylic groups of SBR could remain free to act as adsorption sites. Raman spectroscopy showed characteristic D and G bands of carbon nanotubes at 1346 cm^{-1} and 1598 cm^{-1}, respectively, as shoulders in spectra for composites, which means that supported nanotubes were exposed in a certain way. The total acidic site concentrations of ox-CNx was 0.25 mmol/g, while for C1, C2 and C3, it was 0.05, 0.04 and 0.06 mmol/g, respectively. On the other hand, the maximum cadmium adsorption capacity of ox-CNx was 11.9 mg/g and decreased to 0.16, 0.02 and 0.22 mg/g for C1, C2 and C3, respectively, at pH 6.

Adsorption dynamic tests performed with composites C1 and C3 in bed-packed columns, at a residence time of 20 min, influent concentration of 0.3 ±0.1 mg/L at pH 6 and 3 BV/h, were able to process about 5 and 7 BV, respectively. The bed

123

adsorption capacity for C3 was 5.4 μg/g, near two times higher than for C1. Ideally longer residence time could permit the adsorbate to diffuse deeper into the adsorbent particle, thus utilizing a higher fraction of the bed adsorption capacity. The packed bed with composite C3 had 30% longer life when the EBCT increased to 10 minutes; however, the inlet flux was not the optimal to reach the maximum bed adsorption capacity. The advantage of composite C3 over C1 is, besides a higher bed adsorption capacity, lower production cost due to the smaller nanotube loads.

Three and two consecutive cycles of adsorption-desorption test in packed columns for C3 and C1, respectively, showed that the bed adsorption capacity remained, suggesting that nanotubes are well supported in the polymeric matrix. The configuration of carbon nanotube-based composite could prevent liberation of nanotubes to the environment, and allow their safe application in water treatment systems. Understanding the morphology of nanotubes is fundamental to develop nanotube-based adsorbents; aggregation of nanotubes, interfacial contact and chemical interactions with polymeric matrix are phenomena involved in the reduction of active sites for adsorption. Indeed more studies are necessary to support carbon nanostructures in polymeric matrices while preserving their adsorption capacity.

5.2 FINAL CONCLUSIONS

Nanotechnology has the potential to contribute to long-term water quality through application of carbon nanotubes to remove toxic heavy metals by adsorption. Oxidized carbon nanotubes have a higher adsorption capacity for toxic heavy metals than commercially available activated carbon.

Adsorption capacity is related to the chemical structure and the morphology of carbon nanotubes. Nitrogen-doped carbon nanotubes (CNx) have been developed recently. In this study it was proved that CNx can be modified chemically, in similar form as ox-SWNT and ox-MWNT, and are capable of adsorbing toxic heavy metals as cadmium and lead present in aqueous solution. In general, ox-CNx have two times higher cadmium adsorption capacity than ox-MWNT, but ox-SWNT have 1.3 times higher cadmium adsorption capacity than ox-CNx. In addition, ox-CNx have 1.4 times higher cadmium adsorption capacity than oxidized activated carbon Filtrasorb-400. Thus oxidized SWNT have the highest adsorption capacity for cadmium in solution at pH 6, followed by oxidized CNx and oxidized MWNT. However, the SWNT are the most expensive carbon nanotubes, while ox-MWNT are the cheapest. In the case of ox-CNx, these are not commercially available; their cost of production in laboratory is approximately 10 times higher than ox-MWNT, and much cheaper than SWNT. Hence, ox-CNx would be a cost-effective alternative to be used as adsorbent in future applications of carbon nanotubes in water treatment systems.

The previous assumption is supported by the fastest adsorption kinetic observed for ox-CNx in relation to ox-SWNT and ox-MWNT. Bamboo-type morphology of ox-CNx restrains diffusion of cadmium to the internal tubular spacing close to the open tips; hence cadmium adsorption equilibrium is reached in less than 20 minutes in contrast with the longer and more highly entangled ox-SWNT, where diffusion through their internal spacing delays time to equilibrium to more than 80 min.

Furthermore, this study reports for first time adsorption kinetic parameters calculated by the intraparticle diffusion model, which involves more physical variables, resulting in a better fitting of the experimental data. Although the intraparticle diffusion model has limitations due to the nanometric size of nanotubes, its use is recommended to analyze adsorption kinetics of carbon nanotubes.

Intraparticle diffusion could be a decisive factor in the kinetic mechanism for cadmium adsorption. Reported values are a first measure for cadmium diffusivities through pores on sidewall of carbon nanotubes. Obtained values for D_{ep} are 2.4E-11, 4.2E-9 and 1.1E-9 cm^2/s, for ox-SWNT, ox-CNx and ox-MWNT, respectively, considered as single nanotubes, at initial cadmium concentration of 4 mg/L, pH 6 and 200 rpm. Carbon nanotube systems report unusually higher tortuosities than values between 2 to 10, often reported for other carbonaceous materials. This may suggest the high complexity of water transport and cation adsorption through carbon nanotubes.

Application of carbon nanotubes in water treatment systems requires their effective immobilization in a proper support, in order to prevent their liberation and negative impact on the environment. Also, this research reports for the first time the immobilization of carbon nanotubes (ox-CNx) in a polyurethane matrix, to obtain a nanostructured adsorbent. The adsorption behavior of the obtained composite was evaluated by adsorption dynamic tests in bed-packed columns. Characterization of the nanotubes based-composites by several techniques suggests the chemical interaction between surface oxygenated groups in the nanotubes and the polymer. As a consequence, the availability of surface adsorption sites in the supported nanotubes decreases significantly. However, composites C1 and C3, with nanotube loads of 2.5% and 1% plus 5% SBR, respectively, are able to process about 5 and 7 bed volumes of cadmium solution (residence time of 20 min, influent concentration of 0.3 ±0.1 mg/L at pH 6 and 3 BV/h). The advantage of composite C3 over C1 is a higher cadmium adsorption capacity and lower production cost due to the smaller nanotube loading.

Consecutive cycles of adsorption-desorption test in packed columns with C3 and C1, respectively, showed that the bed adsorption capacity of the composites remains, suggesting that nanotubes are well supported in the polymeric matrix. The configuration of carbon nanotube-based composite can prevent the liberation of nanotubes to the environment, and allow their safe application in water treatment systems. More studies are necessary to support carbon nanostructures in polymeric matrixes while preserving their adsorption capacity. However, it is thought that this research has contributed to the development of nanostructure composites and their use in the water treatment field.

Finally, many techniques can be employed to treat polluted water with heavy metals. Selection of the most suitable treatment depends on the technical applicability, plant simplicity and cost-effectiveness, and in the future, systems developed with nanotechnology would offer a cost-effective alternative to solve water pollution problems.

5.3 PERSPECTIVES FOR FUTURE RESEARCH

Development of carbon nanotube-based filters for water treatment requires further research in order to obtain cost-efficient devices, looking for cheaper solutions that meet government regulations. Several studies, including this one, have demonstrated that oxidized carbon nanotubes have advantages over activated carbon for adsorption of toxic heavy metals in aqueous solutions. Even effects of natural organic material and dissolved ions currently present in water should be evaluated. Studies of adsorption kinetic should include several models as well as geometry, shape and effects at nanometric size.

In respect to supporting carbon nanotubes in a polymeric support, many variables can be explored in order to reduce interfacial contact and chemical interaction between carbon nanotubes and the polymer chains, to preserve the active sites for adsorption of toxic heavy metals in solution:

- Different polymeric matrices with appropriate chemical and mechanical properties for use in liquid phase can be tested
- Different types of carbon nanotubes, such as SWNT or MWNT, can be supported
- Nanotubes can be agglomerated into bigger structures before being supported
- Different additives can be tested to reduce chemical interaction between polymer chains and carbon nanotubes

Once the interactions between carbon nanotubes and the polymer are overcome, keeping the greatest concentration of active adsorption sites of carbon nanotubes, adsorption kinetic should be evaluated, because the polymer chains will necessarily impact the adsorption rate of the adsorbate to reach adsorption sites on the surface of carbon nanotubes. Adsorption column tests will be helpful to evaluate the adsorption behavior of the nanostructured composites, in order to optimize the parameters for column operation to obtain the maximum bed adsorption capacity.

To obtain nanostructured adsorbents based on carbon nanotubes or other nanoparticles is a big challenge. This goal requires demonstrating that the nanoparticle impacts on human health and on the environment are well understood and controlled. The environmental chemistry of even simple nanoparticles could be extraordinarily complicated, even in pure water. Thus understanding interactions with complex polymeric systems will require greater efforts.

Finally, development of nanostructured systems for water treatment will occur in the near future. Challenges such as availability of enough quantities of CNT at reasonable costs will be overcome very soon, due to increasing investments for large scale production of carbon nanotubes and other nanoparticles. Even more interesting, are the wide perspectives for using modified carbon nanotubes. More and more, new ways to modify their structure and properties will be discovered. As a consequence, new advantages will be available. However, it is very important to emphasize the necessity for the assessment of environmental impact of these nanoparticles, in order to have a full scenario for their use. This study did not cover the life cycle assessment of CNT, nor toxicological studies in vitro or in vivo, however, a deep characterization of the studied nanotubes herein would be helpful for future toxicological research.

REFERENCES

Ago H, Kugler T, Cacialli S, Salaneck WR, Shaffer MS, Windle AH, Friend RH (1999) Work functions and surface functional groups of multiwall carbon nanotubes. J. Phys. Chem. B 103: 8116-8121

Ajayan PM, Zhou OZ (2001) Applications of carbon nanotubes. In: Dresselhaus MS, Dresselhaus G, Avouris Ph (eds) Carbon nanotubes: synthesis structure properties and applications. Topics in Applied Physics. Springer, Berlin, pp 391-425

Allen SJ, Whitten LJ, Murray M, Duggan O (1997) The adsorption of pollutants by peat, lignite and activated chars. J. Chem. Technol. Biotechnol. 68: 442-452

Andrade-Espinosa G, Muñoz-Sandoval E, Terrones M, Endo M, Terrones H, Rangel JR (2008) Acid modified bamboo-type carbon nanotubes and cup-stacked-type carbon nanofibres as adsorbent materials: cadmium removal from aqueous solution. J. Chem. Technol. Biotechnol. 84: 519-524

Antunes EF, Lobo AO, Corat EJ, Trava-Airoldi VJ (2007) Influence of diameter in the Raman spectra of aligned multi-walled carbon nanotubes. Carbon 45: 913-921

Baalousha M (2009) Aggregation and disaggregation of iron oxide nanoparticles: Influence of particle concentration, pH and natural organic matter. Sci. Tot. Environ. 407: 2093-2101

Bansal RC, Donnet JB, Stoeckli F (1998) Active carbon. Marcel Dekker Inc., New York

Bansal RC, Goyal M (2005) Activated carbon adsorption. CRC Press, Boca Raton

Basmadjian D (1997) The little adsorption book: a practical guide for engineers and scientists. CRC Press, Boca Raton, Florida

Bassi M, Tonelli C, Di-Meo A (2003) Glass transition behavior of a microphase segregated polyurethane based on PFPE and IPDI. A calorimetric study. Macromol. 36: 8015-8023

B´eguin F, Flahaut E, Linares-Solano A, Pinson J (2006) Surface properties, porosity, chemical and electrochemical applications. In: Loiseau A, Launois P, Petit P, Roche S, JP Salvetat (eds) Understanding carbon nanotubes. From basics to applications. Springer, Netherlands, pp 495-549

Billmeyer FW (1984) Textbook of polymer science. John Wiley & Sons, New York

Blanchard G, Maunaye M, Martin G (1984) Removal of heavy metals from waters by means of natural zeolites. Water Res. 18: 1501-1507

Boehm H (1994) Some aspects of the surface chemistry of carbon blacks and other carbons. Carbon 32: 759-769

Boxall A, Tiede K, Chaudhry Q, (2007) Engineered nanomaterials in soils and water: how do they behave and could they pose a risk to human health?. Nanomedicine 2: 919-927

Bradsher CK, Barker MW (1964) Acridizinium ion chemistry IV. Oxidation with nitric acid. J. Org. Chem. 29: 452-454

Brasquet C, Le Cloirec P (1997) Adsorption onto activated carbon fibers: application to water and air treatments. Carbon 35: 1307-1313

Brasquet C, Roussy J, Subrenat E, Le Cloirec P (1996) Adsorption of micropollutants onto fibrous activated carbon: association of ultrafiltration and fibers. Wat. Sci. Tech. 34: 215-222

Brasquet C, Subrenat E, Le Cloirec P (1999) Removal of phenolic compounds from aqueous solution by activated carbon cloths. Wat. Sci. Tech. (Paris) 39: 201-205

Budinova TK, Gergova KM, Petrov NV, Minkova VN (1994) Removal of metal-ions from aqueous-solution by activated carbons obtained from different raw-materials. J. Chem. Technol. Biotechnol. 60: 177-182

Chen C, Li X, Zhao D, Tan X, Wang X (2007) Adsorption kinetic, thermodynamic and desorption studies of Th (IV) on oxidized multi-wall carbon nanotubes. Colloid. Surf. 302: 449-454

Chen C, Wang X (2006) Adsorption of Ni(II) from aqueous solution using oxidized multiwall carbon nanotubes. Ind. Eng. Chem. Res. 45: 9144-9149

Chen JP, Wu S (2004) Acid/base-treated activated carbons: characterization of functional groups and metal adsorptive properties. Langmuir 20: 2233-2242

Cheung CW, Chan CK, Porter JF, McKay G (2001) Combined diffusion model for the sorption of cadmium, copper, and zinc ions onto bone char. Environ. Sci. Technol. 35: 1511-1522

Choi HC, Bae SY, Park J, Seo K, Kim C, Kim B, Song HJ, Shin HJ (2004) Experimental and theoretical studies on the structure of N-doped carbon nanotubes: Possibility of intercalated molecular N-2. Appl. Phys. Lett. 85: 5742-5744

Choi HC, Park J, Kim B (2005a) Distribution and structure of N atoms in multiwalled carbon nanotubes using variable-energy X-ray photoelectronic spectroscopy. J. Phys. Chem. B 109: 4333-4340

Choi HC, Bae SY, Jang WS, Park J (2005b) Release of N_2 from the carbon nanotubes via high-temperature annealing. J. Phys. Chem. B 109: 1683-1688

Coates J (2000) Interpretation of infrared spectra: a practical approach. In: Meyers RA (ed) Encyclopedia of Analytical Chemistry. http://infrared.als.lbl.gov/BLManual/IR_Interpretation.pdf. Accessed Jan 20 2009

Contescu A, Contescu C, Putyera K, Schwarz JA (1997) Surface acidity of carbons characterized by their continuous pK distribution and Boehm titration. Carbon 35: 83-94

Cooney DO (1999) Adsorption design for wastewater treatment. Lewis Publishers, Boca Raton Florida

Corapcioglu MO, Huang CP (1987) The adsorption of heavy metals onto hydrous activated carbon. Water. Res. 21: 1031-1044

Czerw R, Terrones M, Charlier JC, Blase X, Foley B, Kamalakaran R, Grobert N, Terrones H, Tekleab D, Ajayan PM, Blau W, Rühle M, Carroll DL (2001) Identification of electron donor states in N-doped carbon nanotubes. Nano Lett. 1: 457-460

Di ZC, Ding J, Peng XJ, Li YH, Luan ZK, Liang J (2006) Chromium adsorption by aligned carbon nanotubes supported ceria nanoparticles. Chemosphere 62: 861-865

Dobos D (1994) Handbook for electrochemists in industry and universities. Elsevier Scientific, Amsterdam

Dresselhaus MS (1997) Future directions in carbon science. Ann. Rev. Mat. Res. 27: 1-34

Dresselhaus MS, Dresselhaus G, Avouris Ph (2001) Carbon Nanotubes. Synthesis, structure, properties and applications. Springer, Germany

Duclaux L (2002) Review of the doping of carbon nanotubes (multiwalled and single-walled). Carbon 40: 1751-1764

Dyke CA, Tour JM (2004) Overcoming the insolubility of carbon nanotubes through high degrees of sidewall functionalization. Chem. Eur. J. 10: 812-817

El-Sheikh AH (2008) Effect of oxidation of activated carbon on its enrichment efficiency of metal ions: comparison with oxidized and non-oxidized multi-walled carbon nanotubes. Talanta 75: 127-134

Endo M, Strano MS, Ajayan PM (2008) Potential applications of carbon nanotubes. In: Jorio A, Dresselhaus G, Dresselhaus MS (eds) Carbon Nanotubes: Advanced topics in the synthesis, structure, properties and applications. Springer, Berlin, pp 13-62

Evans RM (1993) Polyurethane sealants. Technology and applications. Technomic Publishing Company Inc., Lancaster, Pennsylvania

Ewels CP, Glerup M (2005) Nitrogen doping in carbon nanotubes. J. Nanosci. Nanotechnol. 5: 1345-1363

Feng-Chin W, Ru-Ling T, Shang-Chieh H, Ruey-Shin J (2009) Characteristics of pseudo-second-order kinetic model for liquid-phase adsorption: A mini-review. Chem. Eng. J. 151: 1-9

Gao Z, Bandosz TJ, Zhao Z, Han M, Liang C, Qiu J (2008) Investigation of the role of surface chemistry and accessibility of cadmium adsorption sites on open-surface carbonaceous materials. Langmuir 24: 11701-11710

Gao Z, Bandosz T, Zhao Z, Han M, Qiu J (2009) Investigation of factors affecting adsorption of transition metals on oxidized carbon nanotubes. J. Hazard. Mater. 167: 357-365

Glerup M, Castignolles M, Holzingeer M, Hug G, Loiseau A, Bernier P (2003) Synthesis of highly nitrogen-doped multi-walled carbon nanotubes. Chem. Commun. (Camb.) 20: 2542-2543

Gomez-Serrano V, Acedo-Ramos M, Lopez-Peinado AJ, Valenzuela-Calahorro C (1997) Mass and surface changes of activated carbon treated with nitric acid. Thermal behavior of the samples. Thermochim. Acta 291: 109-115

Hassellöv M, eadman JW, Ranville JF, Tiede K (2008) Nanoparticle analysis and characterization methodologies in environmental risk assessment of engineered nanoparticles. Ecotoxicology 17: 344-361

He YT, Wan J, Tokunaga T (2008). Kinetic stability of hematite nanoparticles: the effect of particle sizes. J. Nanopart. Res. 10: 321–332

Hirsch A (2002) Functionalization of single-walled carbon nanotubes. Angew. Chem. Int. Ed. 41: 1853-1859

Hristozov D, Malsch I (2009) Hazards and risks of engineered nanoparticles for the ewnvironment and human health. Sustainability 1: 1161-1194

Hu J, Chen C, Zhu Z, Wang X (2009) Removal of chromium from aqueous solution by using oxidized multiwalled carbon nanotubes. J. Hazard. Mater. 162: 1542-1550

Hui CW, Chen B, McKay G (2003) Pore surface diffusion model for batch adsorption processes. Langmuir 19: 4188-4196

Inoue S, Ichikuni N, Suzuki T, Uematsu T, Kaneko K (1998) Capillary condensation of N2 on multiwall carbon nanotubes. J. Phys. Chem. B 102: 4689-4692

Jung YC, Sahoo NG, Cho JW (2006) Polymeric nanocomposites of polyurethane block copolymers and functionalized multi-walled carbon nanotubes as crosslinkers. Macromol. Rapid Commun. 27: 126-131

Kabbashi NA, Atieh MA, Al-Mamun A, Mirghami ME, Alam MDZ, Yahya N (2009) Kinetic adsorption of application of carbon nanotubes for Pb(II) removal from aqueous solution. J. Environ. Sci. 21: 539-544

Kandah MI, Meunier JL (2007) Removal of nickel ions from water by multi-walled carbon nanotubes. J. Hazard. Mater. 146: 283-288

Kiang CH, Endo M, Ajayan PM, Dresselhaus G, Dresselhaus MS (1998) Size effects in carbon nanotubes. Phys. Rev. Lett. 81: 1869-1872

Kim UJ, Gutierrez HR; Gupta AK, Eklund PC (2008) Raman scattering study of the thermal conversion of bundled carbon nanotubes into graphitic nanoribbons. Carbon 46: 729-740

Ko DC, Porter JF, McKay G (2001) Determining of solid-phase loading for the removal of metal ion from effluents using fixed-bed adsorbers. Environ. Sci. Technol. 35: 2797-2803

Koós AA, Dowling M, Jurkschat K, Crossley A, Grobert N (2009) Effect of the experimental parameters on the structure of nitrogen-doped carbon nanotubes produced by aerosol chemical vapour deposition. Carbon 47: 30-37

Kondratyuk P, Yates JT (2007) Molecular views of physical adsorption inside and outside of single-wall carbon nanotubes. Acc. Chem. Res. 40: 995-1004

Kostal J, Prabhukumar G, Lao UL, Chen A, Matsumoto M, Mulchandani A, Chen W (2005) Customizable biopolymers for heavy metal remediation. J. Nanopart. Res. 7: 517-523

Kurniawan TA, Chan GY, Lo WH, Babel S (2006) Physico-chemical treatment techniques for wastewater laden with heavy metals. Chem. Eng. J. 118: 83-98

Lachman N, Bartholome C, Miaudet P, Maugey M, Poulin P, Wagner HD (2009) Raman response of carbon nanotube/ PVA fibers under strain. J. Phys. Chem. C 113: 4751-4754

Lambin Ph, Loiseau A, Monthioux M, Thibault J (2006) Structural analysis by elastic scattering. In: Loiseau A, Launois P, Petit P, Roche S, JP Salvetat (eds) Understanding carbon nanotubes. From basics to applications. Springer, Netherlands, pp 131-198

Leyva-Ramos R, Geankoplis CJ (1985) Model simulation and analysis of surface diffusion of liquids in porous solids. Chem. Eng. Sci. 40: 749-807

Leyva-Ramos R, Rangel-Mendez JR, Bernal-Jacome LA, Berber-Mendoza MS (2005) Intraparticle diffusion of cadmium and zinc ions during adsorption from aqueous solution on activated carbon. J. Chem. Technol. Biotechnol. 80: 924-933

Leyva-Ramos R, Diaz-Flores PE, Leyva-Ramos J, Femat-Flores R (2007) Kinetic modeling of pentachlorophenol adsorption from aqueous solution on activated carbon fibers. Carbon 45: 2280-2289

Li YH, Wang S, Wei J, Zhang X, Xu C, Luan Z, Wu DH, Wei BQ (2002) Lead adsorption on carbon nanotubes. Chem. Phys. Lett. 357: 263-266

Li YH, Ding J, Luan ZK, Di ZC, Zhu YF, Xu CL, Dehai W, Bingqing W (2003a) Competitive adsorption of Pb^{2+}, Cu^{2+} and Cd^{2+} ions from aqueous solutions by multiwalled carbon nanotubes. Carbon 41: 2787-2792

Li YH, Luan ZK, Xiao X, Zhou XW, Xu CL, Wu DH, Wei BQ (2003 b) Removal of Cu^{2+} ions from aqueous solutions by carbon nanotubes. Adsorpt. Sci. Technol. 21: 475-485

Li YH, Wang SG, Luan ZK, Ding J, Xu CL, Wu DH (2003c). Adsorption of cadmium (II) from aqueous solution by surface oxidized carbon nanotubes. Carbon 41: 1057-1062

Li YH, Di ZC, Ding J, Wu DH, Luan ZK, Zhu YQ (2005) Adsorption thermodynamic, kinetic and desorption studies of Pb^{2+} on carbon nanotubes. Water Res. 39: 605-609

Li XQ, Zhang WX (2006) Iron nanoparticles, the core-shell structure and unique properties for Ni(II) sequestration. Diam. Relat. Mater. 15: 90-94

Li YH, Zhu YQ, Zhao YM, Wu DH, Luan ZK (2006) Different morphologies of carbon nanotubes effect on the lead removal from aqueous solution. Diam. Relat. Mater. 15: 90-94

Li YH, Zhao YM, Hu WB, Ahmad I, Zhu YQ, Peng XJ, Luan ZK (2007) Carbon nanotubes: the promising adsorbent in wastewater treatment. J. Phys. Conference Series 61: 698-702

Liu Y, Pan C, Wang J (2004) Raman spectra of carbon nanotubes and nanofibers prepared by ethanol flames. J. Mat. Sci. 39: 1091-1094

Loiseau A, Blase X, Charlier J, Gadelle P, Journet C, Laurent Ch, Peigney A (2006) Synthesis methods and growth mechanisms. In: Loiseau A, Launois P, Petit P, Roche S, JP Salvetat (eds) Understanding carbon nanotubes. From basics to applications. Springer, Netherlands, pp 49-130

Lu C, Chiu H (2006) Adsorption of zinc (II) from water with purified carbon nanotubes. Chem. Eng. Sci. 61: 1138-1145

Lu C, Chiu H (2008) Chemical modification of multiwalled carbon nanotubes for sorption of Zn^{2+} from aqueous solution. Chem. Eng. J. 139: 462-468

Lu C, Chiu H, Liu C (2006) Removal of Zinc (II) from aqueous solution by purified carbon nanotubes: kinetics and equilibrium studies. Ind. Eng. Chem. Res. 45: 2850-2855

Lu C, Liu C, Rao GP (2008) Comparison of sorbent cost for the removal of NI^{2+} from aqueous solution by carbon nanotubes and granular activated carbon. J. Hazard. Mater. 151: 239-246

Maldonado S, Morin S, Stevenson KJ (2006) Structure, composition, and chemical reactivity of carbon nanotubes by selective nitrogen doping. Carbon 44: 1429-1437

Mauter MS, Elimelech M (2008) Environmental applications of carbon nanomaterials. Environ. Sci. Technol. 42: 5843-5859

McKee GS, Vecchio KS (2006) Thermogravimetric analysis of synthesis variation effects on CVD generated multiwalled carbon nanotubes. J. Phys. Chem. B 110: 1179-1186

Misra A, Tyagi PK, Rai P, Misra DS (2007) FTIR spectroscopy of multiwalled carbon nanotubes: A simple approach t study the nitrogen doping. J. Nanosci. Nanotech. 7: 1820-1823

Nakamoto K (1997) Infrared and Raman spectra of inorganic and coordination compounds. John Wiley & Sons, Inc. New York

Natale FD, Erto A, Lancia A, Musmarra D (2009) A descriptive model for metallic ions adsorption from aqueous solutions onto activated carbons. J. Hazard. Mater. 169: 360-369

Nevidomskyy AH, Csanyi G, Payne MC (2003) Chemically active substitutional nitrogen impurity in carbon nanotubes. Phys. Rev. Lett. 91: 1-4

Newman J (1973) Electrochemical Systems. Prentice Hall, Englewood Cliffs, NJ

Nightingale ER (1959) Phenomenological theory of ion solvation. Effective radii of hydrated ions. J. Phys. Chem. 63: 1381-1387

Niyogi S, Hamon MA, Hu H, Zhao B, Bhowmik P, Sen R, Itkis ME, Haddon RC (2002) Chemistry of single-wall carbon nanotubes. J. Phys. Chem. B 102: 4689-4692

Noy A, Park HG, Fornasiero F, Holt JK, Grigoropoulos CP, Bakajin O (2007) Nanofluidics in carbon nanotubes. Nanotoday 2: 22-29

Nyquist RA, Kagel RO (2000) Handbook of Infrarred and Raman spectra of inorganic compounds and organic salts. Academic Press, San Diego

NOM-127-SSA1-1994 (2000) Modificación a la Norma Oficial Mexicana NOM-127-SSA1-1994: Salud ambiental. Agua para uso y consumo humano. Límites permisibles de calidad y tratamientos a que debe someterse el agua para su potabilización.

Otake Y, Jenkins RG (1993) Characterization of oxygen-containing surface complexes created on a microporous carbon by air and nitric acid treatment. Carbon 31: 109-121

Ovejero G, Sotelo JL, Romero MD, Rodríguez A, Ocana MA, Rodríguez G, Garcia J (2006) Multiwalled carbon nanotubes for liquid-phase oxidation. Functionalization, characterization and catalytic activity. Ind. Eng. Chem. Res. 45: 2206-2212

Pamula E, Rouxhet PG (2003) Bulk and surface chemical functionalities of type III PAN-based carbon fibres. Carbon 41: 1905-1915

Pan B, Xing B (2008) Adsorption mechanism of organic chemicals on carbon nanotubes. Environ. Sci. Technol. 42: 9005-9013

Pappas AJ, Osterman FA, Powell HB (1970) Differential thermal analysis of some pyridine 1 -oxide coordination compounds. Inor. Chem. 9: 2695-2698

Peng Y, Liu H (2006) Effects of oxidation by hydrogen peroxide on the structures of multiwalled carbon nanotubes. Ind. Eng. Chem. Res. 45: 6483-6488

Perez-Aguilar NV, Muñoz-Sandoval E, Diaz-Flores PE, Rangel-Mendez JR (2010) Adsorption of cadmium and lead onto oxidized nitrogen-doped multiwall carbon nanotubes in aqueous solution. J. Nanopart. Res. 12: 467-480

Pillay K, Cukrowska EM, Coville NJ (2009) Multi-walled carbon nanotubes as adsorbents for the removal of parts per billion levels of hexavalent chromium from aqueous solution. J. Hazard. Mater. 166: 1067-1075

Pinto ML, Pires J, Carvalho AP, Bordado JC, Carvalho MB (2004) Synthesis and characterization of polyurethane foam matrices for the support of granular adsorbent materials. J. Appl. Polym. Sci. 92: 2045-2053

Pinto ML, Pires J, Carvalho AP, Carvalho MB Bordado JC, (2006) Synthesis and regeneration of polyurethane/adsorbents composites and their characterization by adsorption methods. Microporous Mesoporous Mater. 89: 260-269

Radovic LR (ed) (2001) Chemistry and physics of carbon. Vol 27. Marcel Dekker Inc., New York

Rao GP, Lu C, Su F (2007) Sorption of divalent metal ions from aqueous solution by carbon nanotubes: a review. Sep. Purif. Technol. 58: 224-231

Reddad Z, Gerente C, Andres Y, Le Cloirec P (2002) Adsorption of several metal ions onto a low-cost biosorbent: kinetic and equilibrium studies. Sep. Purif. Technol. 36: 2067-2073

Renn O, Roco MC (2006) Nanotechnology and the need for risk governance. J. Nanopart. Res. 8: 153-191

Ricordel S, Taha S, Cisse I, Dorange G (2001) Heavy metals removal by adsorption onto peanut husks carbon: characterization, kinetic study and modeling. Sep. Purif. Technol. 24: 389-401

Rouquerol F, Rouquerol J, Sing K (1999) Adsorption by powders and porous solids. Principles, methodology and applications. Academic Press, London

Rubner MF (1986) Synthesis and characterization of polyurethane-diacetylene segmented copolymers. Macromol. 19: 2114-2128

Saito R, Grüneis A, Samsonidze GG, Brar VW, Dresselhaus G, Dresselhaus MS, Jorio A, Cançado LG, Fantini C, Pimenta MA, Souza-Filho AG (2003) Double resonance Raman spectroscopy of single-wall carbon nanotubes. New J. Phys. 5-157: 1-15

Salipira KL, Mamba BB, Krause RW, Malefetse TJ, Durbach SH (2007) Carbon nanotubes and cyclodextrin polymers for removing organic pollutants from water. Environ. Chem. Lett. 5: 13-17

Savage N, Diallo MS (2005) Nanomaterials and water purification: Opportunities and challenges. J. Nanopart. Res. 7: 331-342

Schaefer DW, Justice RS (2007) How nano are nanocomposites?. Macromol. 40: 8501-8517

Shannon MA, Bohn PW, Elimelech M, Georgiadis JG, Marinas BJ, Mayes AM (2008) Science and technology for water purification in the coming decades. Nature 452: 301-310

Srivastava A, Srivastava ON, Talapatra S, Vajtai R, Ajayan PM (2004) Carbon nanotube filters. Nat. Mater. 3: 610-614

Stafiej A, Pyrzynska K (2007) Adsorption of heavy metals ions with carbon nanotubes. Sep. Purif. Technol. 58: 49-52

Stumm W, Morgan JJ (1996) Aquatic chemistry. Wiley, New York

Sumpter BG, Meunier V, Romo-Herrera JM, Cruz-Silva E, Cullen DA, Terrones H, Smith DJ, Terrones M (2007) Nitrogen-mediated carbon nanotube growth: diameter reduction, metallicity, bundle dispersability, and bamboo-like structure formation. ACS Nano 1: 369-375

Suzuki M (1990) Adsorption engineering. Elsevier, Tokio

Tasis D, Tagmatarchis N, Bianco A, Prato M (2006) Chemistry of carbon nanotubes. Chem. Rev. 106: 1105-1136

Tay T, Candan Mehmet, Erdem M, Çimen Y (2009) Biosorption of cadmium ions from aqueous solution onto non-living lichen *Ramalina fraxinea* biomass. Clean 37: 249-255

Terrones H, Terrones M, Moran-Lopez JL (2001) Curved nanomaterials. Curr. Sci. India 81: 1011-1029

Terrones M (2003) Science and technology of the twenty-first century: Synthesis, properties and applications of carbon nanotubes. Ann. Rev. Mat. Res. 33: 419-501

Terrones, M (2004) Carbon nanotubes: synthesis and properties, electronic devices and other emerging applications. Int. Mater. Rev. 49: 325-377

Terrones M, Ajayan PM, Banhart F, Blase X, Carroll DL, Charlier JC, Czerw R, Foley B, Grobert N, Kamalakaran R, Kohler-Redlich P, Ruhle M, Seeger T, Terrones H (2002) N-doping and coalescence of carbon nanotubes: synthesis and electronic properties. Appl. Phys. A-Mater. 74: 355-361

Terrones M, Jorio A, Endo M, Rao AM, Kim YA, Hayashi T, Terrones H, Charlier JC, Dresselhaus G, Dresselhaus MS (2004) New direction in nanotube science. Mat. Today 7: 30-45

Terrones M, Souza AG, Rao AM (2008) Doped carbon nanotubes: Synthesis, characterization and applications. In: Jorio A, Dresselhaus G, Dresselhaus MS (eds) Carbon Nanotubes: Advanced topics in the synthesis, structure, properties and applications. Springer, Berlin, pp 531-566

Theron J, Walker JA, Cloete TE (2008) Nanotechnology and water treatment: Applications and emerging opportunities. Crit. Rev. Microbiol. 34: 43-69

Thomas WJ, Crittenden B (1998) Adsorption technology and design. Elsevier, Netherlands

Tiede K, Boxall ABA, Tear SP, Lewis J, David H, Hassellöv M (2008) Detection and characterization of engineered nanoparticles in food and the environment. Food Addit. Contam. 25: 795-821

Tiede K, Hasellöv M, Breitbarth E, Chaudhry Q, Boxall ABA (2009) Considerations for environmental fate and ecotoxicity testing to support environmental risk assessments for engineered nanoparticles. J. Chromatogr. A 1216: 503-509

Tománek D, Jorio A, Dresselhaus MS, Dresselhaus G (2008) Introduction to the important and exciting aspects of carbon-nanotube science and technology. In: Jorio A, Dresselhaus G, Dresselhaus MS (eds) Carbon Nanotubes: Advanced topics in the synthesis, structure, properties and applications. Springer, Berlin, pp 1-12

Tour JM (2007) Transition to organic materials science, passive, active, and hybrid nanotechnologies. J. Org. Chem. 72: 7477-7496

Tsai CJ, Pui DY (2009) Recent advances and new challenges of occupational and environmental health of nanotechnology. J. Nanopart. Res. 11: 1-4

USEPA (1999) Introduction to the National Pretreatment Program. Office of Wastewater Management. U.S. Environmental Protection Agency. Washington, DC 20460

USEPA (2007) Nanotechnology white paper. Science Policy Council. U.S. Environmental Protection Agency. Washington, DC 20460

van Dommele S, Romero-Izquirdo A, Brydson R, de Jong KP, Bitter JH (2008) Tuning nitrogen functionalities in catalytically grown nitrogen-containing carbon nanotubes. Carbon 46: 138-148

Vaisman L, Wagner HD, Marom G (2006) The role of surfactants in dispersion of carbon nanotubes. Adv. Colloid. Interface. Sci. 128-130: 37-46

Wade LG (1993) Organic Chemistry. Prentice Hall, Mexico

Wang HJ, Zhou AL, Peng F, Yu H, Yang J (2007a) Mechanism study on adsorption of acidified multiwalled carbon nanotubes to Pb(II). J. Colloid. Interf. Sci. 316: 277-283

Wang HJ, Zhou AL, Peng F, Yu H, Chen LF (2007b) Adsorption characteristic of acidified carbon nanotubes for heavy metal Pb (II) in aqueous solution. Mater. Sci. Eng. A-Struct. 466: 201-206

Wang SG, Wong WX, Liu XW, Yao YW, Gao BY, Yue QY (2007c) Removal of lead (II) from aqueous solution by adsorption onto manganese oxide-coated carbon nanotubes. Sep. Purif. Technol. 58: 17-23

Wang Z, Shirley MD, Meikle ST, Whitby RLD, Mikhalovsky SV (2009) The surface acidity of acid oxidized multi-walled carbon nanotubes and the influence of in-situ generated fulvic acids on their stability in aqueous dispersions. Carbon 47: 73-79

Weber WJ (2002) Distributed optimal technology networks. Water Sci. Technol. 46: 241-246

WHO (World Health Organization) (2006) Guidelines for drinking-water quality [electronic resource]: incorporating first addendum, vol 1, recommendations, 3rd edn. Electronic version for the Web. Available via DIALOG. http://www.who.int/water_sanitation_health/dwq/gdwq0506.pdf . Accesed 20 Jan 2009

WWAP (World Water Assessment Programme) (2003) The United Nations World Water Development Report 1: Water for People, Water for Life. Paris: UNESCO and New York: Berghahn Books.

WWAP (World Water Assessment Programme) (2006). The United Nations World Water Development Report 2: Water, a shared responsibility. Paris: UNESCO and New York: Berghahn Books.

WWAP (World Water Assessment Programme) (2009). The United Nations World Water Development Report 3: Water in a changing world. Paris: UNESCO, and London: Earthscan.

WWF4 (2006a) Final Report. 4th World Water Forum. Available from the World Wide Web site

http://www.worldwaterforum4.org.mx/uploads/TBL_DOCS_16_59.pdf . Last date access Jan 20, 2010

WWF4 (2006b) Water for Growth and development. A theme document for the 4th World Water Forum. Available from the World Wide Web site http://www.worldwaterforum4.org.mx/uploads/TBLDOCTOSB_1_5.pdf . Last date access Jan 20, 2010

Xiong Y, Li Z, Guo Q, Xie Y (2005) Synthesis of multi-walled and bamboo-like well-crystalline CNx nanotubes with controllable nitrogen concentration (x=0.05-1.02). Inorg. Chem. 44: 6505-6508

Xiong J, Zheng Z, Qin X, Li M, Li H, Wang X (2006) The thermal and mechanical properties of a polyurethane/multi-walled carbon nanotube composite. Carbon 44: 2701-2707

Xiong J, Zheng Z, Wenhui S, Dongsheng Z, Wang X (2008) Microstructure and properties of polyurethane nanocomposites reinforced with methylene-bis-ortho-chloroaniline-grafted multi-walled carbon nanotubes. Composites A 39: 904-910

Yang RT (2003) Adsorbents: fundamentals and applications. Wiley, New Jersey

Yang S, Li J, Shao D, Hu J, Wang X (2009) Adsorption of Ni(II) on oxidized multi-walled carbon nanotubes: Effect of contact time, pH, foreign ions and PAA. J. Hazard. Mater. 166: 109-116

Yin CY, Aroua MK, Daud WM (2007) Review of modifications of activated carbon for enhancing contaminants uptakes from aqueous solution. Sep. Purif. Technol. 52: 403-415

Zagorodni AA (2007) Ion Exchangers. Properties and Applications. Elsevier, Amsterdam

Zamudio A, Elias AL, Rodriguez-Manzo JA, Lopez-Urias F, Rodriguez-Gattorno G, Lupo F, Rühle M, Smith DJ, Terrones H, Diaz D, Terrones M (2006) Efficient

anchoring of silver nanoparticles on N-doped carbon nanotubes. Small 2: 346-350

Zawadski J (1980) IR Spectroscopic investigations of the mechanism of oxidation of carbonaceous films with HNO_3 solution. Carbon 18: 281-285

Zhang J, Zou H, Qing Q, Yang Y, Li Q, Liu Z, Guo X, Du Z (2003) Effect of chemical oxidation on the structure of single-walled carbon nanotubes. J. Phys. Chem. B 107: 3712-3718

Zeng H, Arashiro M, Giammar DE (2008) Effects of water chemistry and flow rate on arsenate removal by adsorption to an iron oxide-based sorbent. Water Res. 42: 4629-4636

LIST OF PUBLICATIONS

Perez-Aguilar NV, Muñoz-Sandoval E, Diaz-Flores PE, Rangel-Mendez JR (2010) Adsorption of Cadmium and Lead onto Oxidized Nitrogen-doped Carbon Nanotubes in Aqueous Solutions: Equilibrium and Kinetics. *J Nanopart Res,* 12: 467-489

Perez-Aguilar NV, Muñoz-Sandoval E, Diaz-Flores PE, Rangel-Mendez JR. Effect of the Morphology of Three Different Types of Carbon Nanotubes on the Cadmium Adsorption Kinetic. *(In preparation)*

Perez-Aguilar NV, Escobar-Barrios VA, Muñoz-Sandoval E, Rangel-Mendez JR. Carbon Nanotube-based Composites for Adsorption of Toxic Metals from Aqueous Solutions. *(In preparation)*

EXTENDED ABSTRACTS

Perez-Aguilar NV, Rangel-Mendez JR, Escobar-Barrios VA, Terrones H, Muñoz-Sandoval E. CNx Based Nanocomposite as Adsorbent of Heavy Metals (Cd, Pb) Present in Aqueous Solutions. *International Conference on Carbon, Jul 13-18 (2008), Nagano, Japan*

Perez-Aguilar NV, Rangel-Mendez JR, Escobar-Barrios V, Terrones H, Terrones M, Muñoz-Sandoval E. Nitrogen-doped Carbon Nanotube-Polyurethane Composites to Adsorb Cadmium and Lead from Aqueous Solutions. *XX National Conference of the Polymeric Mexican Society, Oct 30-Nov 2 (2007), Guanajuato, Mexico*

PE Diaz-Flores, **NV Perez-Aguilar**, JR Rangel-Mendez. Functionalized Carbon Nanotubes: A choice to remove toxic pollutants from water effluents. *IV Annual Meeting on Woman in Science, May 24-25, (2007), Leon, Mexico*

ATTENDANCE AT CONFERENCES

Perez-Aguilar NV, Rangel-Mendez JR, Escobar-Barrios VA, Muñoz-Sandoval E. "Modification and supporting of CNx for toxic metals adsorption from aqueous solution". *VI Annual Meeting on Woman in Science, Aug 19-21, (2009), Leon, Mexico. (Poster presentation)*

Perez-Aguilar NV, Rangel-Mendez JR, Escobar-Barrios VA, Muñoz-Sandoval E. "Improvement of a CNx-based polymeric nanocomposite to adsorb heavy metals in water". *1st US-Mexico Symposium on Advances in Polymer Science, Dec 7-10, (2008), Baja California, Mexico. (Poster presentation)*

Perez-Aguilar NV, Rangel-Mendez JR, Escobar-Barrios VA, Terrones H, Muñoz-Sandoval E. "CNx Based Nanocomposite as Adsorbent of Heavy Metals (Cd, Pb) Present in Aqueous Solutions". *International Conference on Carbon, Jul 13-18 (2008), Nagano, Japan. (Oral presentation)*

Perez-Aguilar NV, Rangel-Mendez JR, Escobar-Barrios V, Terrones H, Terrones M, Muñoz-Sandoval E. "Nitrogen-doped Carbon Nanotube-Polyurethane Composites to Adsorb Cadmium and Lead from Aqueous Solutions". *XX National Conference of the Polymeric Mexican Society, Oct 30-Nov 2 (2007), Guanajuato, Mexico. (Oral presentation)*

PE Diaz-Flores, **NV Perez-Aguilar**, JR Rangel-Mendez. Functionalized Carbon Nanotubes: A choice to remove toxic pollutants from water effluents". *IV Annual Meeting on Woman in Science, May 24-25, (2007), Leon, Mexico (Poster presentation)*
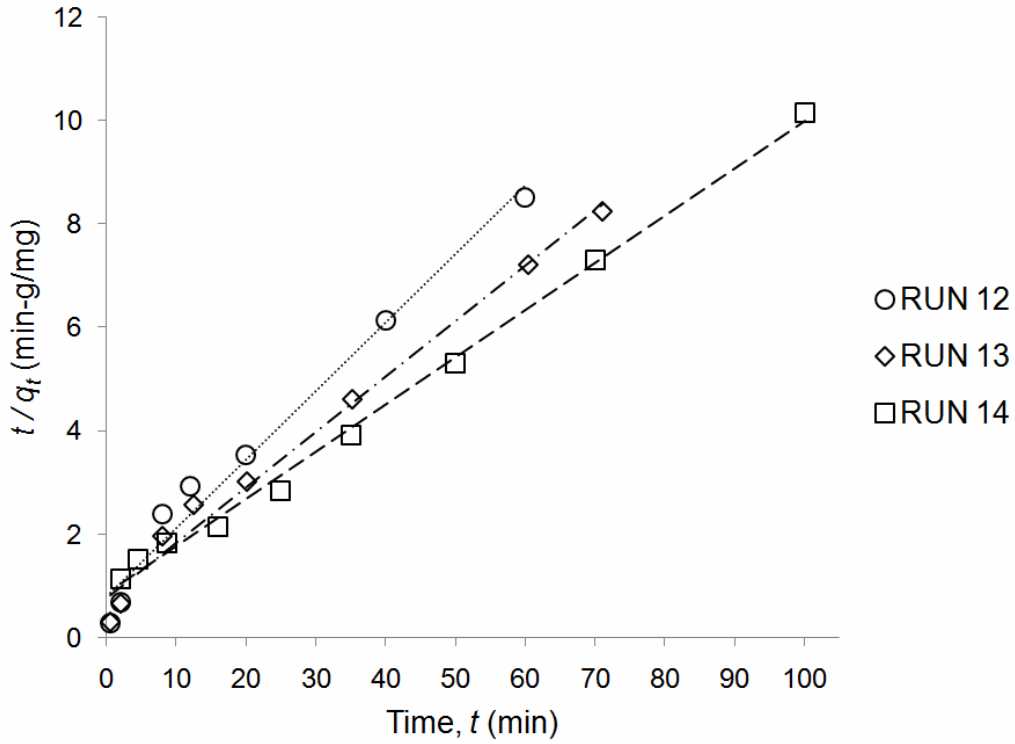
APPENDICES

Appendix A
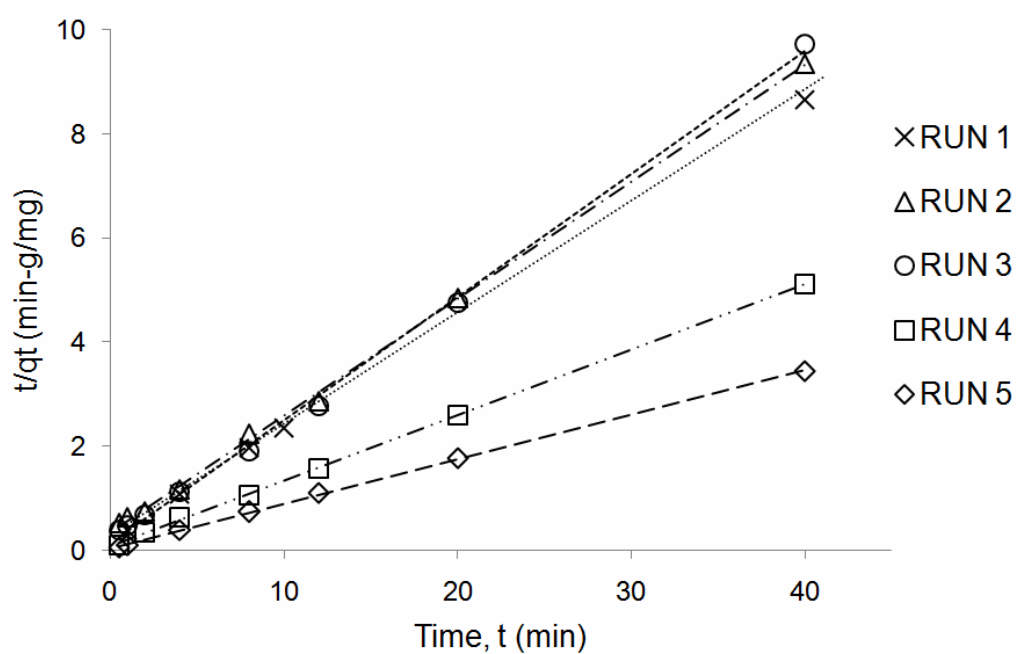
Fig. A1 Adsorption kinetic data for cadmium adsorption onto ox-CNx without pH control, fitted to pseudo-second order model. Runs 1 and 2 were performed at C_{A0}~ 4 mg/L and 150 rpm; Runs 3 to 5 were performed at 200 rpm and C_{A0} near 4, 9 and 19 mg/L respectively.
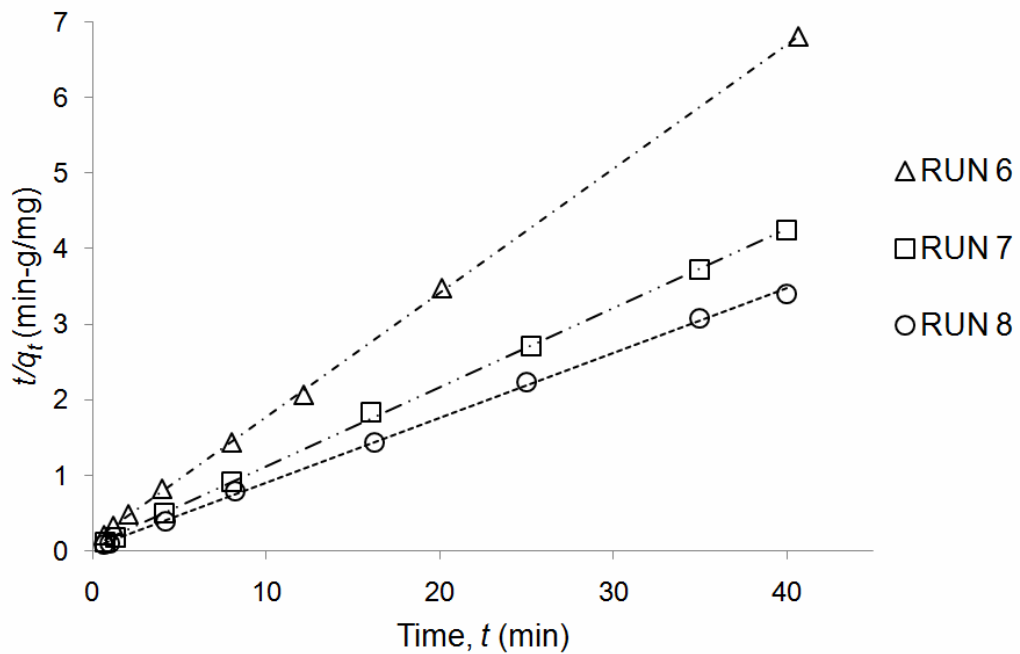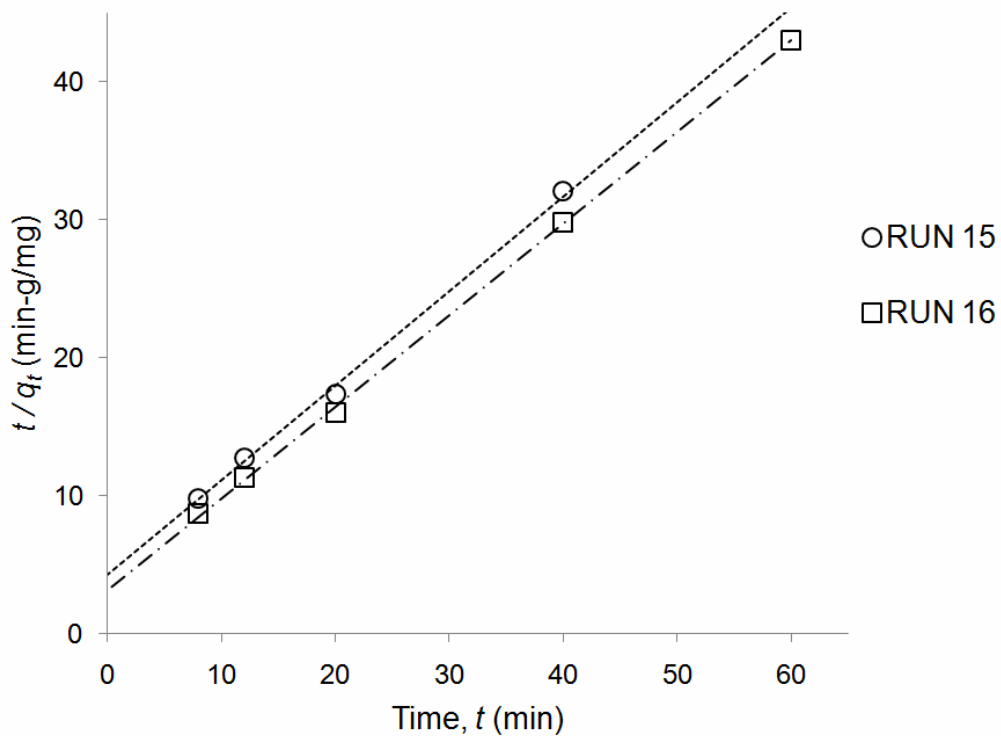
Fig. A2 Adsorption kinetic data for cadmium adsorption onto ox-CNx at pH 6, fitted to pseudo-second order model. Runs 6 to 8 were performed at 200 rpm and C_{A0} near 4, 9 and 19 mg/L respectively.
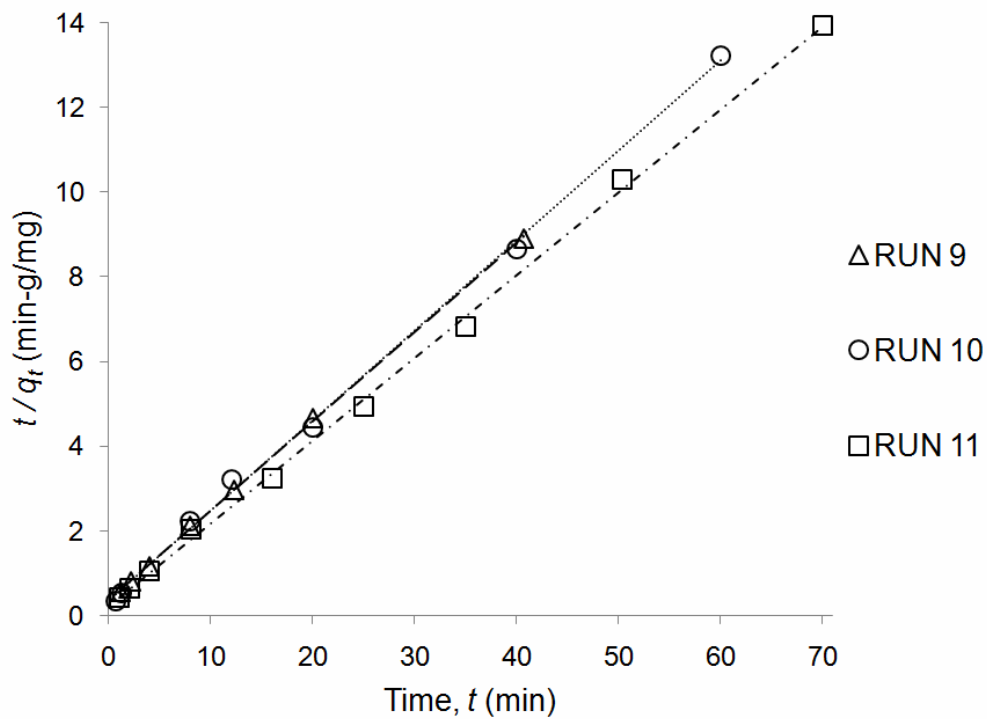
Fig. A3 Adsorption kinetic data for cadmium adsorption onto ox-MWNT fitted to pseudo-second order model. Cadmium initial concentration C_{A0} was approximately 4 mg/L; Run 9 was performed without pH control and 200 rpm, Run 10 was performed at pH 6 and 200 rpm, Run 11 was performed at pH 6 and 250 rpm.

Fig. A4 Adsorption kinetic data for cadmium adsorption onto ox-SWNT fitted to pseudo-second order model. Cadmium initial concentration C_{A0} was approximately 4 mg/L; Run 12 was performed without pH control and 200 rpm, Run 13 was performed at pH 6 and 200 rpm, Run 14 was performed at pH 6 and 350 rpm.

Fig. A5 Adsorption kinetic data for cadmium adsorption onto non-porous iron nanoparticles, FeOOH, fitted to pseudo-second order model. Cadmium initial concentration C_{A0} was approximately 4 mg/L; Run 15 was performed without pH control and 200 rpm, Run 16 was performed at pH 6 and 200 rpm.
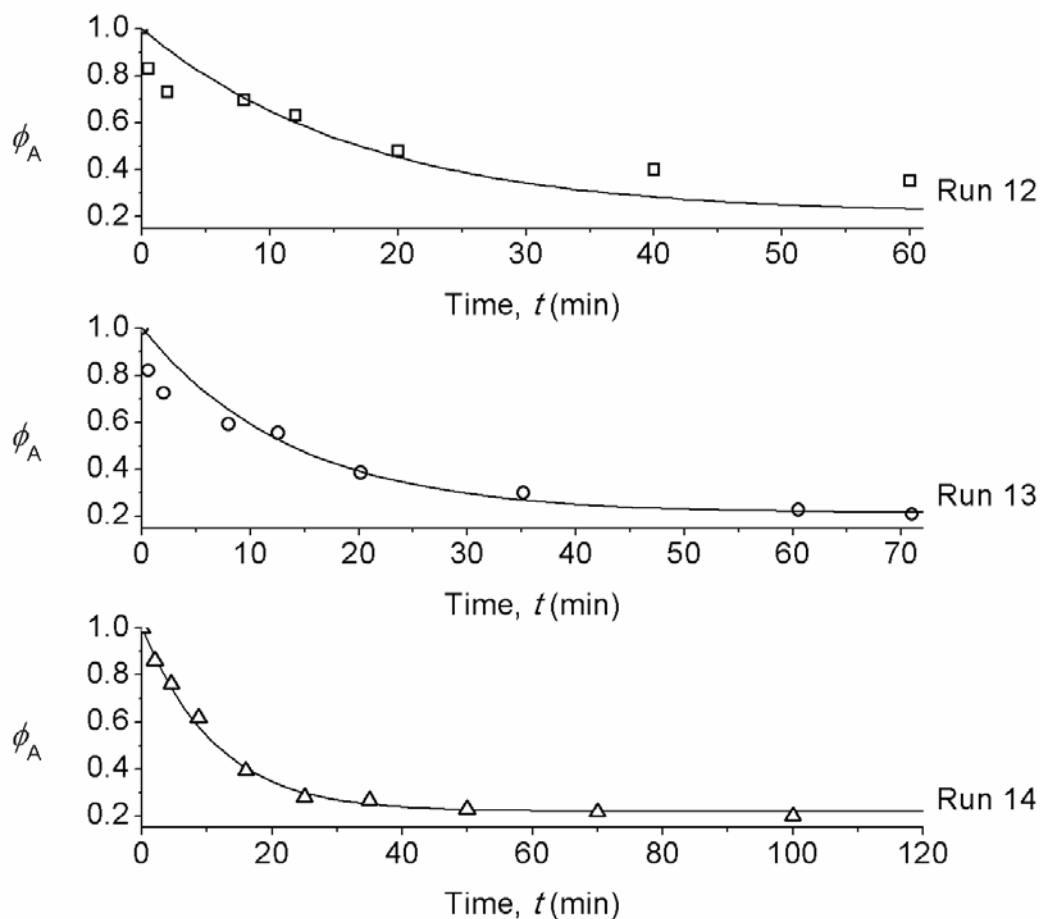
Appendix B
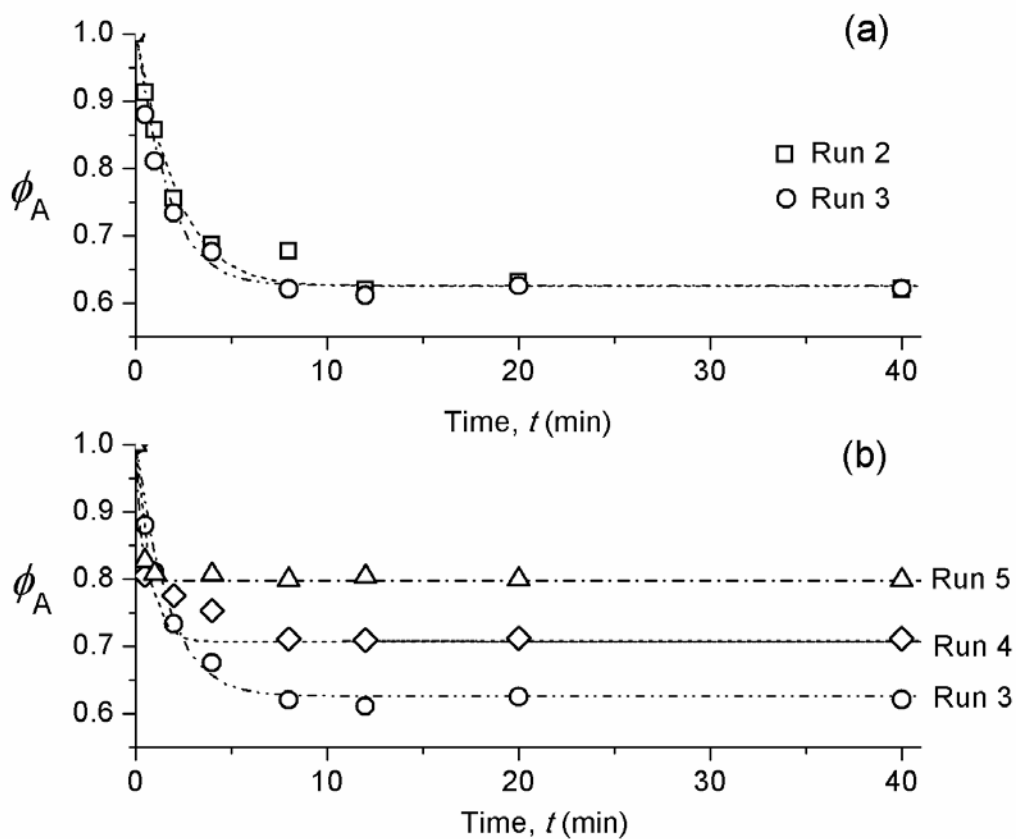
Fig. B1 Concentration decay curves with experimental data fitted by the external mass transfer model for cadmium adsorption onto ox-CNx. Runs were performed without pH control. (a) Runs 2 and 3 were performed at $C_{A0} \sim$ 4 mg/L and 150 rpm; (b) Runs 3, 4 and 5 were performed at 200 rpm and C_{A0} near 4, 9 and 19 mg/L respectively.
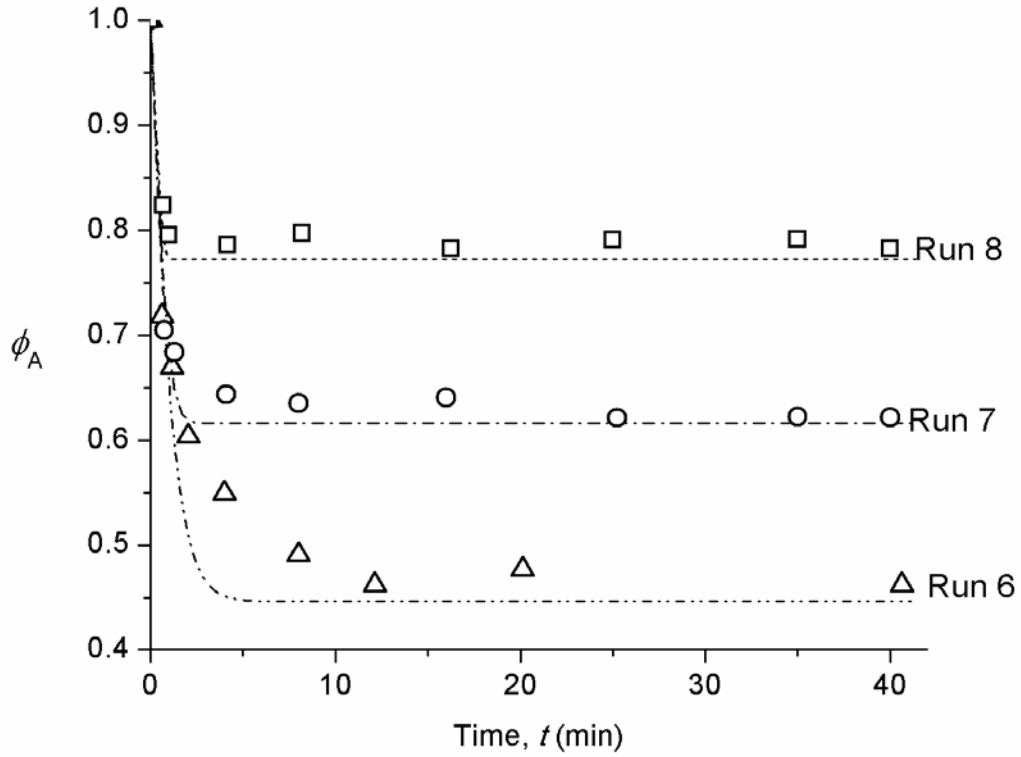
Fig. B2 Concentration decay curves with experimental data fitted by the external mass transfer model for cadmium adsorption onto ox-CNx. Runs 6, 7 and 8 were performed at initial cadmium concentration of approximately C_{A0} 4, 9 and 19 mg/L respectively, at pH 6 and 200 rpm.
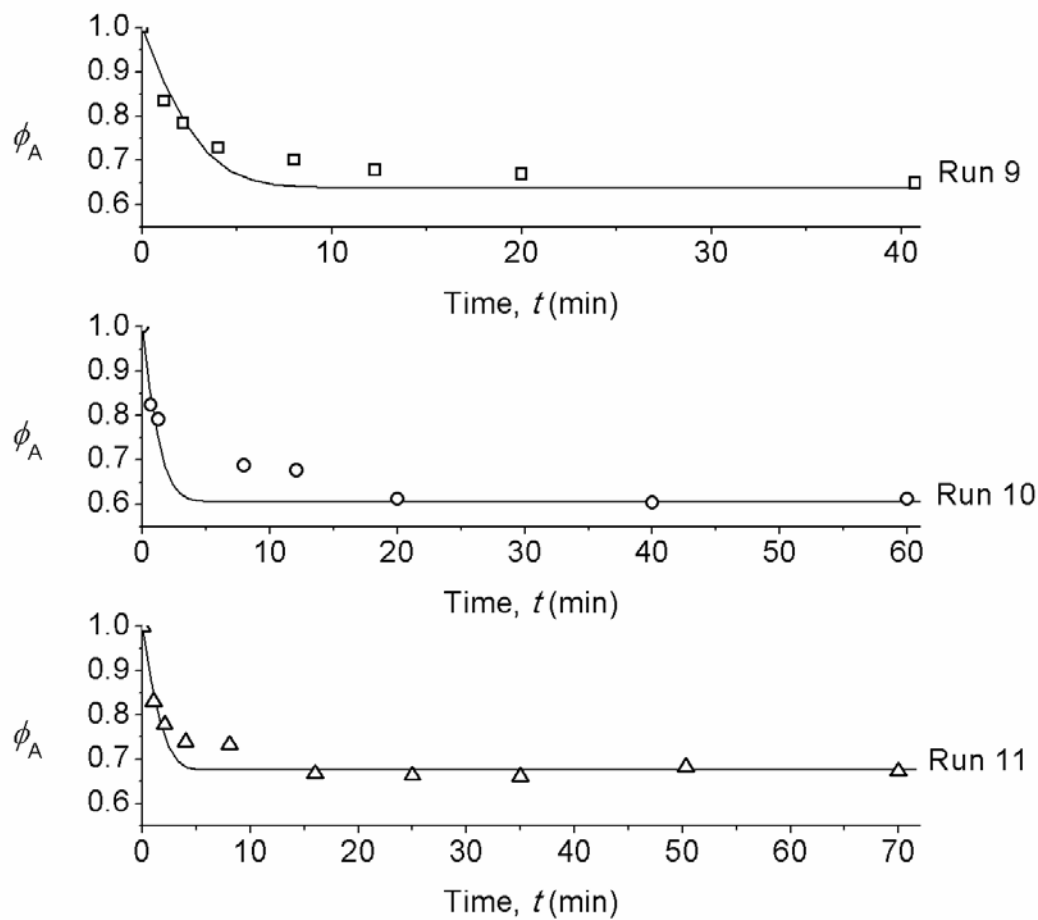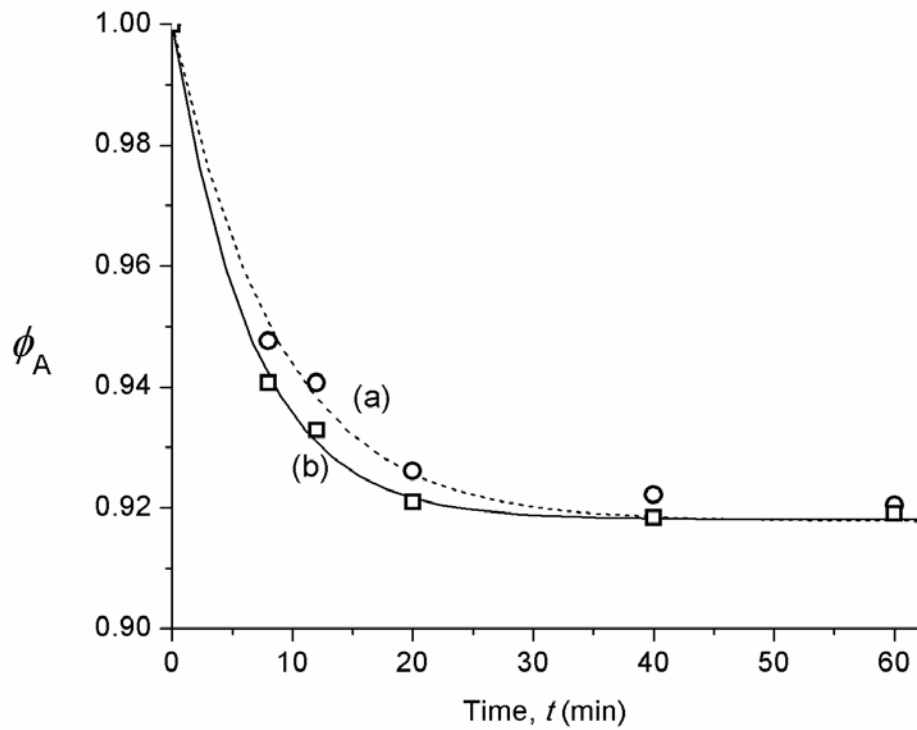
Fig. B3 Concentration decay curves with experimental data fitted by the external mass transfer model for cadmium adsorption onto ox-MWNT at initial cadmium concentration of approximately C_{A0} 4 mg/L. Run 9 was performed without pH control and 150 rpm; Run 10 was performed at pH 6 and 200 rpm; Run 11 was performed at pH 6 and 250 rpm.
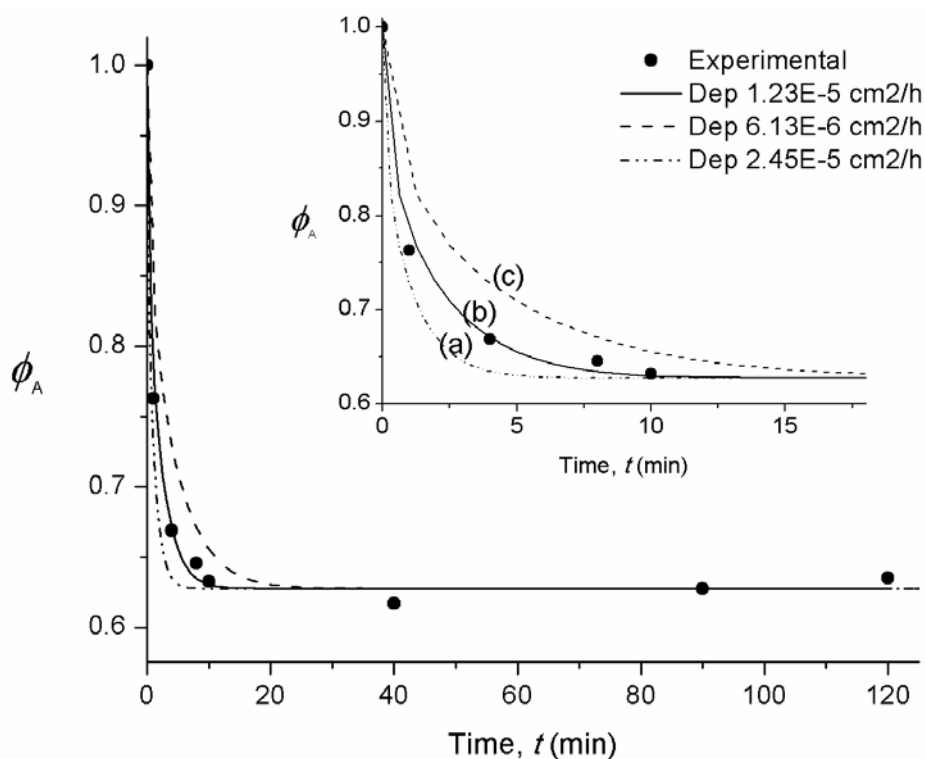
Fig. B4 Concentration decay curves with experimental data fitted by the external mass transfer model for cadmium adsorption onto ox-SWNT at initial cadmium concentration of approximately C_{A0} 4 mg/L. Run 12 was performed without pH control and 200 rpm; Run 13 was performed at pH 6 and 200 rpm; Run 14 was performed at pH 6 and 350 rpm.
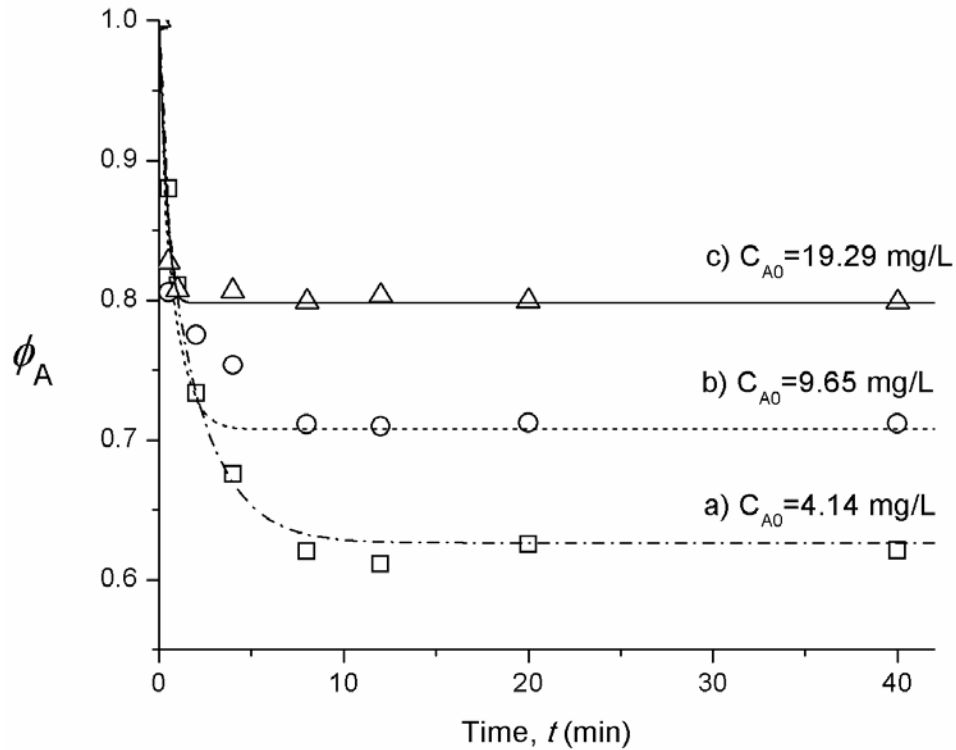
Fig. B5 Concentration decay curves with experimental data fitted by the external mass transfer model for cadmium adsorption onto FeOOH at initial cadmium concentration of approximately C_{A0} 4 mg/L. Run 15 was performed without pH control and 200 rpm; Run 16 was performed at pH 6 and 200 rpm.

Appendix C

Fig. C1 Sensitivity test of the intraparticle diffusion model to predict concentration decay curves (lines) that best fitting to the experimental adsorption kinetic data (symbols). Different values of diffusivity coefficients ($D_{e,p}$) were tested for run 1, performed at initial cadmium concentration of 4 mg/L, initial pH 6 without control and 150 rpm.

Fig. C2 Experimental adsorption kinetic data (symbols) and concentration decay curves (lines) predicted by the intraparticle diffusion model, for cadmium adsorption onto ox-CNx. Runs 3, 4 and 5 were performed at 200 rpm and (a) C_{A0}=4.14 mg/L without pH control, (b) C_{A0} =9.65 mg/L at pH 6 and (c) C_{A0} =19.29 mg/L at pH 6.
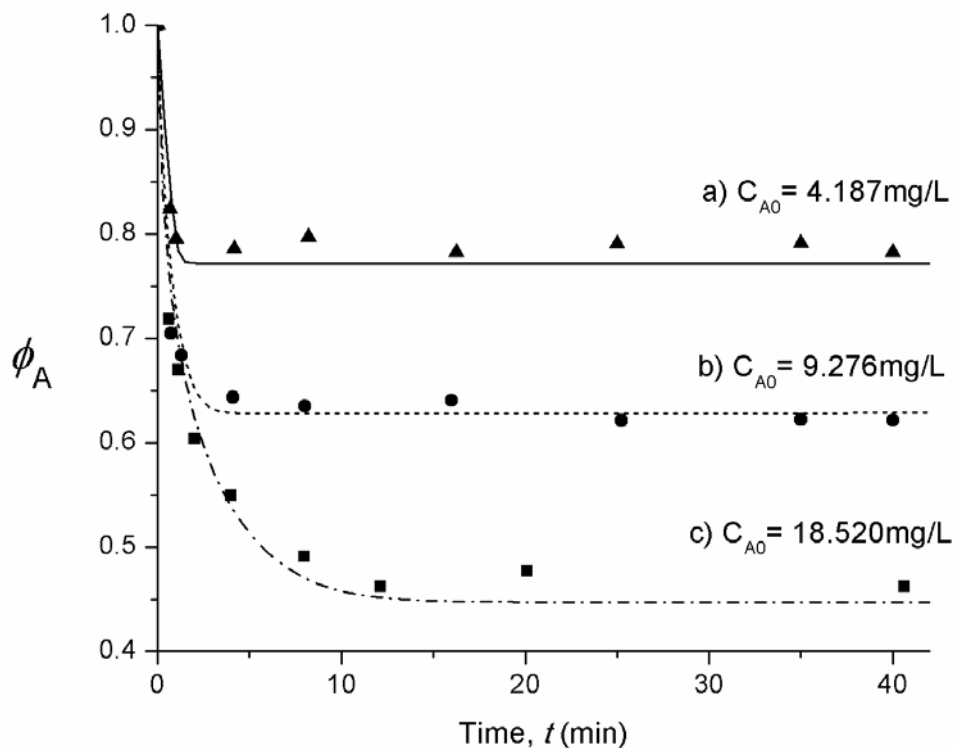
Fig. C3 Experimental adsorption kinetic data (symbols) and concentration decay curves (lines) predicted by the intraparticle diffusion model, for cadmium adsorption onto ox-CNx. Runs 6, 7 and 8 were performed at 200 rpm, pH 6 and (a) C_{A0} =4.14 mg/L, (b) C_{A0} =9.65 mg/L and (c) C_{A0} =19.29 mg/L.
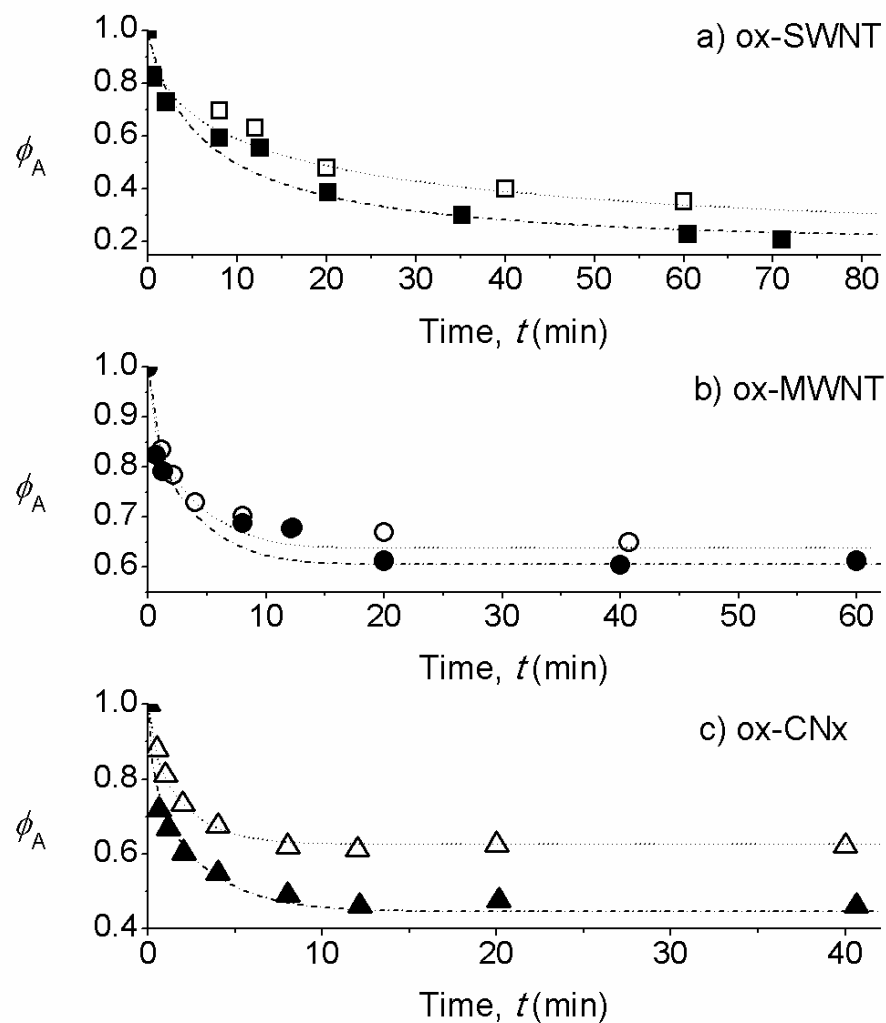
Fig. C4 Effect of pH control on the decay concentration curves with experimental data fitted by the intraparticle diffusion model, for cadmium adsorption onto (a) ox-SWNT, Runs 12 and 13, (b) ox-MWNT, Runs 9 and 10, and (c) ox-CNx, Runs 3 and 6. Experimental data were obtained at cadmium initial concentration of 4 mg/L, 200 rpm, without pH control (empty symbols) or pH 6 (full symbols).
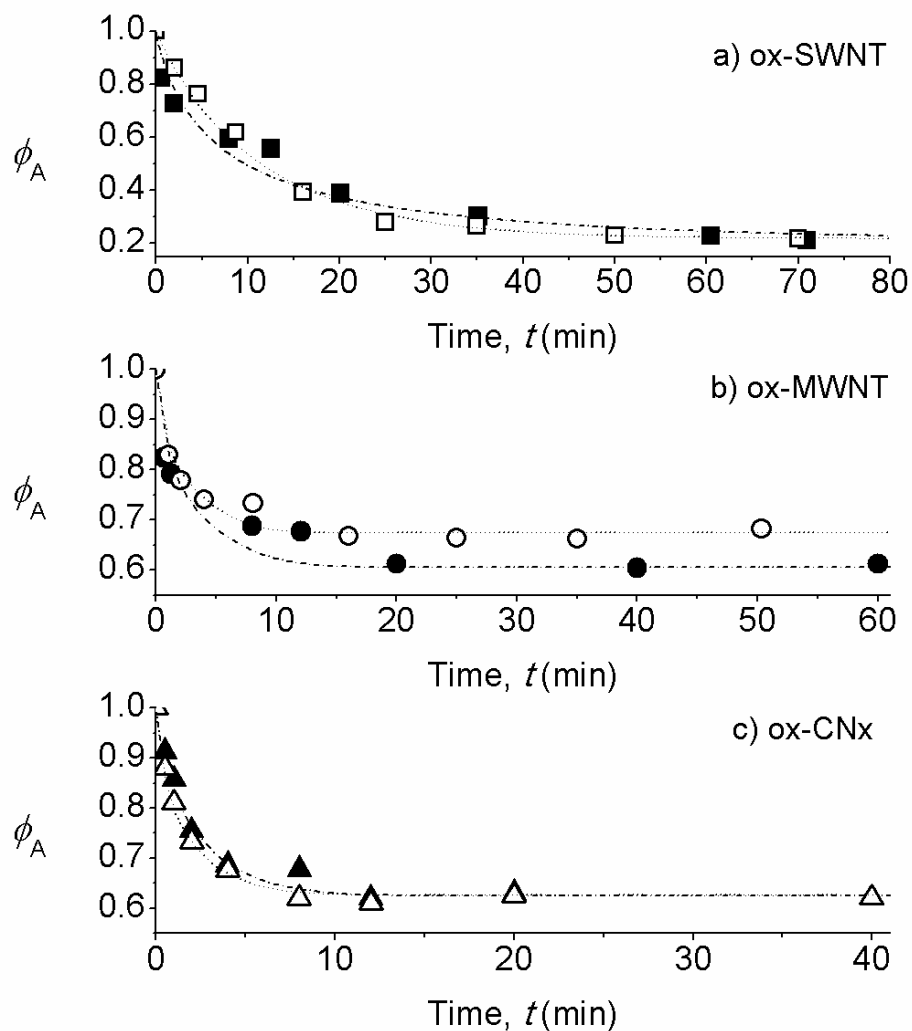
Fig. C5 Effect of shaking rate on the decay concentration curves with experimental data fitted by the intraparticle diffusion model. Experimental data were obtained at initial cadmium concentration of 4 mg/L, for cadmium adsorption onto (a) ox-SWNT, runs 13 and 14, at 200 and 350 rpm respectively, (b) ox-MWNT, runs 10 and 11, at 200 and 250 rpm respectively, and (c) ox-CNx, runs 2 and 3, at 150 and 200 rpm respectively. Empty symbols represent low rate data and full symbols high rate data.